An Investigation of the Soldering and Brazing Behaviour of Mg-Mg Joints using Sn, Zn and Mg containing Filler Metals

by

Viren Pravin Trivedi

A thesis
presented to the University of Waterloo
in fulfillment of the
thesis requirement for the degree of
Master of Applied Science
in
Mechanical Engineering

Waterloo, Ontario, Canada, 2012

© Viren Pravin Trivedi 2012

Author’s Declaration

I hereby declare that I am the sole author of this thesis. This is a true copy of the thesis, including any required final revisions, as accepted by my examiners.

I understand that my thesis may be made electronically available to the public.

Abstract

In order to evaluate the feasibility of forming Pure Mg – Pure Mg and Mg Alloy – Mg Alloy joints using soldering and brazing, four filler metals (Sn, Sn-9Zn, Sn-9Zn+X wt%Mg and Mg:Zn:X(Sn-9Zn)) were used at peak heating temperatures of ~250°C, 350°C and 450°C. Differential Scanning Calorimetry (DSC) and microstructure characterization were used to evaluate the successful joints.

When using Sn as a filler metal, a joint forms, at temperatures as low as 235°C, which consists of a Mg-Sn eutectic filler layer and a continuous Mg_2Sn intermetallic layer at the filler metal/Mg interface. This joint microstructure persists up to peak temperatures of 350°C and 450°C. The main effect of increasing the peak temperature causes an increase in the thickness of the Mg_2Sn layer.

Joints formed using Sn-9Zn prealloyed filler metal, developed a filler metal composition according to a Sn rich Mg-Sn-Zn ternary microstructure. A continuous Mg_2Sn layer still formed in the joint. Ternary phase diagram predictions support the development of a number of Mg_xZn_y intermetallic compounds. However, only isolated experimental evidence of Mg-Zn liquid formation was present at peak heating temperature of 350°C and no evidence of Mg_xZn_y intermetallic layers was observed for both base metal systems using Sn-9Zn filler metal at 250°C and 350°C. Upon further heating above 350°C, a Mg_7Zn_3 layer forms which eventually leads to a Mg-Zn eutectic liquid formation as 450°C is reached.

Wide gap Transient Liquid Phase Bonding (TLPB) was carried out by adding Mg to Sn-9Zn filler metal. Decrease in liquid volume fraction during solidification was noted with increase in Mg wt% as well as an increase in heating temperatures. Complete consumption of the filler metal was observed at 30wt% Mg and 450°C.

Microstructural events were noted to be similar to Mg-Mg couples using Sn-9Zn filler metal.

Mg-Zn, 50:50 wt% filler metal was thus used to evaluate joints without Mg_2Sn intermetallic formation. Mg-Zn binary liquid phase formation was found to correspond to 342°C upon initial heating and presence of solid Mg_7Zn_3 in microstructure was found in samples heated to 350°C. Increase in diffusional solidification of Zn into the unreacted Mg powder and Mg base metal was noticed upon further heating to 450°C.

Significant influence on the microstructure was noticed with addition of prealloyed Sn-9Zn powder to Mg-Zn filler metal mixture. Sn-9Zn was observed to be consumed in solid state during initial heating while alloying and dissolution of Pure Mg particles was seen to be accelerated. All Pure Mg powder was consumed indicating a large volume fraction present at 450°C in the case of filler containing 10% Sn-9Zn. The primary cellular grains of (Mg) grow from the Mg base metal substrate and Mg_7Zn_3 solidifies in the intercellular region. In the original filler metal portion of the diffusion couple, a mixture of (Mg), Mg_7Zn_3 and eutectic appears with a more dispersed character indicative of an equiaxed growth process. Promising results from 45Mg:45Zn:10(Sn-9Zn) wt% and peak heating temperature of 450°C could form basis for future work which can eventually lead to a commercial application.

Acknowledgements

First and foremost I thank my supervisor Dr. Stephen Corbin, who gave me the opportunity that has today turned out to be a time which has changed my life personally and academically. I am truly grateful for the freedom he has given me to wonder, question, research, answer and discover many a things some known, some new because of which I have come to appreciate and love the work and will always strive to continuously learn and advance as best as I can in the field of engineering. His guidance and mentorship during this time has been an absolute delight.

I would like to thank Dr. Mary Wells, my co-supervisor for her support and insight on this study.

I would also like to thank my thesis readers Dr. Shahrzad Esmaeili and Dr. John Wen for their comments, criticisms and insights on my MASc thesis. I greatly appreciate it.

I would like to thank MagNET and NSERC for funding this study as well as all the industrial partners especially Dana/Long Manufacturing to allow me to visit their facility and provide a perspective.

I would absolutely like to thank Mark Whitney, Dan Cluff, Dr. Ryan Clemmer, Dr. Dennis Turriff, Dr. Yuquan Ding and Dr. Jeffery McIssac for their guidance and support during my MASc. I would also like to thank Dr. Mark Pritzker who gave me an opportunity to see if I could perform chemical engineering on magnesium and Millennium Plating Co. for actually performing the chemical engineering on magnesium which made a great contribution to this study.

Lastly, I would like to thank my family and friends especially Sanju Vashist, Palak Patel, Dhaval Mistry and Ankit Mathur for their support while I sailed through this adventure of a life time.

For my parents and grandparents- my teachers in life, source of inspiration and values.

“All that we are is the result of what we have thought. The mind is everything. What we think we become.”

- **Gautama Buddha**

Table of Contents

List of Figures

List of Tables

1.0 Introduction

1.1 Background

Global warming is a pressing issue in the world. Impact of green house gas emissions on the environment is of a great concern. United States uses 71.4% of its petroleum consumption in the transportation industry and 66.0% of its petroleum is used by light-duty vehicles. The transportation sector in the United States emits 1945.8 million metric tonnes of greenhouse gas emissions which is 27.5% of total greenhouse gas emissions in United States trailing the industrial sector which emits 35.6%. Fuel economy of cars has increased from 15.9 miles per gallon (14.79L/100km) in 1980 to 22.6 miles per gallon (10.41L/100km) in 2008 and has been mandated by United States government to reach 34.1 miles per gallon (6.9L/100km) for all light duty vehicles in 2016 [1]. Due to research and development of technology, a 33% weight reduction in vehicles is expected by the United States Department of Energy, translating to a 23% reduction in fuel consumption by 2020 [2].

Engine performance and weight of the vehicle are the two very important factors that affect fuel economy [3]. In order to decrease the weight of vehicles, materials like Zinc, Copper and Steel will have to be replaced by lighter materials like Aluminum and Magnesium. As a norm; every 10% reduction in vehicle weight corresponds to a 6-8% decrease in fuel consumption. [2] Aluminum is 63% lighter than Steel and Magnesium is 33% lighter than Aluminum which makes Magnesium a worthwhile metal to explore for potential automotive and aerospace applications. Magnesium is being used as powertrain castings, intake manifolds, suspension supports etc. and has potential to be used to make pistons, engine blocks, doors, seats etc [4, 5] to reduce the overall weight of the vehicle and thus reduce the greenhouse

gas emissions as well as increase the fuel economy. Historically, Volkswagen was the first to introduce a 25kg of magnesium castings in transmission housing [2]. Since then magnesium casting usage has increased from 4 lbs in 1995 to 11 lbs in 2008 for domestic light duty vehicles [1].

In addition to being the sixth most abundant element and lowest density metal, magnesium has high specific strength & specific stiffness, good castability, excellent machinability, excellent sound damping and electromagnetic shielding capabilities, dent resistance, low toxicity, hot formability, recyclability, is resistant to ageing, etc. [2, 6, 7]. Along with casting, machining, forming, hot working etc., joining of magnesium as an integral part of manufacturing process is studied with care and in detail. Magnesium alloys are easily recycled with low energy costs and with minimal pollution with the most common technology for Mg recycling being flux remelting [2].

Along with the automotive sector, an increased need for magnesium technologies have been seen in the aerospace industry as well [8]. Applications of magnesium in the aerospace industry include structural reliability to decrease the payload weights for satellites as well as civil and military transportation to increase the fuel efficiency and reduce the operation costs [9]. Airbus A320 approximately consists of 65% Aluminum, 9% Steel, 7% Titanium, 13% Composites and 6% of Magnesium and other metals. With advances in light metals technology, European Union targets reduction in operating costs of an aircraft by 20% (short term) to 50% (long term) [10]. Active effort in reducing the weights of fuel connectors, seats, box doors, electrical and mechanical insulation parts etc. is already under way for aircrafts [11]. Applications for reduction of weight for space robots, satellites etc. also actively seek lighter metals like magnesium [9].

State of the art research programs are carried out in various countries in an effort to increase the collaboration and innovation of light weight materials [12]. Medical industry seeks applications of magnesium as a possible bone replacement material [13] while, electronics industry seeks to make gadgets lighter by making structural components as well as batteries (MgH_2) from magnesium [14]. The benefits of light weight material are even sought for light weight armors [15] and ballistics [16].

In summary, applications of magnesium are many however; in order to realize its application in many areas, methods of joining Mg to itself and to other metals must be better understood and developed.

1.2 Basics of Transient Liquid Phase Bonding and Sintering

The first commercial production of magnesium can be dated back to 31st August, 1864 when the first company producing magnesium was founded in the United Kingdom [17]. Casting, forging, forming, cold working etc. are some of the ways used to create functional Mg parts for assemblies. Joining can be included as the most important process for finished parts & final assemblies. Almost all processes associated with the usage of the powder form of magnesium fall under sintering while, plates can be joined by hot (welding, brazing, hybrid methods etc.) or cold (mechanical joining etc.) processes. Various researchers have successfully been able to demonstrate joining processes for Mg as described below. As a detailed overview of all processes is out of the scope of this chapter, focus shall be maintained on joining through the use of filler metal (eg. solder and brazing) and the related technology of Liquid Phase Sintering for the case of mixed powder filler metals.

In the automotive industry, the application of furnace brazing is particularly useful for the manufacturing of automotive heat exchangers [18]. The brazing sheets have a clad/core layered structure where the clad layers (with a lower melting point) act as an interlayer to join the two cores (Figure 1.2.1). The joining is promoted by removing the oxide film by the application of flux and heating, thus forming a bond through Transient Liquid Phase Bonding. During bonding, the clad layers melt such that there is liquid formation. Over time, due to solute diffusion, a homogenous bond is formed.

Another such interesting application of Liquid Phase Bonding is its application to turbine repair [19] where the damaged portion of the turbine blade is removed and an insert is fabricated which is then joined to the existing blade by

Transient Liquid Phase Bonding (TLPB). It has been proven to form high quality bonds.

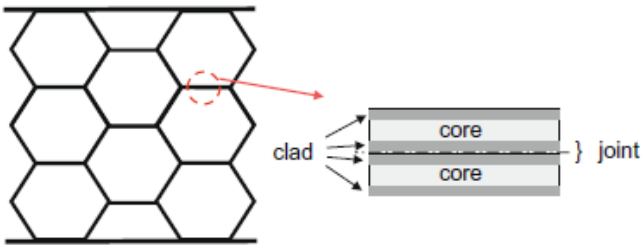

Figure 1.2.1: A typical schematic of clad/core structure used for manufacturing automotive heat exchangers [18]

Transient Liquid Phase Bonding (TLPB) and Sintering (TLPS) are liquid processes in which liquid disappears due to dissolution into the solid, thus forming a bond [20]. However, it is also known as diffusion brazing or soldering; a variation which depends on liquid formation at the faying surfaces by interlayer melting, resolidification and then an epitaxial growth of the substrate through isothermal solidification [21]. Typical geometry of the joint in this kind of process is achieved by a thin interlayer which can be a foil or coating on to the base substrate. At times, powders with fluxing agent or powders pressed against the base metal to break the oxide layers are also used in the filler metal region. TLPB goes through four steps in order to form a uniform joint which approaches the strength of the base material [21]. These four steps are (i) heating, (ii) dissolution and widening, (iii) isothermal solidification and (iv) homogenization. A schematic of the process can be seen in Figure 1.2.2.

(i) Heating:

During the heating stage, the joint structure (Figure 1.2.2 a) is heated up to the melting point of the low melting point interlayer, T_1 in this case

assumed to be of a eutectic composition C_E(Figure 1.2.2f). While reaching the eutectic temperature, solid state interaction is promoted given there is no oxidation contamination between the interlayer and the faying surfaces. When solid state diffusion occurs, the joint is effectively formed. Also it is during this step that solid state intermetallics can be formed. In essence, the bond can be formed even during the heating stage. However, it would require a perfect contact without asperities, thus a uniform bond is proven to be extremely difficult at this stage. Solid state interactions are generally found to be very slow and as a result to promote a rapid joint formation, presence of liquid is desired. At times, if the interlayer is very thin, the solid state kinetics use up all the interlayer material and no liquid is formed above the eutectic temperature [21].

(ii) Dissolution and widening

As the temperature profile (Figure 1.2.2e) continues heating the joint structure along with the entire assembly, the first liquid starts to appear at the faying surfaces within the joint geometry. During this step, depending upon the solubility of the solid in the liquid material, the widening of the joint width due to an increase in liquid occurs (Figure 1.2.2b). This occurs after the eutectic first liquid appears at the faying surfaces. Due to lowering of Gibbs free energy, the liquid zone widens accepting the solid up to the concentration limitations $C_{L\alpha}$ governed by concentration at the temperature of the joint assembly. The dissolution of solid in liquid swiftly moves to reach the maximum width of liquid that can be formed.

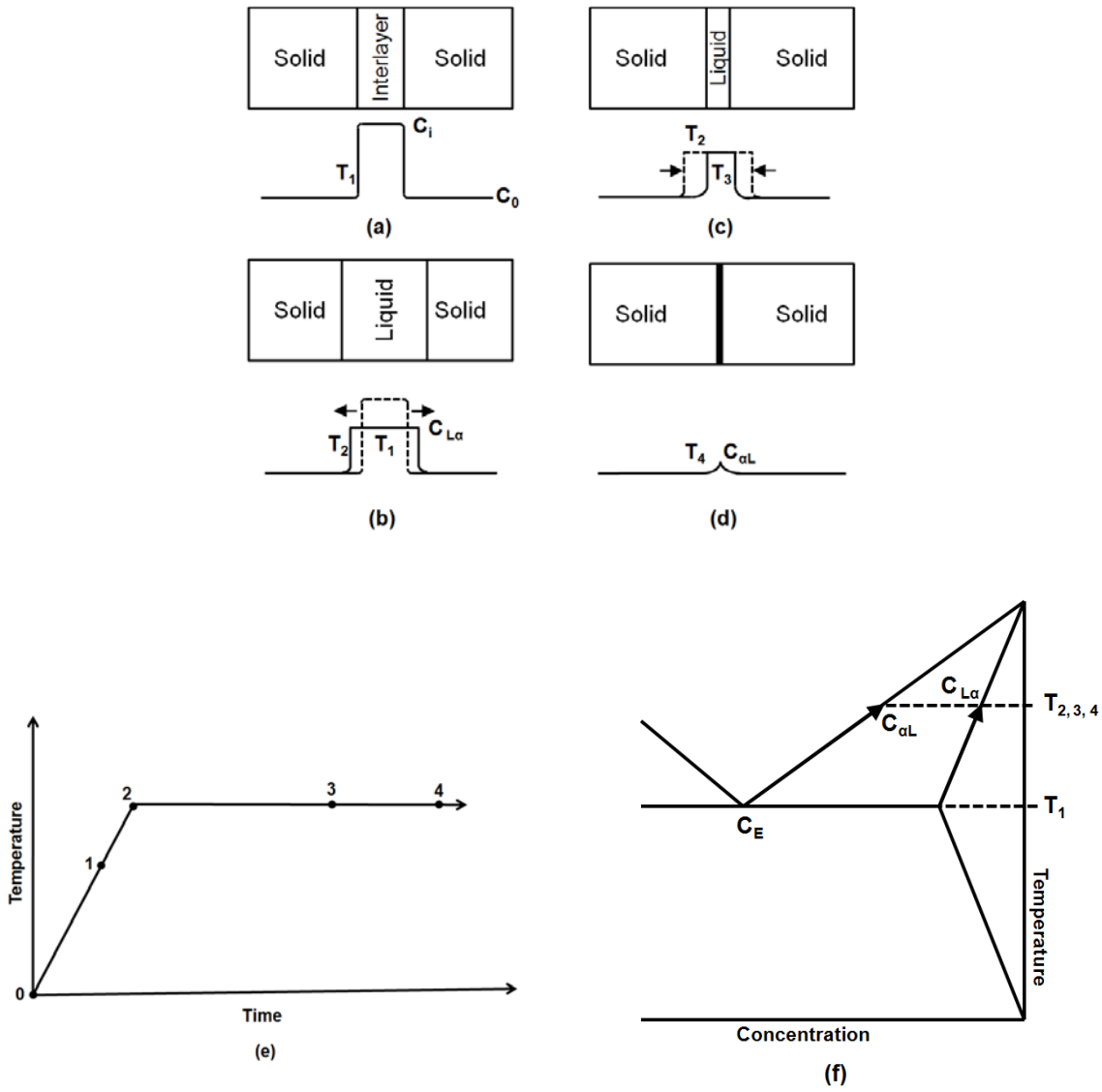

Figure 1.2.2: TLP stages (a) Heating, (b) Dissolution and Widening, (c) Isothermal Solidification, (d) Homogenization, (e) Temperature Profile and (f) Process on Phase Diagram [adapted from [21]**]**

(iii) Isothermal Solidification

As the temperature remains at the brazing temperature T_3, more and more solute moves into the solid base metal through diffusion at the solid/liquid interface. This process is known as isothermal solidification (Figure 1.2.2c). As the temperature is held at a desired temperature; based on diffusion coefficients, the solidification rate increases or decreases. It

should be noted here that solid state intermetallic boundaries could form at the solid/ liquid interface lengthening the time required for isothermal solidification to complete. The isothermal solidification stage is completed when the liquid zone is entirely consumed and diffused into the solid base metal and no liquid is present. During this process the solid/liquid interface starts moving towards the centerline of the joint geometry (Figure 1.2.2c). The time required for the completion of this stage largely depends on the width of the liquid, extent of intermetallic formation as well as the diffusion rate between the solid base material and the liquid.

(iv) Homogenization

There is a residual peak of solute concentration at the joint centerline as the isothermal solidification stage is complete [21]. This magnitude of solute concentration $C_{\alpha L}$ is slowly reduced by further diffusion into the base material. This process is known as homogenization (Figure 1.2.2d). As this is solid/solid diffusion, the extent of time required for this process to complete could be very long. Intermetallics could slow the process further as well as in some cases degrade the joint properties.

A variation of TLPB which is Transient Liquid Phase Sintering (TLPS) typically exhibits the same process stages such as diffusion bonding, powder based filler metal brazing and soldering and is essentially a method by which parts or objects are made from powder. A comprehensive map of the sintering process can be found in Figure 1.2.3. A solid state sintering is achieved by diffusion of atoms of one material into another based on favourable metallurgical conditions. A liquid phase sintering process is essentially an extension of solid state sintering but, in the

presence of liquid that is facilitated by elevated temperatures or favourable metallurgical conditions to promote liquid phase formation. In liquid phase sintering, the liquid usually wets the solid if it has solubility for the solid. Conceptual summary of the interactions and sintering behaviour during liquid phase sintering can be referred to from Figure 1.2.4.

In order to investigate a system of interest for liquid phase sintering, a phase diagram can become an excellent guide. Binary phase diagram portraying favourable conditions for a successful liquid phase sintering can be referred to from Figure 1.2.5.

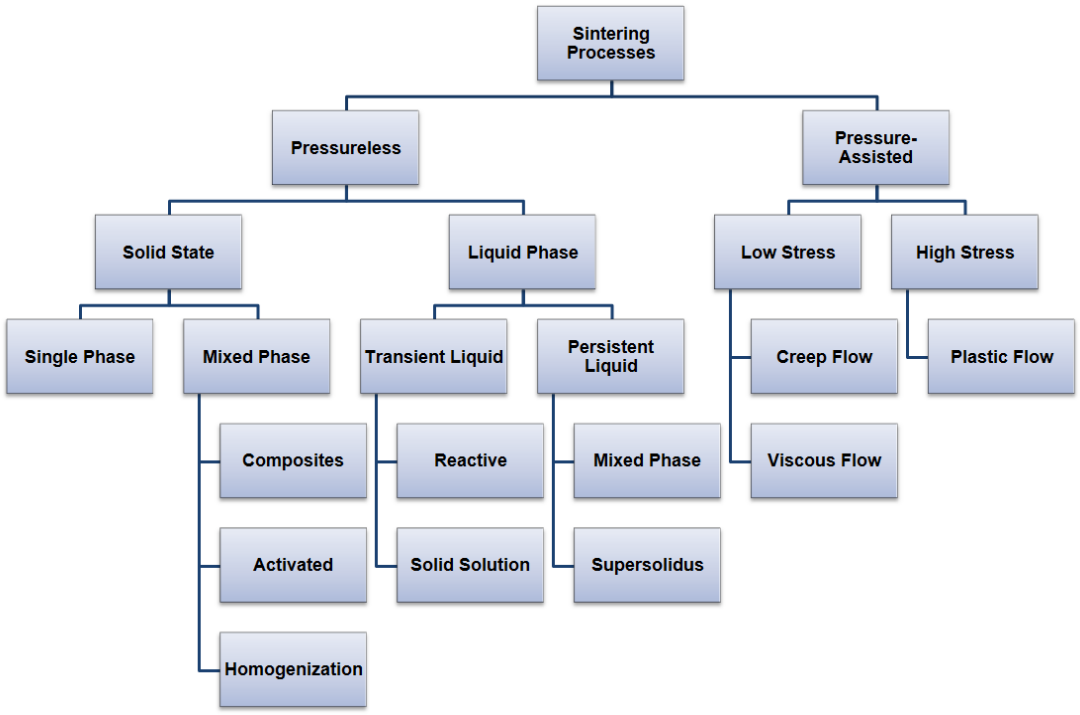

Figure 1.2.3: Sintering processes map [22]

		Solid Solubility in Liquid	
		Low	**High**
Liquid Solubility in Solid	**Low**	Limited Densification, Rearrangement	Extensive Densification
	High	Swelling, Transient Liquid	Mixed Effect Swelling and Densification

Figure 1.2.4: Conceptual summarization of the interactions and sintering behaviour as dictated by solubility interactions during liquid phase sintering [22]

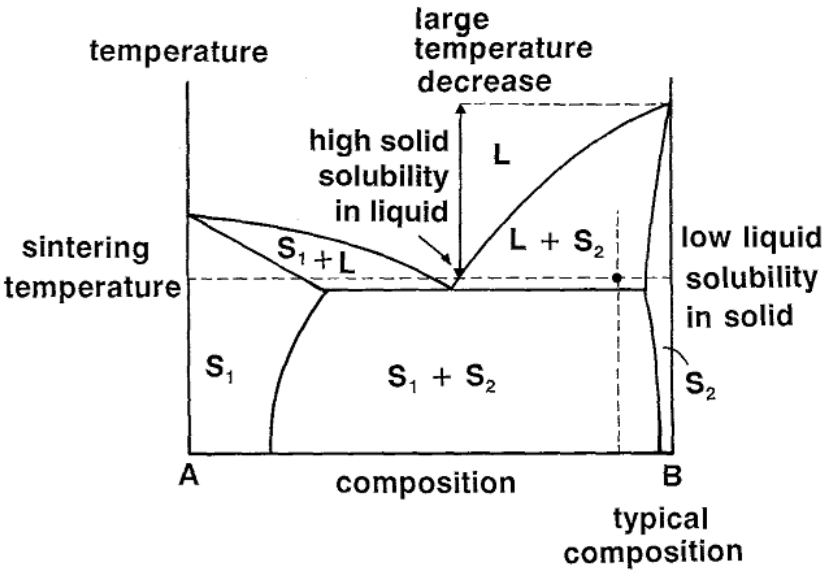

Figure 1.2.5: Favourable attributes for liquid phase sintering as mapped on a binary phase diagram [22]

R.M.German [23] identifies the following five criteria as favourable for successful liquid phase sintering:

1) Solubility of the solid in liquid
2) Low contact angle
3) Small dihedral angle
4) Low degree of solid state inter-particle bonding
5) Loose powder structure

The progress of the liquid phase sintering process can be divided into three stages: Initial, Intermediate and Final [23].

Initial stage of liquid phase sintering is solubility and rearrangement and it typically lasts for the first 10 minutes [23]. As the heat input to the system slowly increases with the temperature rise, the first liquid formation occurs at a melting onset temperature which depends on the system. However, shrinkage can occur within the system if the system has provisions for solid state diffusion or even solid state intermetallic formation. The other possibility is swelling of the system which can occur if there is a low solubility ratio. Once the liquid forms, the repacking of the solid particles due to liquid wetting starts under capillary forces. The densification or rate of densification depends on the degree of interaction between the solid and liquid by wetting and solubility within the systems. Densification occurs due to rearrangement which primarily depends on rate at which the melted liquid can spread through the system. Along with spreading, due to the capillary forces and wetting of solid particles by liquid, clustering of particles is promoted, as well; penetration through the solid grain particles where possible occurs by breaking the solid particle into fragments and thus assists mixing of the systems. The proportion of liquid formation has a direct effect on rearrangement as high volume fraction of liquid means higher capillary forces. Thus, viscosity and capillary forces optimization

(optimum quantity of liquid) is critical for densification. A high green density (non reacted packing density) is unfavourable as the liquid movement within the system is restricted and thus causes swelling. However, pore formation due to the changes in density by solubility, diffusivity or reactions within systems is common. This stage is followed by an intermediate stage of solution – reprecipitation.

After the first melt formation and start of liquid phase sintering, the initial stage makes a transition into an intermediate stage (dissolution and reprecipitation). Densification, grain growth, grain accommodation, coalescence and pore elimination are prominent in the intermediate stage of liquid phase sintering. The aim for liquid phase sintering is always towards pore free densification of a system. Densification is highly associated with the grain growth, dissolution of small grains into large grains, grain boundary migration by coalescence and cooperative solution reprecipitation between solid and liquid systems.

Grain shape accommodation is perhaps one of the most important parameters in achieving high densification in a system. When grain shapes deviate from minimum energy shape, it accommodates to remove porosity, thus promoting the densification process. Coalescence of contacting grains promotes grain boundary accommodation. A chemical potential difference aids coalescence however; where small grains are involved, high energy barrier obstructs coalescence which then requires co-operative solution-reprecipitation. Pore filling has been identified as the final action during the intermediate stage and thus marks the start of the final stage. Elimination of the largest pores requires further grain growth and grain shape accommodation. Grain growth essentially squeezes the liquid and allows capillary refilling of the pores.

The final stage of liquid phase sintering is essentially an extension of the intermediate stage where the entire system approaches equilibrium. The densification rate for completion of liquid phase sintering depends on diffusion and solubility of the solid in the liquid. It is important to optimize the time a system should go through the heating cycles as during prolonged heating, the residual pores can be affected by Ostwald ripening and coalescence. The behaviour of such events can either be beneficial or harmful to the system as they may cause densification or promote swelling. An atmosphere in which the liquid phase sintering is executed also has a significant impact on the densification of the system. As a result, sintering in a vacuum helps rapid densification as pressurization occurs with soluble trapped gases while insoluble trapped gases assist pore formation.

Ostwald ripening and coalescence events are characteristic features of the final stage of liquid phase sintering. The mean grain size increases with time and it also increases the mean separation between the grains. The separation allows the larger grains to grow further depending on the liquid volume fraction available. The mean grain size increase has been correlated with time as time to the $1/3^{rd}$ power [23]. Impurities, intermetallics and non consistent green densities can impede the grain growth. Many analytical models have been developed to predict the time required for the liquid phase sintering to achieve completion however, the models do not include the effects of irregular grain shapes, high volume fractions of the solid, grain shape accommodation, grain contact, intermetallics and non zero dihedral angles [24, 25, 26, 27]. Thus, the effect of time, temperature, solubility, grain size, atmosphere and composition are understood in terms of microstructure coarsening and final densification however, a number of other factors do effect the process which can only by studied by experimental evaluation. The schematic diagram of classic liquid phase sintering involving non-reactive systems can be referred to from Figure 1.2.6.

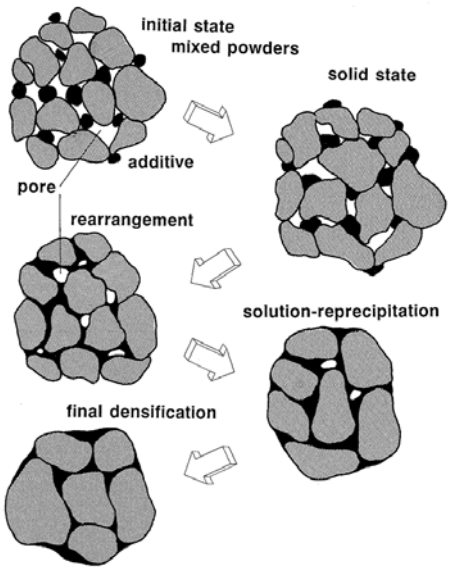

Figure 1.2.6: Schematic diagram of the classic liquid phase sintering stages involving non reactive systems [22]

1.3 Prior Art of Magnesium Soldering and Brazing

Wielage et al. [28] developed a fluxless ultrasonic assisted soldering method with 100 N load using Al-Mg-Zn filler metal at 340°C-350°C for 10-15 seconds to join Mg alloys. They also used Sn based filler metal (96Sn:4Ti:3Ag) at 235°C for 10-15 seconds to join Mg alloys and Steel to evaluate the corrosion behaviour of solder joints. The joints appeared to be complete with eutectic and intermetallics formations. The authors observed that the Mg-Mg joints had better corrosion behaviour than the Mg-Steel joints.

Weilage and Muechlich [29] used Mg-Zn-Al based filler metals at temperatures above 340°C to join Mg(AZ31)-Mg(AZ31) and Mg-Al binary couples. $Mg_{17}Al_{12}$ intermetallic was prominent in both Mg-Mg and Mg-Al binary couples and the filler metal composition of 40Mg:50Zn:10Al was found to have the best shear strength characteristics.

Liu et al. [30] investigated reaction brazing of Mg alloy (AZ31B) and Al alloy (6061) by first plating Aluminum with Zinc and then applying 4 MPa pressure at 360°C and 446°C with different hold times. Specimens joined using 10µm, 20µm and 30µm braze metal thickness at 360°C and 30 min hold exhibited significant cracking at the bond line and the development of a reaction zone with intermetallics. The bond was not found to be repeatable. However, with a 3µm layer of zinc plating, significant improvement in joint microstructure as well as shear strength was noted at 360°C and 10, 20 and 30 min holds.

Bobzin et al [31] outlined criteria for the development of suitable filler metals for magnesium joining applications as:

1) Minimize contact corrosion
2) Joining temperature must be lower than the critical temperature: approx <450°C.
3) Third element should build a ternary eutectic.

The authors performed numerous experiments of joining AZ31B alloy with filler metal compositions of Mg-Al-Ga, Mg-Al-Cu and Mg-Al-Zn at 360°C - 475°C with flux in an Argon environment. Best results were found with the Mg-Al-Ga system with no significant pores in the joint microstructure and the joint was found to have the highest shear strength. However, corrosion tests were poor and cracks were found at the joint interface of all three filler metal systems.

Sun et al. [32] performed transient liquid phase bonding of a magnesium alloy using an aluminum interlayer. The bond was performed using two Mg Alloy sheets (Mg-3Al-1Zn) with a 10µm Al interlayer at a heating rate of 0.13°C/s (7.8°C/min) up to 1, 5, 10, 30, 60 & 120 min hold at bonding temperature of 440°C, 460°C, 480°C & 500°C in a 4.5 Pa vacuum furnace. The joint was observed to grow to 51µm from 10µm at 480°C and 1 min hold. The composition at the interface was noted to decrease to 41.9wt% Al from the 99.99wt% aluminum (before bonding). $Al_{12}Mg_{17}$ intermetallic was notable with 10 min hold and joint was observed to have increased to 86µm with further decrease in the Al (wt%) content at the joint interface, suggesting significant metallurgical interactions and dissolution of the substrate. At 60 min hold, the joint width was observed to decrease suggesting an isothermal solidification phase of transient liquid phase joining. The Al content was observed to drop to 10.8wt% with completion of isothermal solidification stage. Intermetallics were observed to decrease with an increase in bonding time. Grain growth was

observed with further decrease of Al content at the joint interface with increase in time from 60 min to 120 min. The authors also report shear strength increase from 33.8 MPa at 1 min to 76.1 MPa (92.4% of base metal) at 60 min hold and decreased to 70.4% at 120 min hold. It was also observed that bonding temperature of 480°C, out of 440°C, 460°C, 480°C and 500°C resulted in best shear strength. The authors attribute the high joint shear strength to the $Al_{12}Mg_{17}$ intermetallic compound and grain coarsening.

1.4 Objectives and Concept Joint

The main purpose of this study is to develop and investigate a method to join magnesium (pure or alloy) to magnesium (pure or alloy) at temperatures as low as possible with commercially viable materials. The application targeted is manufacturing of an automotive heat exchanger by furnace brazing. The intent is to be able to develop and evaluate a process to join magnesium via Transient Liquid Phase Bonding lowering the joining temperature (which reduces the thermal expansion effects) and without use of an organic flux to obtain a microstructure that can be classified as a metallurgically good bond. The objectives of this study are:

- Research on low temperature joining of Mg to obtain good metallurgical contact between the Mg surface and a Sn-Zn or Mg-Sn-Zn containing filler metal.
- Develop a complete methodology to examine the melting and re-solidification behaviour of a filler/base metal couple with use of the Differential Scanning Calorimeter.
- Characterize the microstructure evolution in Pure Mg and Mg Alloy based joint systems at different temperatures and different hold times using various Sn-Zn or Mg-Sn-Zn containing filler metal compositions.

Thus, in light of previous studies and results found in the literature, the concept joint proposed can be seen from Figure 1.4.1. The joint was proposed based on the fact that one of the lowest melting temperatures of a metal that is widely used in the industry is 231.5°C for Sn [33]. Zn and Sn have eutectic composition temperature of 199°C [33] while the ternary eutectic for Mg-Zn-Sn is reported to occur at 7.39:11.47:81.14 at% and 183°C [34]. Due to magnesium's tenacious oxide, direct wetting of Sn based filler metal would not be possible without use of flux or

other oxide eliminating techniques. Thus a surface treatment of magnesium can assist the process and the fact that zinc has a higher solubility in magnesium than tin; zinc immersion coating was selected as in interlayer to assist low temperature joining of magnesium by Transient Liquid Phase Bonding process. Based on Figure 1.4.1, an additional objective of this work was to assess the feasibility of developing a TLPB process for Mg-Mg joining.

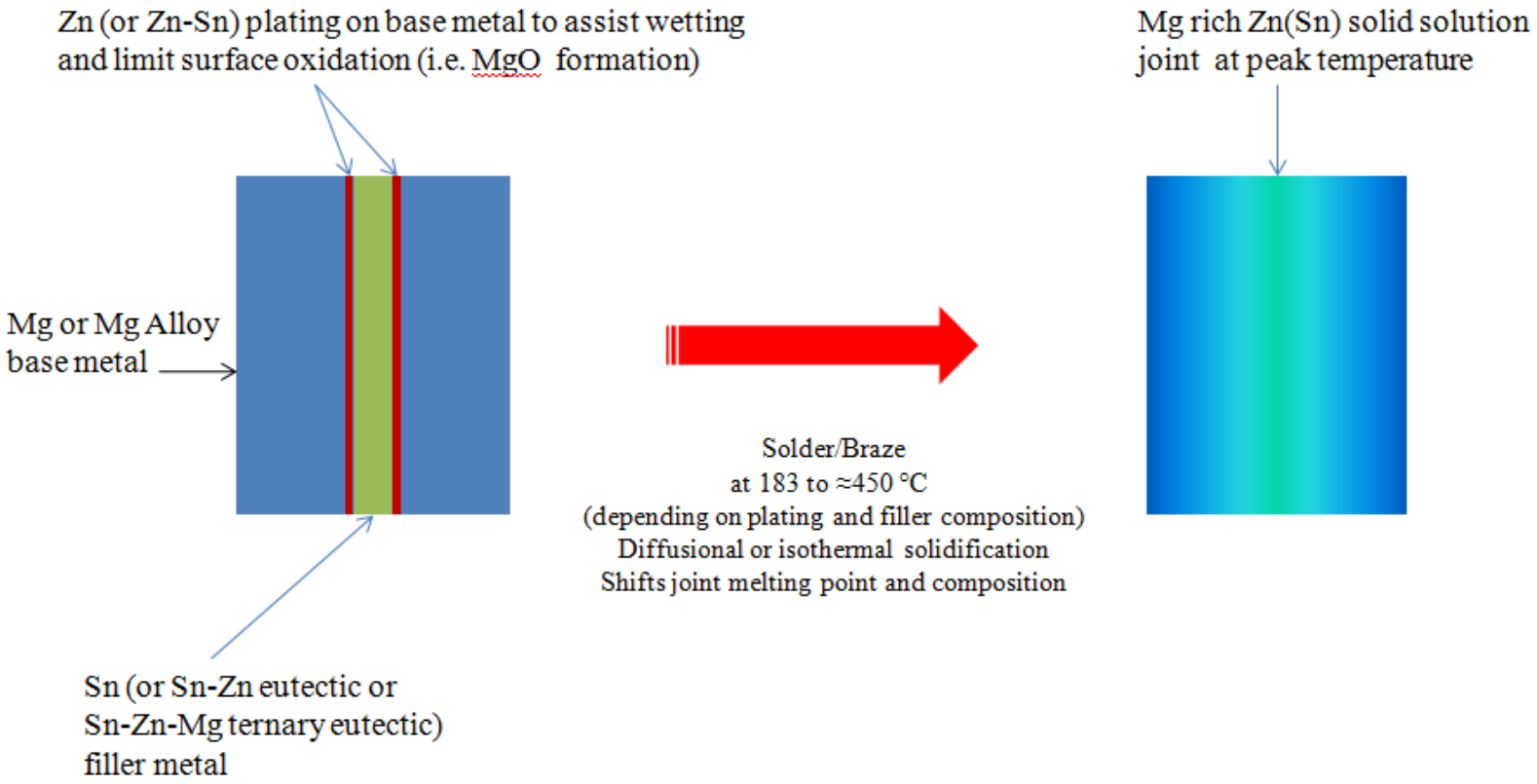

Figure 1.4.1: The Concept Joint

2.0 Differential Scanning Calorimetry

2.1 Differential Scanning Calorimeter Instrumentation

Differential Scanning Calorimetry is defined as “the measurement of the change of the difference in the heat flow rate to the sample and to a reference sample while they are subjected to a controlled temperature program” [35] Evolution of Differential Scanning Calorimetry (DSC) comes from Differential Thermal Analysis (DTA) which is defined as “the measurement of the change of the difference in temperature between the sample and the reference sample while they are subjected to a controlled temperature program” [35]. Controlled temperature program, or in simple terms heating and cooling cycles, affects any material or a combination of materials in a different manner. These combinations of materials could go through solid state, liquid state or gaseous state reactions and release or absorb energy as exothermic or endothermic reactions respectively. The fundamental difference between DTA and DSC is the measurement of temperature difference in DTA while heat flux in DSC. In principle a DSC operates by measuring the sample in question and the reactions within the sample which are either endothermic or exothermic reactions to measure the voltage difference between the empty reference crucible and the reaction sample crucible to plot with respect to time in a computer program while DTA measures temperature difference directly.

Uniqueness of these experimental procedures allows for characterization of materials, kinetic investigations, phase transitions due to changes in temperature by recording the thermal events [35]. Instrumentation for both DSC and DTA are typically configured in a similar fashion. The schematic for the DSC instrumentation can be seen in Figure 2.2.1. Reference crucible (R) which is empty and the sample

crucible (S) which holds the material or combination of materials for investigation can be seen in the schematic shown in the Figure 2.1.1. These crucibles are placed in the furnace which is also an atmospheric control chamber. These thin walled crucibles are placed in a sample carrier which holds these crucibles in the hot atmospheric controlled zone. Thermocouples are directly below these crucibles and record events at different rates while the crucibles are subjected to a predetermined temperature program.

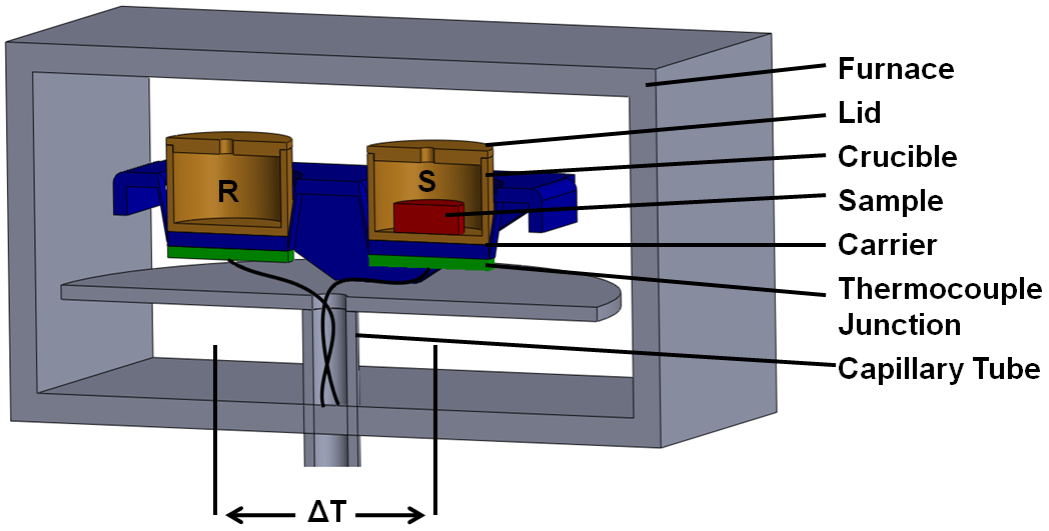

Figure 2.1.1: Schematic of Differential Scanning Calorimeter

A differential scanning calorimeter could provide two outputs, the average temperature of the two cells and the difference in power supplied to the cells [36], which is why two types of DSC instrumentation are available; namely, power compensated differential scanning calorimeter and heat flux differential scanning calorimeter. The differential method of measurement for both types of DSC's is defined as "a method of measurement in which the measurand is compared with a quantity of the same kind, of known value only slightly different from the value of the measurand, and in which the difference between the two values is measured" [35]. In

principle, phase changes as well as reactions within the samples are recorded in a similar fashion in both DSC's by heating and cooling the sample and reference material.

A power compensated differential scanning calorimeter works on the principle that if the temperatures of both, sample and reference are individually controlled, any event in the sample crucible will either increase or decrease the requirement of electrical energy for the reference crucible and can be recorded as the difference in required power to compensate the lead or lag of temperature. While, in a heat flux differential scanning calorimeter which operates slightly differently than the power compensated differential scanning calorimeter, both crucibles are heated symmetrically in a chamber with predetermined heat flow rates and any event that occurs in the sample crucible will either increase or decrease the temperature of the sample crucible with respect to the reference crucible which can be recorded as the temperature difference.

Heat flux differential scanning calorimeters are further classified into disk type and cylinder type measurement systems. As the names suggest, in disk type measurement systems material of interest are in small disk form while in cylinder type system the crucible size is large enough to incorporate small cylinder type samples. The main difference between the two measurement systems is that because of its larger size, cylinder type measurement systems can accommodate more thermocouples or thermopile for a larger signal from the more useful volume of material in question but it comes with the price of higher thermal inertia while disc type measurement systems have higher sensitivity per volume of material in question [35]. A complete schematic of disk type differential scanning calorimeter with the

measurement recording procedure, which is also the type of differential scanning calorimeter used in the experimental work presented here, is shown in Figure 2.1.2.

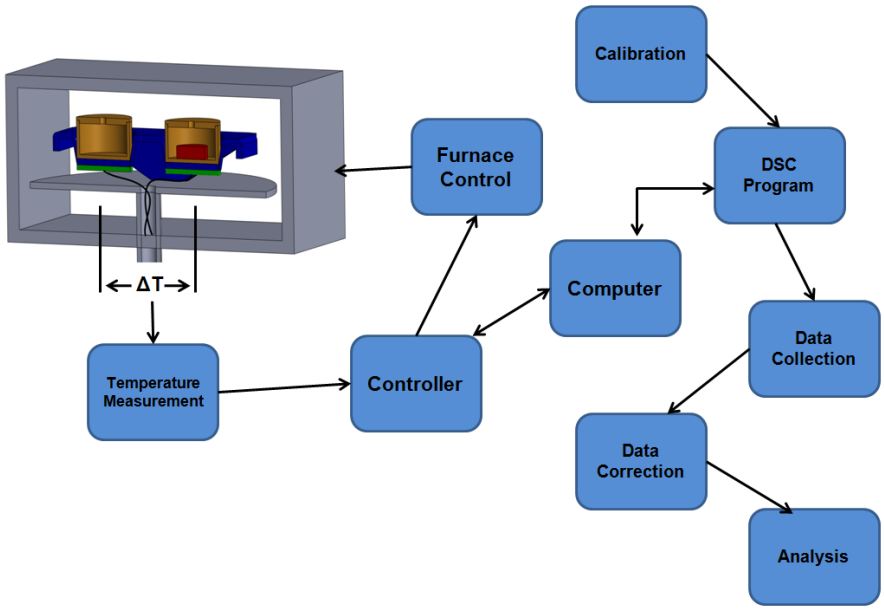

Figure 2.1.2: Schematic of DSC measurement procedure

The understanding of operation and data output of a heat flux differential scanning calorimeter can be enhanced by examining equations governing for the system. As can be seen in Figure 2.1.1, there are no heating elements near the crucibles and also that there is no contact between the furnace surface and the carrier. Therefore, it can be easily said that the heat transfer through the system is carried out by convective heat transfer. The rate of convection heat transfer is expressed by Newton's law of cooling [37] as:

$$\dot{Q} = kA_s(T_s - T_\infty) \qquad (2.1\text{-}1)$$

where $\dot{Q}$ is *dq/dt*, *k* is the convection heat transfer coefficient, A_s is the surface area through which convection heat transfer takes place, T_s is the surface temperature and T_∞ is the ambient steady temperature through which heat is transferred. It is also

known that the thermal resistance R for convective heat transfer is 1/(kA) and incorporating the parameters for this system, the equation 2.1-1 for sample becomes

$$\frac{dq_s}{dt} = \frac{(T_f - T_s)}{R} \tag{2.2-2}$$

where T_f is the heat source temperature from the furnace and T_s is the measured sample temperature by the thermocouple at the carrier. Similarly for reference side the governing equation is:

$$\frac{dq_r}{dt} = \frac{(T_f - T_r)}{R} \tag{2.1-3}$$

It is assumed that $R = R_{sample} = R_{reference}$ as the crucibles are made of the same material. Rearranging and subtracting equation 2.1-3 from 2.1-2 provides with the equation for the change in temperature.

$$\Delta T = T_s - T_r = R \cdot \left(\frac{dq_s}{dt} - \frac{dq_r}{dt}\right) \tag{2.1-4}$$

It is necessary to incorporate the expressions for heat capacity into the equations for which it should be noted that as the furnace heats the surroundings of the carrier, it convectively heats the sample crucible as well as the carrier base where the thermocouples are mounted. For sake of simplicity, it is assumed that no thermal events occur in the sample carrier. Then, the relation of the changes in temperature at the sample side can only be incorporated to the heat capacity of the carrier under the sample crucible (C_{sc}) and heat capacity of the sample and crucible (C_s) which can be expressed in equation form as [38]:

$$\frac{dq_s}{dt} = C_s \cdot \frac{dT_s}{dt} + C_{sc} \cdot \frac{dT_{sc}}{dt} \tag{2.1-5}$$

Similarly, the reference side governing equation is

$$\frac{dq_r}{dt} = C_r \cdot \frac{dT_r}{dt} + C_{rc} \cdot \frac{dT_{rc}}{dt} \tag{2.1-6}$$

As can be seen in Figure 2.1.1, the sample carriers are incorporated in one carrier and made of one material, the single structure is assumed to have the same heat capacity ($C_{sc} = C_{rc}$). It is assumed that no thermal events occur in the sample carrier. The sample carrier contains a material of interest while the reference crucible is empty; therefore the heat capacities of the sample and reference crucibles are not the same ($C_s \neq C_r$). Also, due to the furnace being the source of heat and assuming a uniform heating rate, $\left(\frac{dT}{dt} = \frac{dT_s}{dt} = \frac{dT_r}{dt}\right)$, subtracting equation 2.1-6 from 2.1-5 and equating it to equation 2.1-4, the equation for the measured values within the heat flux differential scanning calorimeter shown in Figure 2.1.1 becomes:

$$T_s - T_r = R \cdot \frac{dT}{dt} \cdot (C_s - C_r) = \Delta T \qquad (2.1\text{-}7)$$

As stated earlier T_s and T_r in the equation 2.1-7 represent the measured values of the reference and sample crucibles. dT/dt represents the heating rate from the furnace and R is the thermal resistance of the instrument. Thus, the expression shows that the difference in temperature is directly controlled by the difference in specific heats of the empty reference crucible and heat capacity of the sample with the material of interest. The experimental accumulation of the data set and with respect to equation 2.1-7 provides a trace or a graph typically known as a thermal profile. As the reference crucible is empty while the sample crucible holds the material of interest and as both the sample and reference crucible are made of the same material, the change in the thermal profile comes from the effective difference in specific heat value of the material of interest and the events within the material of interest. A schematic thermal profile can be seen in Figure 2.1.3. The profile consists of a heating and a cooling curve that is affected by the predetermined heating rate and cooling rate. The schematic profile displays the melting and solidification thermal events within the material of interest.

Some of the characteristic features of such a thermal profile are shown in Figure 2.1.4. T_i represents the initial peak temperature while T_f represents the final peak temperature. T_{io} and T_{fo} represent the initial and final onset thermal events that are calculated by extrapolated tangent line to the peak and baseline on respective sides. T_p represents the peak temperature where highest energy absorption or desorption takes place.

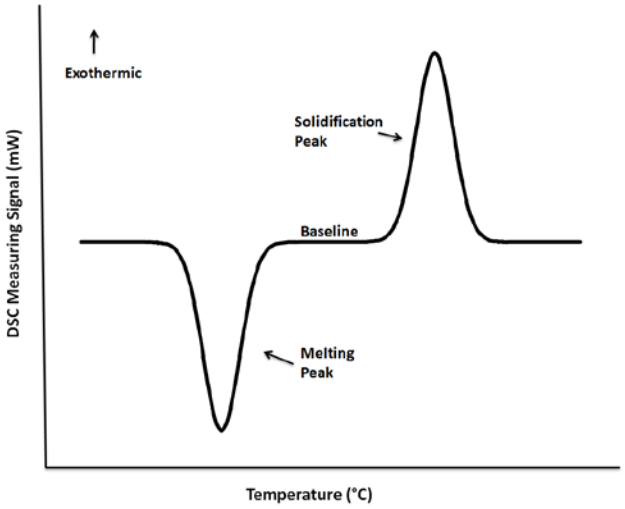

Figure 2.1.3: Schematic DSC thermal profile

In a heat flux differential scanning calorimeter, as the thermocouples are bonded directly below the crucibles, some amount of thermal resistance between the thermocouples and the crucibles is observed [38]. But, as these thermocouples are located outside the crucibles, the thermal resistance depends only on instrumentation and not on the material of investigation or any thermal events occurring within the material of investigation. Thermal resistance is a temperature dependent value and thus a calibration needs to be carried out in order to minimize the noise induced by the measurement signal due to these thermal resistances. In order to calibrate the equipment for the value of thermal resistance, standard pure metals with known melting point and enthalpy of melting are measured in the differential scanning

calorimeter. The selection of these pure reference materials is based on the temperature range that is required for additional experimentation of different material combination systems. These materials are processed multiple times in order to get more precise data sets for the melting points and enthalpy of melting. As the differential temperature is known, the heating rate is known and the specific heat of the standard materials is known, it allows calculation of the thermal resistance with equation 2.1-7. The values of reference sample material are compared to standard theoretical values and the results are considered to be acceptable if the tolerance is ±3% of the theoretical values [39].

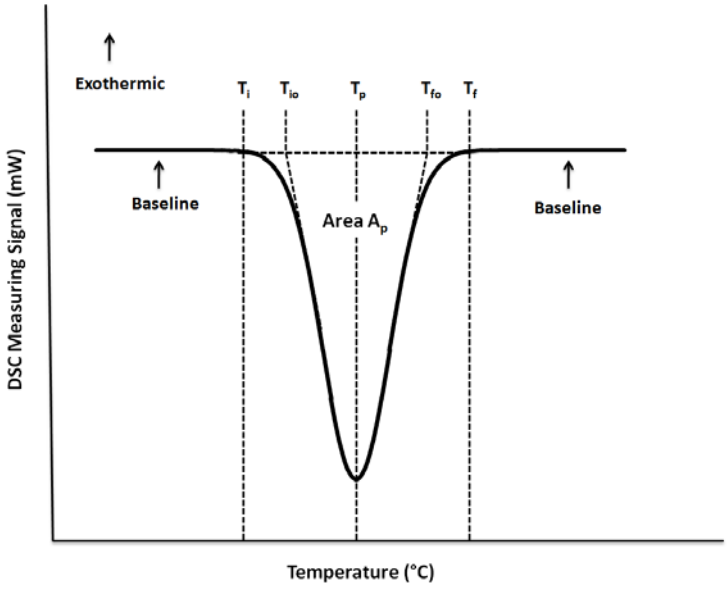

Figure 2.1.4: DSC thermal profile's characteristic features [38]

When a DSC is coupled with the appropriate software, measurement signal obtained as voltage is then filtered and adjusted to the signal by the calibration for the signal. The signal which is mainly controlled by the specific heats of C_s and C_r respectively forms a baseline in the thermal profile. Any thermal events such as phase transformation due to the heating and cooling of the material of interest or any reactions within the material is recorded on the thermal profile as a deviation from the

base line. This energy that is recorded is either exothermic or endothermic. Typically, before a material of interest is investigated, a correction file [39] is run in the differential scanning calorimeter to record any thermal changes of the sample and reference crucibles as well as to record any noise created by machine effects, crucible or the carrier during the thermal profile desired for the material at interest. Thus, for good baseline stability, the correction file is subtracted from the sample file automatically in the analysis software. Enthalpy of transition for phase transformation due to increase or decrease in thermal energy or for a specific phase transformation can be obtained by integrating the area between the initial and final onset temperatures within a thermal profile.

The area (A_p) bound by the baseline and initial and final onset temperature is proportional to the mass of the material of interest as well as the actual enthalpy of transition (ΔH) during heating or cooling [38]. The governing equation is:

$$A_p \propto m \cdot \Delta H \quad \text{or} \quad A_p = K \cdot m \cdot \Delta H \tag{2.1-8}$$

where K is the enthalpy calibration constant obtained experimentally and m is the mass of the material of interest. Equation 2.1-8 can be rearranged to find the expression for ΔH. The percent of melting or solidification can thus be provided by the equation [40]:

$$\Delta H_{\%} = \left[\frac{\Delta H_{meas}}{w_{element} \cdot \Delta H_{element}}\right] \cdot 100\% \tag{2.1-9}$$

where ΔH_{meas} is the measured enthalpy from the area of the exotherm or endotherm, $w_{element}$ is the weight fraction of the element of interest and $\Delta H_{element}$ is the theoretical enthalpy of the element of interest.

The area (A_p) required in equation 2.1-8 is obtained by integration of the exotherm or the endotherm and requires a horizontal baseline. However, in most cases, the thermal profile does not result in a horizontal baseline and thus, correction methods have to be employed in order to compensate for the baseline shift. Figure 2.1.5 shows a few baseline correction methods [40]. These methods include (i) linear method, (ii) tangential sigmoidal method, (iii) horizontal sigmoidal method, (iv) horizontal left method and (v) horizontal right method of integration.

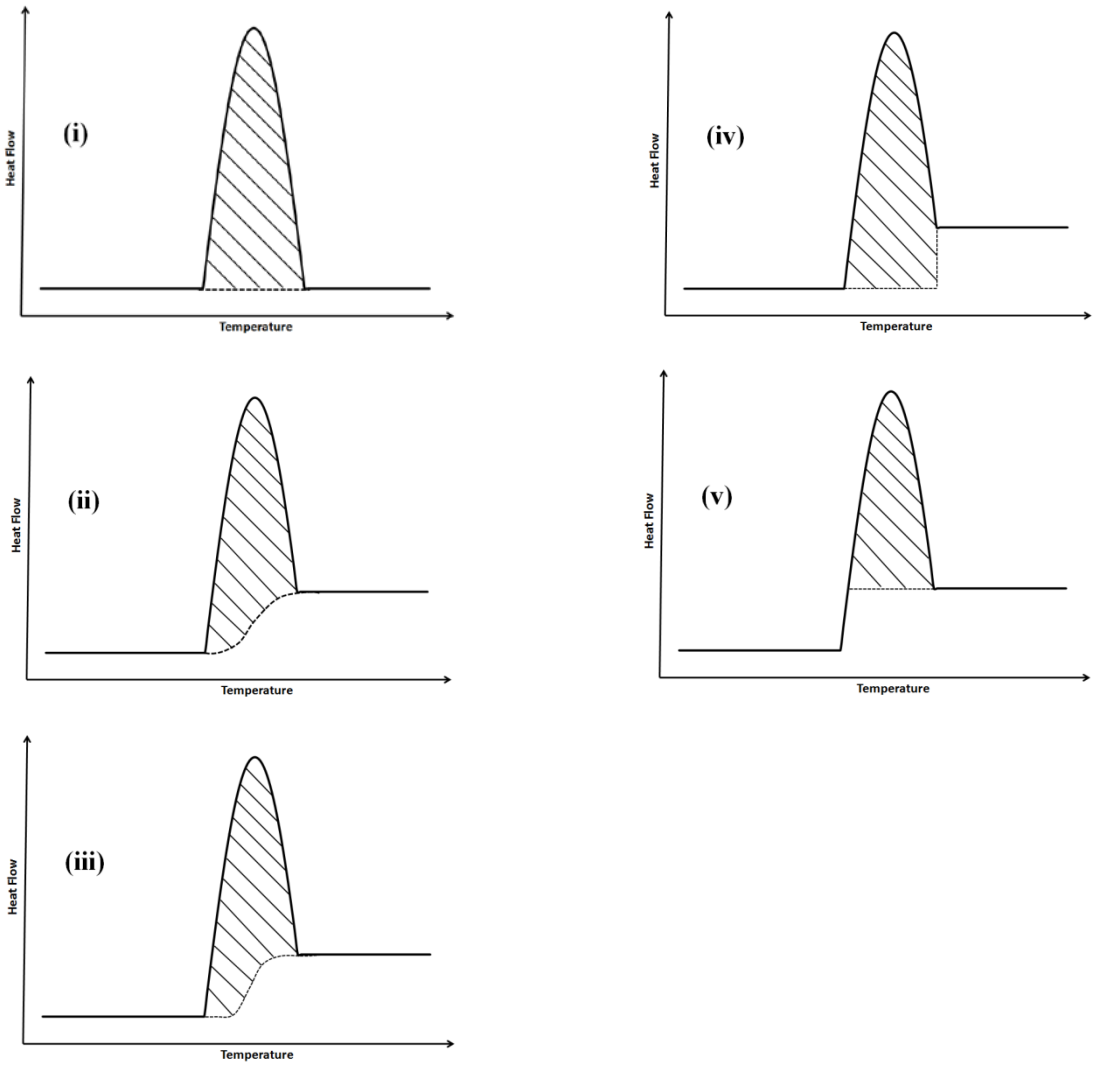

Figure 2.1.5 Baseline correction methods [40]

2.2 Using Differential Scanning Calorimetry to measure TLP processing

A comprehensive description of the differential scanning calorimeter instrumentation can be found in the previous section. Although, theoretical models [24, 26] exist, it is necessary to understand how differential scanning calorimeter is used to measure the kinetics within the transient liquid phase bonding or sintering process. Experimental investigation using DSC can be found in the work of various authors [27, 41, 42, 43, 44] but an excellent understanding of the results obtained from using the differential scanning calorimeter can be found in the work of Corbin and Lucier [45]. In order to measure solidification, it is necessary to compare the enthalpy of formation while melting as well as while solidification. The idea is that if melting and solidification behaviour of a system can be observed repeatedly over time, it is possible to measure and predict the time that is required for the liquid phase to dissipate to form a solid transient bond otherwise known as homogenization. Due to the heating and melting of the eutectic liquid, some amount of interlayer would alloy with the base solid to form an alloy which has higher melting temperature due to a concentration shift. However, if the time is cut short and the system is cooled, the non isothermally solidified liquid would solidify upon cooling (e.g. through eutectic reaction). When the joint is reheated, this eutectic phase would re-melt. By measuring the reduction in the area under the peak and confirming that the solidification peak on the first cycle is the same as the melting peak of the system during reheating, one can conclude that some amount of eutectic liquid was isothermally solidified during each thermal cycle event. Thus, if this cycle is repeated again and again (Figure 2.2.1a), time can be measured when the liquid volume fraction is lost due to isothermal solidification. The total time can only be represented when the interlayer is in liquid

form thus ignoring solid state interactions. The time recorded is from the onset of eutectic liquid melting to the time unreacted liquid solidifies in each cycle. Adding all the time fractions and calculating the percentage eutectic liquid remaining gives the experimental data plotted in Figure 2.2.1b with respect to the models derived from Crank solutions, etc.

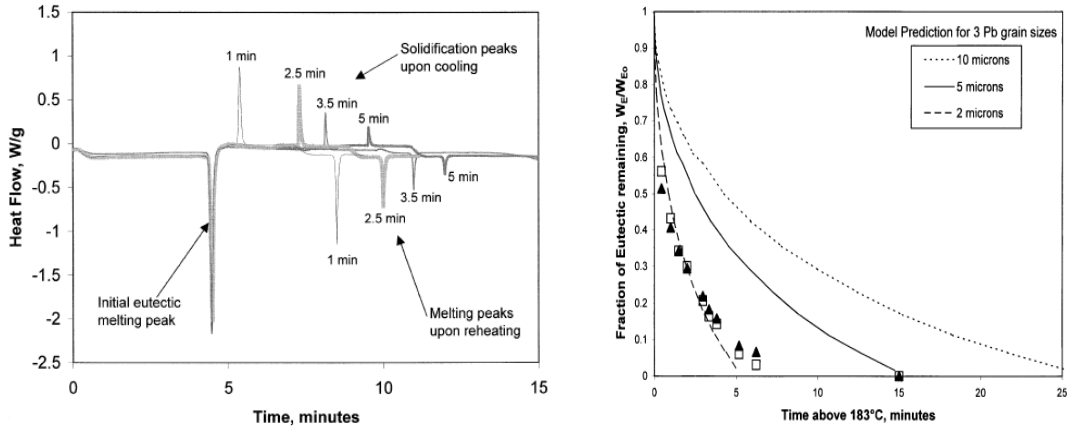

(a) **(b)**

Figure 2.2.1: (a) DSC thermal trace for a repeated thermal cycle event, (b) Comparison between data obtained from DSC (experimental) and the modified Crank solution (model) [45]

DSC has not only been used to measure the phase transformations or measuring the time required for the liquid fraction to dissipate into base metal but also for various other studies including metallurgical study of joint evolution presented in this work. WU-Yu-Feng et al. [44] used non-isothermal differential scanning calorimetry to measure the synthesis kinetics of Mg_2Sn in Mg-Sn powder mixture. A 95:5 ratio of 99.9% pure metals was mixed and pressed at approximately 20 MPa and heated to temperatures of 798°K, 813°K, 828°K and 843°K in inert Argon atmosphere. The microstructural evolution in that study can be referenced in Figure 2.2.2. It can very clearly be seen that interactions between the magnesium and tin particles increase with a rise in temperature. Also, the synthesis of Mg_2Sn appears

to be increasing for the first three temperature sets. As the temperature increases a eutectic Mg+Mg_2Sn phase can be seen developing at temperature of 843°K. These phase transformations were recorded in DSC traces and used to calculate the activation energy for Mg_2Sn to be 281.7 kJ/mol.

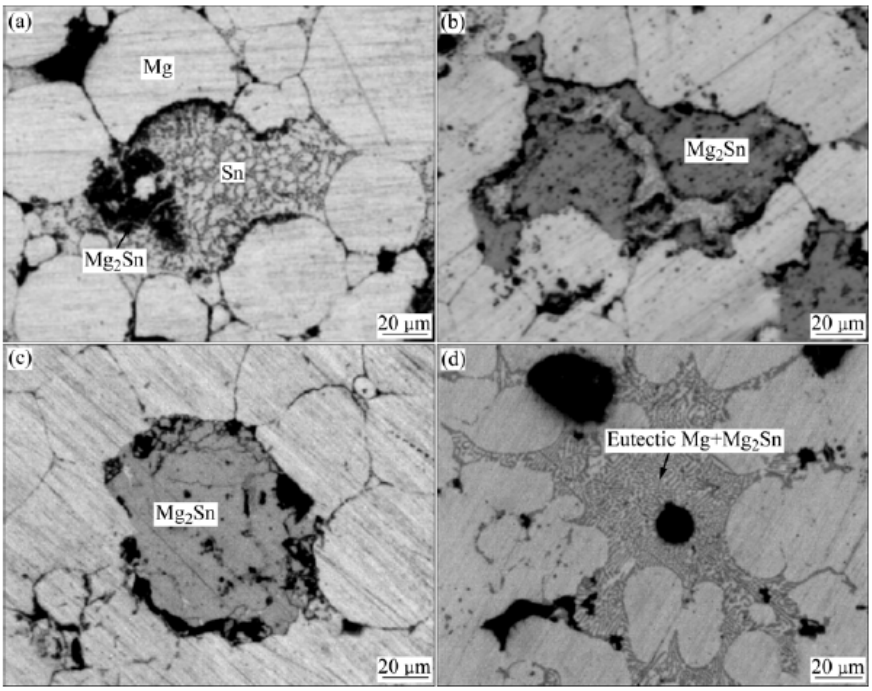

Figure 2.2.2: Microstructures of samples quenched at different temperatures: (a) 798°K, (b) 813°K, (c) 828°K and (d) 843°K [44]

Another excellent example of using the differential scanning calorimetry to study metal bonding can be seen in the work of T.D'Hondt and Corbin [43]. The authors present a systematic evolution of the transient liquid phase joint through a DSC trace which has been referenced in Figure 2.2.3. The stages presented in Section 1.2 can be related to the trace. A very interesting microstructure evolution at temperatures ranging from 150°C to 260°C has also been presented in the study. Using DSC analysis, eutectic solidification enthalpies at various temperatures were also experimentally derived. Formation of intermetallic phases and exothermic peaks associated with the interaction in the DSC thermal profile had been briefly noted and

explained by the authors. Also, how the compositional shift in the mixed powder during the heating cycles results into long range solidification is indicated in this study.

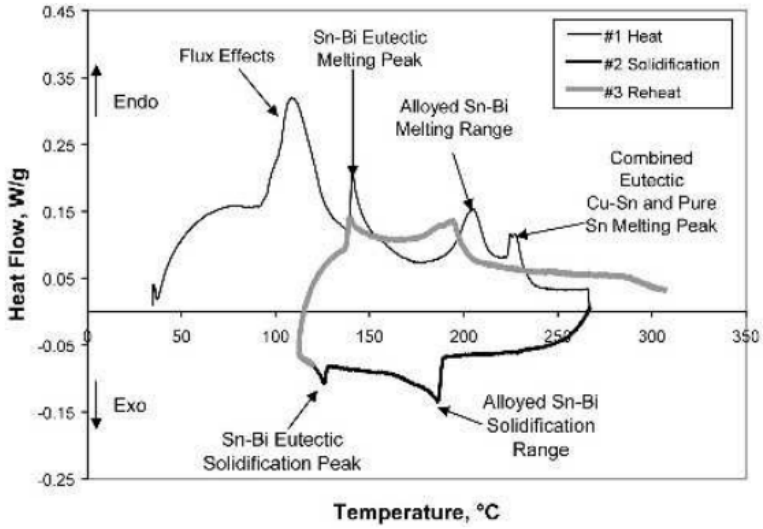

Figure 2.2.3: The DSC trace of the full heating cycle for Cu-45 wt% Sn-5% Bi, with coarse Cu powder and 15-min hold time [43]

A major focus of the current work is to adapt and extend the DSC techniques described above to study Mg based joining (i.e. soldering and brazing).

3.0 Experimental methods

Differential Scanning Calorimetry (DSC) (using a NETZSCH PEGASUS 404C DSC) was the main experimental technique used in this study. However, sample preparations, microstructural characterization using SEM and EDX analysis, wetting tests and plating were also used in this study.

3.1 Zinc Immersion Plating

Pure Mg and Mg Alloys form a tenacious oxide layer on the surface which causes a colour change from metallic to matte grey indicating a macroscopically uniform layer of the oxide [46].

In light of the concept joint proposed in Section 1.4, an attempt was made to limit the continuous oxide layer formation through the development of Zinc plating on Pure Mg and Mg Alloy base plates. It was anticipated that this would prevent the formation of MgO and, any ZnO formation could be reduced by a wettable molten metal or flux such that Sn or Sn-9Zn filler metal could be used in the joining process.

Overall plating on magnesium has been summarized in three methods [47] as:

1) Electroplating over an immersion Zinc coating
2) Direct electroplating with Nickel
3) Plating with electroless Nickel

However, the intention in this study is to take advantage of Zinc plating by using Sn based filler metals. In summary, the Zinc immersion process uses the following steps [47]:

1) Surface conditioning
2) Activation
3) Zinc Immersion

Using the cumulative information provided by Zhu et al. [48], Chen et al., [49] and ASM international [50], numerous experimental sets were performed using various chemicals and processes in an attempt to recreate the plating results as can be referenced from the following Figure 3.1.1

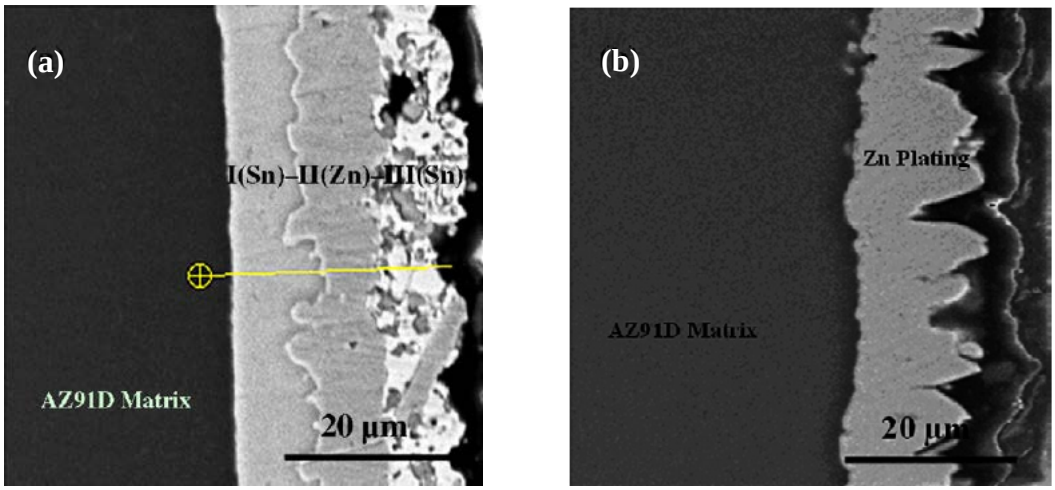

Figure 3.1.1: (a) Cross-section image of Zn-Sn coating on Mg Alloy, (b) Cross-section image of Zn coating on Mg Alloy [48]

The plating results documented by the above references could not be achieved in the current study. Comparing the results and review papers [46, 47, 48, 49, 50, 51, 52, 53] as well as the experimental results obtained (not shown here), it was concluded that proprietary chemicals or processes were not identified in the above references and thus recreating the results would require further research into plating which was out of the scope of this work.

After further industrial survey, Millennium Plating Co. [54] from Massachusetts agreed to perform research grade proprietary plating without revealing the plating process. The plated Zn was tested and cross section examined. Investigations, which will be presented in more detail in Chapter 4 revealed that significantly better wetting between the filler metals and the Zn immersion plated Pure Mg and Mg Alloy samples occurred.

3.2 Initial Experiments

It was further necessary and required to investigate the wetting properties between the Zn layer and Sn based filler metals under flux and fluxless conditions. Dimethylamine (DMA) and Tacky Flux (both organic acid based fluxes) were used to observe interaction, spreading and wetting properties of Sn on a Zn foil. Using both fluxes, it was noted that a uniform bonded interface was achieved with the Sn layer being transformed to approximate Sn-Zn eutectic level (Figure 3.2.1a & b) through dissolution with the base Zn metal. Also, from the literature [23] it is known that a wetting angle of 0° to 90° is acceptable; zero being perfect spreading. It was noted that the Sn layer forms an approximate angle of about 30° (Figure 3.2.1b). It was therefore concluded that, with a Zn immersion coating on Mg in place, Sn based filler metals should exhibit good wetting.

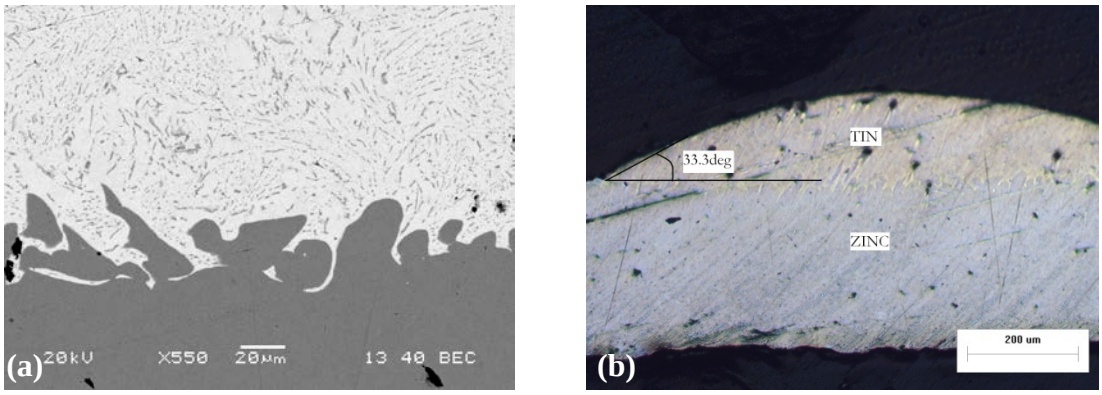

Figure 3.2.1: (a) Sn wetting on Zn foil test with Tack flux, (b) Wetting angle measurement

3.3 Raw Materials

The powders used for preparing the filler metal samples for this study were Pure Sn, Eutectic Sn-9Zn, Pure Mg and Pure Zn. While plates (or foils) used were Pure Mg, Mg Alloy, Pure Sn and Pure Zn. Details about the raw materials used during the study are summarized in the Table 3.3.1. Each material was checked in SEM and EDX analyses were performed to confirm the specifications provided by the respective supplier. SEM micrographs of these powders can be found in Appendix I. EDX analyses confirmed all manufacturer specifications. Also, DSC thermal profiles for Sn and Sn-9Zn can be referred to from Figure 3.3.1

Table 3.3.1: Raw materials [55, 56]

Name	Size	Type	Purity	Manufacturer
Sn	-325 mesh	Powder	99.8% metals basis	Alfa Aesar
Zn	-140+325 mesh	Powder	99.9% metals basis	Alfa Aesar
Mg	-100+200 mesh	Powder	99.6% metals basis	Alfa Aesar
Sn-9Zn	-325 mesh	Powder	Sn:Zn; 91.2:8.8 wt %	AM&M
Mg	1mm thickness	Foil	99.9% metals basis	Alfa Aesar
Mg Alloy	N/A	Foil	Mg:Al:Zn; 96:3:1wt %	Alfa Aesar
Sn	3.2 mm thickness	Foil	99.85% metals basis	Alfa Aesar
Zn	0.62 mm thickness	Foil	99.9% metals basis	Alfa Aesar

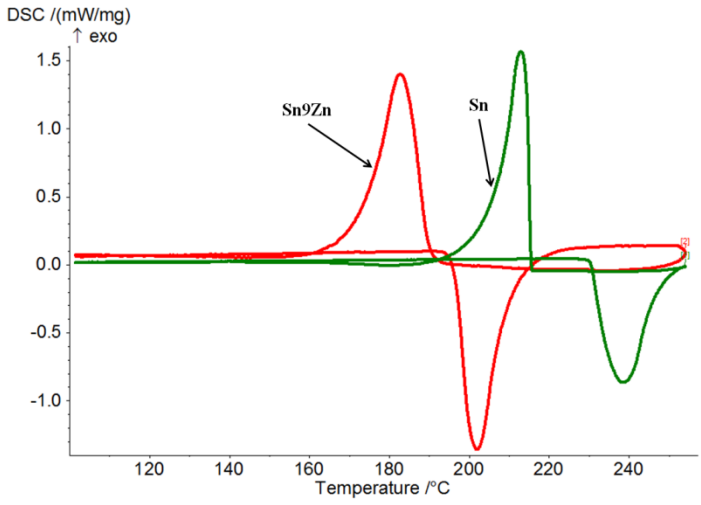

Figure 3.3.1: DSC graphs for Pure Sn and Sn-9Zn powders

3.4 Filler/Base Metal Couple Preparation

Preparation of the samples was carried out in a custom made die depicted in Figure 3.4.1. All plate and powder samples followed one technique while powder presses followed another technique. No organic flux was added since preliminary work indicated a strong and detrimental reaction with Mg.

Powders were stored in an inert gas glove box and introduced in air environment for a brief period of time for mixing by weight percent. The powders were then contained in a small jar with an Argon environment and milled for approximately 2 hours in order to achieve complete mixing and limit contamination from the atmosphere. The powders were then used for sample preparation technique as following:

The plate samples were mounted according to the following steps:

1. Using a punching press, a disc was punched from the Zn immersion coated Mg Plate (or Mg Alloy Plates) such that the Zn immersion coated side faced down, away from the “punched” surface.
2. The disc was press fit into the die cavity of Figure 3.4.1, Part 5. Note: some excess material removal around the edges of the punched disc was sometimes necessary in order the fit the disc into the 3/16” diameter die cavity.
3. The powder was introduced into the die cavity from top of the die on the unaltered Zn plating side slowly using a scale to control the amount added.
4. The die cavity was then introduced into an ultrasonic bath in a dry environment for 2 minutes to allow the powder to evenly distribute over the top of the base metal disc. This was necessary since only a limited and

controlled amount of powder was added to the die to control the weight fraction of the filler/base metal couple.

5. The die was then assembled and placed in a hand press with a calibrated pressure gauge.
6. The pressure was introduced and kept at approx. 1000 psi and maintained for a brief period of time. Slight reduction in pressure was sometimes noted due to the powder compaction; however, the process was continued until the applied pressure was steady.

The powder samples were prepared according to following steps:

1. Portion of the die (Parts 4-7 from Figure 3.1.4) were assembled such that Part 5 facing up would allow introduction of powders.
2. Using a modified pipette drip to be used as a funnel, powders were introduced in the die cavity to avoid powder deposition on the inside walls of Part 5 due to static forces.
3. The die was then assembled and placed in a hand press with a calibrated pressure gauge.
4. The pressure was introduced and kept at approx. 1000 psi and maintained for a brief period of time. Slight reduction in pressure was sometimes noted due to the powder compaction; however, the process was continued until the applied pressure was steady.

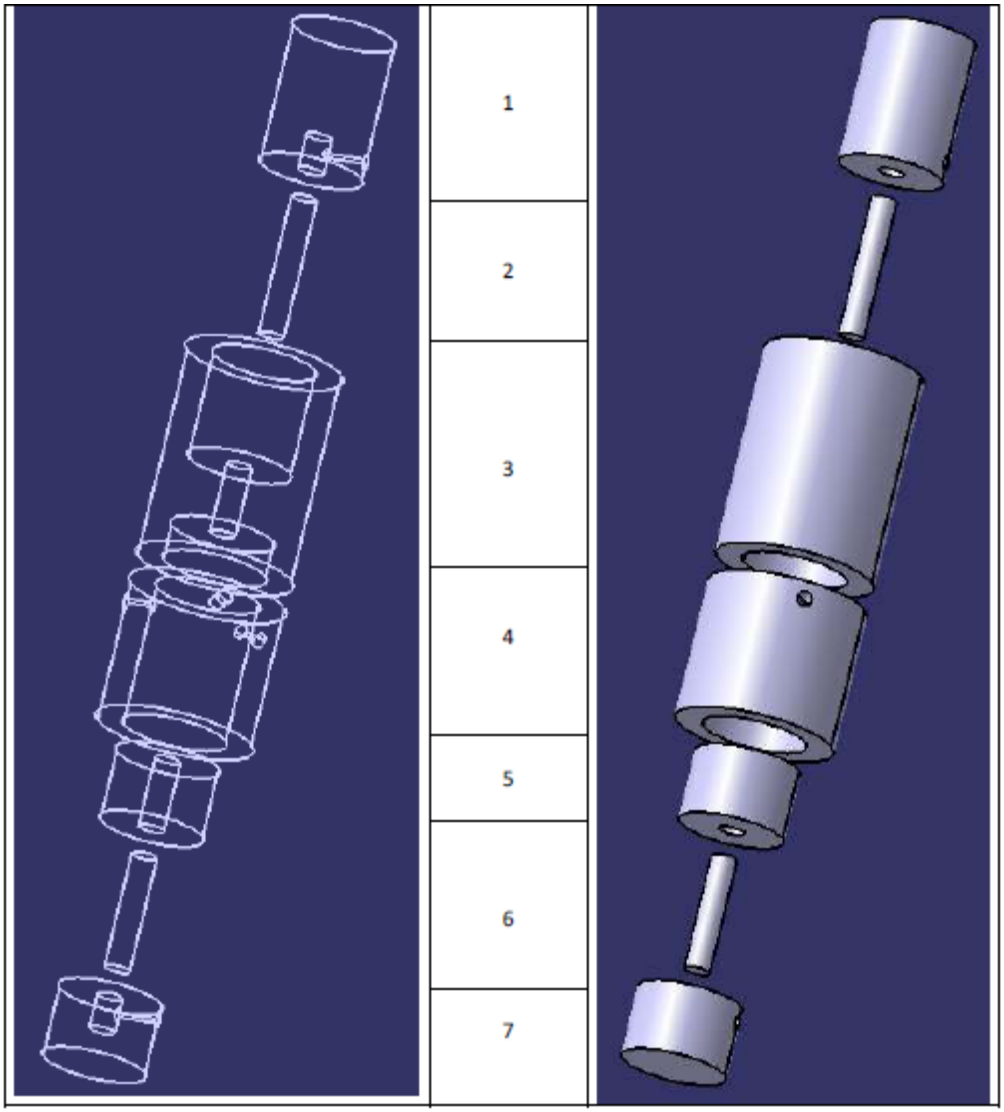

Figure 3.4.1: Sample preparation die (Note: Part 5 & 6 represents the location where the sample is placed and pressed)

3.5 Temperature Profiles

The Netzsch [57] software available with the DSC instrument used for this study allows the user to program a desired thermal cycle. The thermal rate was optimized to be 10°C/min for heating and cooling purposes at or under 250°C while heating at 10°C/min and cooling at 5°C/min for samples at or over 350°C. The thermal cycles used during experiments are summarized in the Tables 3.5.1 - 3.5.3

Table 3.5.1: Cyclic Temperature at 250°C

Segment	Process	Hold time
-	Start Temperature (20°C)	-
1	Heat to 250°C (10°C/min)	-
2	Cool to 120°C (10°C/min)	-
3	Heat to 250°C (10°C/min)	-
4	Isothermal	1h
5	Cool to 120°C (5°C/min)	-
6	Heat to 250°C (5°C/min)	-
7	Isothermal	3h
8	Cool to 120°C (5°C/min)	-
9	Heat to 250°C (5°C/min)	-
10	Isothermal	3h
11	Cool to 120°C (5°C/min)	-
12	Heat to 250°C (5°C/min)	-
13	Isothermal	3h
14	Cool to 25°C (5°C/min)	-

Table 3.5.2: Cyclic Temperature at 350°C

Segment	Process	Hold time
-	Start Temperature (20°C)	-
1	Heat to 250°C (10°C/min)	-
2	Cool to 120°C (10°C/min)	-
3	Heat to 350°C (5°C/min)	-
4	Cool to 120°C (5°C/min)	-
5	Heat to 350°C (5°C/min)	-
6	Isothermal	2h
7	Cool to 120°C (5°C/min)	-
8	Heat to 350°C (5°C/min)	-
9	Isothermal	2h
11	Cool to 120°C (5°C/min)	-
12	Heat to 350°C (5°C/min)	-
13	Isothermal	2h
14	Cool to 25°C (5°C/min)	-

Table 3.5.3: Cyclic Temperature at 450°C

Segment	Process	Hold time
-	Start Temperature (20°C)	-
1	Heat to 250°C (10°C/min)	-
2	Cool to 120°C (10°C/min)	-
3	Heat to 450°C (5°C/min)	-
4	Cool to 120°C (5°C/min)	-
5	Heat to 450°C (5°C/min)	-
6	Isothermal	30 min
7	Cool to 120°C (5°C/min)	-
8	Heat to 450°C (5°C/min)	-
9	Isothermal	30 min
10	Cool to 25°C (5°C/min)	-

3.6 Sample Preparation after DSC Testing

In order to examine the cross sections of samples after DSC testing, all samples were mounted in an epoxy resin (Streurs Specifix-20) which is a room temperature cold-mount epoxy. All samples followed the same preparation technique as follows:

1. All samples were held in plastic clip and then cold mounted using Specifix-20 epoxy.
2. Samples were then introduced in vacuum to extract the air bubbles from the epoxy as well as to allow epoxy to reach the sample surface completely. This step was followed by a 24 hour curing time to allow epoxy to solidify.
3. Samples were then systematically taken through P320, P800, P2000, P4000 ISO grit silicon carbide grinding papers with isopropyl alcohol as a lubricant to avoid corrosion on magnesium surface due to water with each sample introduced into ultrasonic bath (isopropyl alcohol) for cleaning after each grit step.
4. Polishing was then performed using 9µm, 6µm, 3µm, 1µm and 1/4µm diamond suspension for water sensitive products along with using alcohol based lubricant (Struers DP-lubricant yellow, brown) on soft polishing cloth with each sample introduced into ultrasonic bath (isopropyl alcohol) for cleaning after each polishing step.
5. The sample cross sections were then analysed in a JEOL JSM-840 Scanning Electron Microscope. The chemical compositions were also analysed using a Oxford systems energy dispersive x-ray spectrometry (EDX).

3.7 Sample Numbering

For ease of reading and referencing, all samples referred to in this work follow a numbering system:

A.B.C - (D)Mg - E - F - G - H

Where,

A – Chapter Number

B – Section Number

C – Numeric Sample Number

D – Indicates if the base metal is Pure Mg or Mg Alloy with a designation of (P) for Pure and (A) for Mg Alloy.

E – Filler metal composition in wt% (example: Sn9Zn refers to 91wt%Sn – 9wt%Zn)

F – Temperature in °C

G – Hold time at peak temperature in minutes or CYL if the sample undergoes a cyclic heating profile.

H – If necessary, will indicate F for Full Cell with extension R if the sample is reheated.

Example:

4.2.24 – (P)Mg - Sn9Zn- 350 - 30 – FR, refers to a Pure Mg based metal / Sn-9Zn eutectic filler metal couple which was heated to 350°C and held at that temperature for 30 minutes. The sample was a full cell which was reheated.

4.0 Experimental results

4.1 Experimental results for Joining Mg using Sn Filler Metal

Theoretically, it should be possible to join Mg-Mg couple with Pure Sn as a filler metal at 231.5°C if wetting conditions are met. Upon completion of initial wetting experiments as described in Chapter 3.0 & in reference to the concept joint proposed in Chapter 1.4; initial experiments with Mg/Sn were performed at a temperature (235°C), slightly higher than the melting temperature of Sn (231.5°C) and at different hold times to evaluate microstructural evolution on route to isothermal solidification of the joint. These tests are summarized in Table 4.1.1. The testing involved Pure Sn/Zn coated Pure Mg and Pure Sn/Zn coated Mg Alloy couples where samples were made using the technique described in Chapter 3.0. The DSC thermal profiles can be referred to from Figures 4.1.1 and 4.1.2. A prominent shift in lowering the onset solidification temperature during cooling was noted. The extent of this onset shift depended on the hold time at peak heating temperature. At short hold times, the onset temperature of solidification of the filler metal began in the range of 222°C to 227°C. However, at longer times the onset temperature stabilized to a temperature of ~198°C for both couple types.

Table 4.1.1: Experiments with Sn Filler metal at 235°C

Sample ID.	Base Metal	Maximum Testing Temperature	Hold Time
4.1.1-(P)Mg-Sn-235-0	Zn Plated Pure Mg	235°C	0 min
4.1.2-(P)Mg-Sn-235-1	Zn Plated Pure Mg	235°C	1 min
4.1.3-(P)Mg-Sn-235-5	Zn Plated Pure Mg	235°C	5 min
4.1.4-(P)Mg-Sn-235-15	Zn Plated Pure Mg	235°C	15 min
4.1.5-(P)Mg-Sn-235-60	Zn Plated Pure Mg	235°C	60 min
4.1.6-(A)Mg-Sn-235-0	Zn Plated Mg Alloy	235°C	0 min
4.1.7-(A)Mg-Sn-235-1	Zn Plated Mg Alloy	235°C	1 min
4.1.8-(A)Mg-Sn-235-5	Zn Plated Mg Alloy	235°C	5 min
4.1.9-(A)Mg-Sn-235-15	Zn Plated Mg Alloy	235°C	15 min
4.1.10-(A)Mg-Sn-235-60	Zn Plated Mg Alloy	235°C	60 min

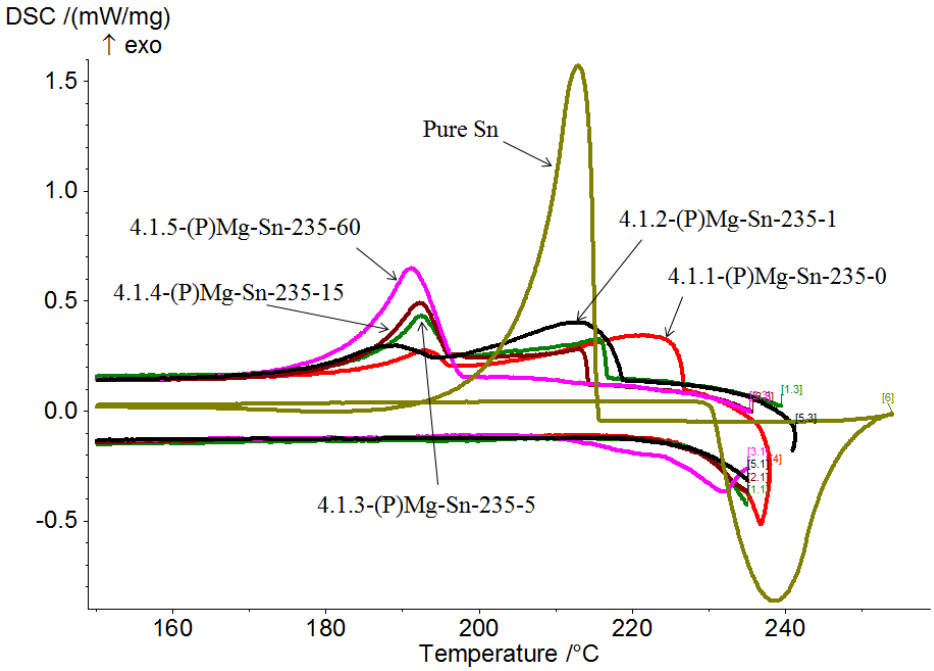

Figure 4.1.1: DSC thermal profiles for Zn Plated Pure Mg with Sn filler metal at 235°C (Hold times: 0, 1, 5, 15, and 60 minutes respectively)

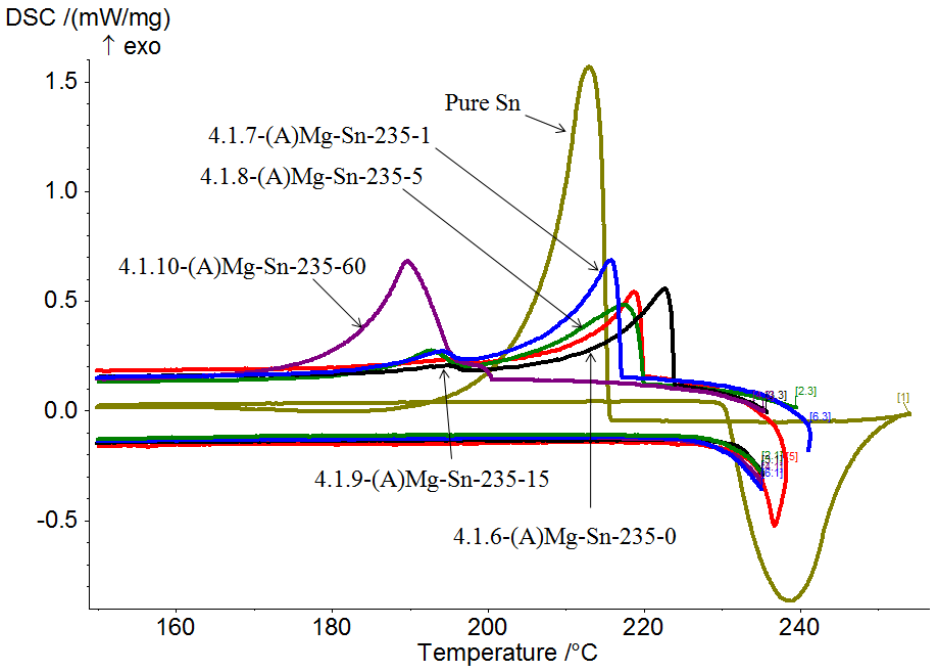

Figure 4.1.2: DSC thermal profiles for Zn Plated Mg Alloy with Sn filler metal at 235°C (Hold times: 0, 1, 5, 15, and 60 minutes respectively)

Comparing the DSC profiles in Figure 4.1.1 and Figure 4.1.2, the decrease in the solidification peak onset to ~198°C and comparison to Pure Sn DSC thermal profile, signifies increasing metallurgical interactions between the filler and base metal. This is noted to be more gradual with the Mg Alloy samples than in Pure Mg samples. The SEM micrographs for the samples referred to in Table 4.1.1 can be referenced from Figure 4.1.3 and 4.1.4.

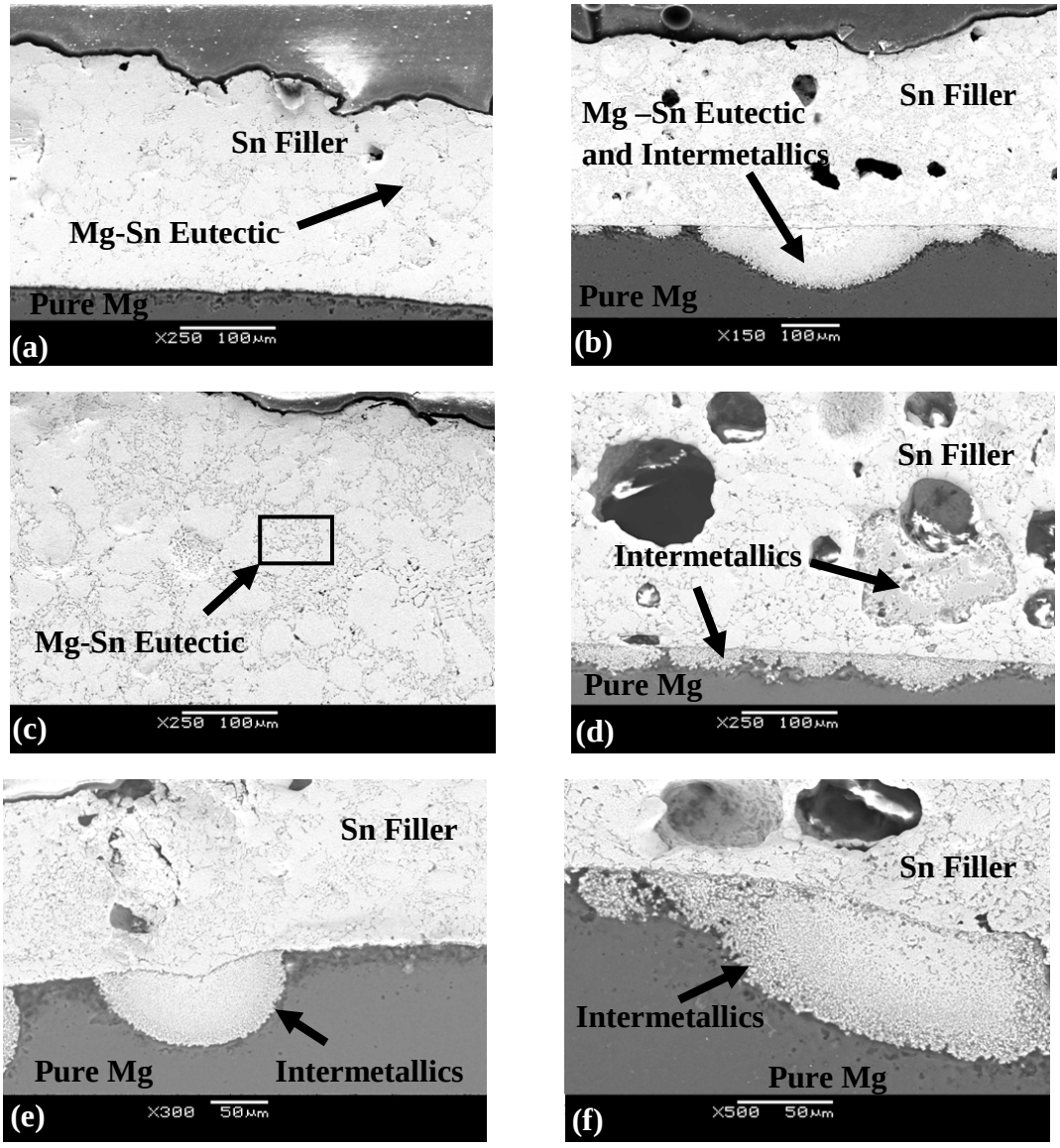

Figure 4.1.3: SEM Micrographs for samples (a) 4.1.1-(P)Mg-Sn-235-0, (b) 4.1.2-(P)Mg-Sn-235-1, (c) 4.1.2-(P)Mg-Sn-235-1, (d) 4.1.3-(P)Mg-Sn-235-5, (e) 4.1.4-(P)Mg-Sn-235-15 and (f) 4.1.5-(P)Mg-Sn-235-60

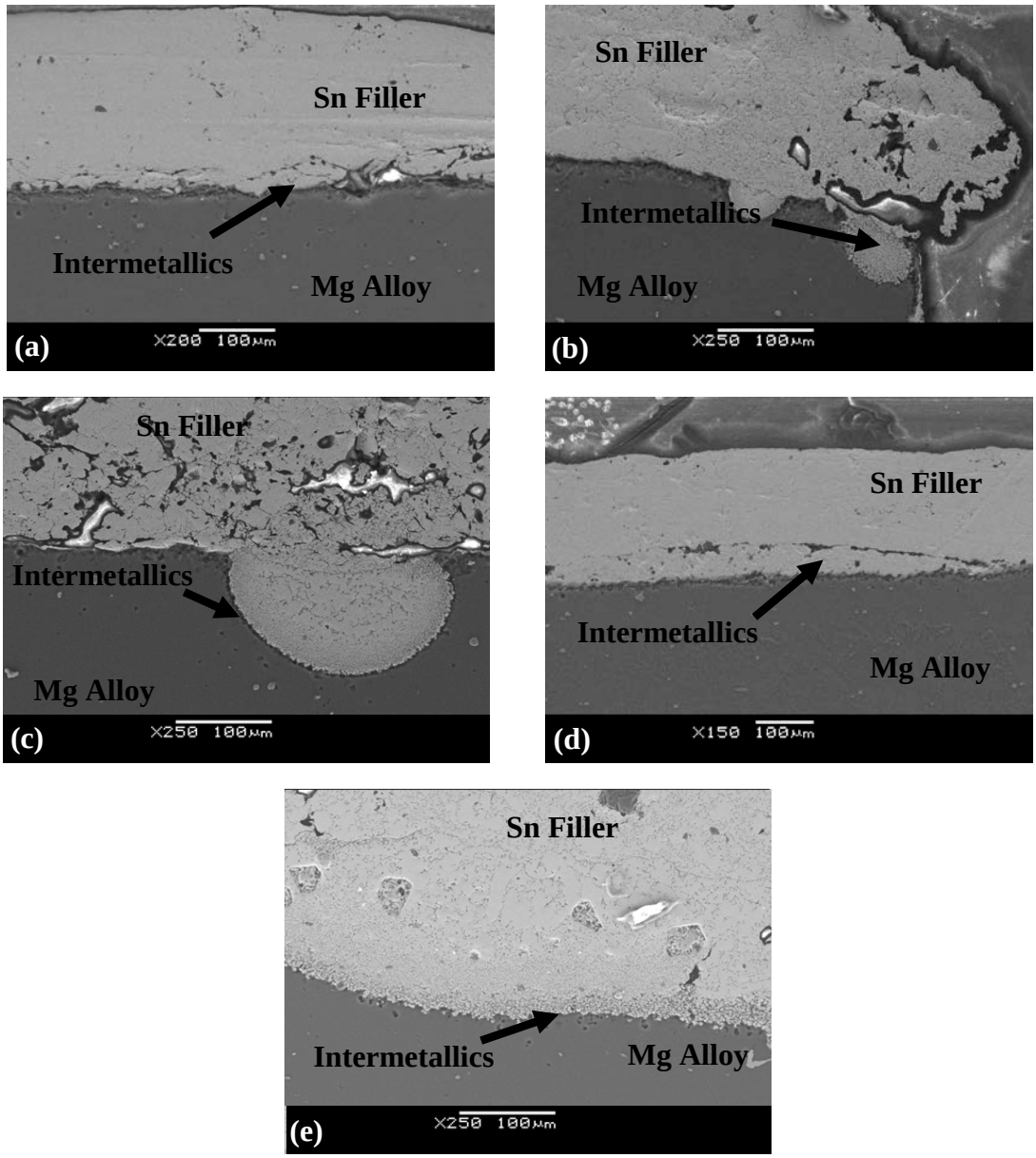

Figure 4.1.4: SEM Micrographs for samples (a) 4.1.6-(A)Mg-Sn-235-0, (b) 4.1.7-(A)Mg-Sn-235-1, (c) 4.1.8-(A)Mg-Sn-235-5, (d) 4.1.9-(A)Mg-Sn-235-15 and (e) 4.1.10-(A)Mg-Sn-235-60

From SEM images, an incremental growth in intermetallics is observed from 0 min to 60 min hold time in the Pure Mg samples (4.1.1-(P)Mg-Sn-235-0 to 4.1.5-(P)Mg-Sn-235-60). Mg-Sn eutectic composition was measured at the particle boundaries in the pressed powder joint geometry. The Mg Alloy system was noted to

behave in a similar fashion as the Pure Mg system with respect to the intermetallic growth and eutectic Mg-Sn composition with increasing time. From the DSC thermal profiles, there does appear to be a slight decrease in the solidification peak onset temperature in Mg Alloy samples than Pure Mg samples however, noticeable quantities of Zn or Al from the dissolution of the alloy base metal were absent in the EDX analysis and microstructure.

Due to thermal lag within the DSC, it broadens a melting endotherm by a few degrees. This resulted in incomplete development of a melting peak in the DSC traces heated to 235°C (Figures 4.1.1 and 4.1.2). It was found that heating to 250°C allowed a full melting endotherm to be measured which was absent in profiles at 235°C. Thus, experiments were performed at 250°C with various hold times at the peak melting temperature. The set has been summarized in Table 4.1.2. The DSC thermal profiles can be referenced from Figures 4.1.5 and 4.1.6. In both DSC thermal profiles; a significant change in solidification peaks were not noticed suggesting the initial reactions for joint formation to have completed. Solidification onset for Pure Mg samples appears to be ~198°C while that for Mg Alloy to be ~195°C regardless of the hold times.

Table 4.1.2: Experiments with Sn Filler metal at 250°C

Sample ID.	**Base Metal**	**Maximum Testing Temperature**	**Hold Time**
4.1.11-(P)Mg-Sn-250-0	Zn Plated Pure Mg	250°C	0 min
4.1.12-(P)Mg-Sn-250-15	Zn Plated Pure Mg	250°C	15 min
4.1.13-(P)Mg-Sn-250-30	Zn Plated Pure Mg	250°C	30 min
4.1.14-(A)Mg-Sn-250-0	Zn Plated Mg Alloy	250°C	0 min
4.1.15-(A)Mg-Sn-250-15	Zn Plated Mg Alloy	250°C	15 min
4.1.16-(A)Mg-Sn-250-30	Zn Plated Mg Alloy	250°C	30 min

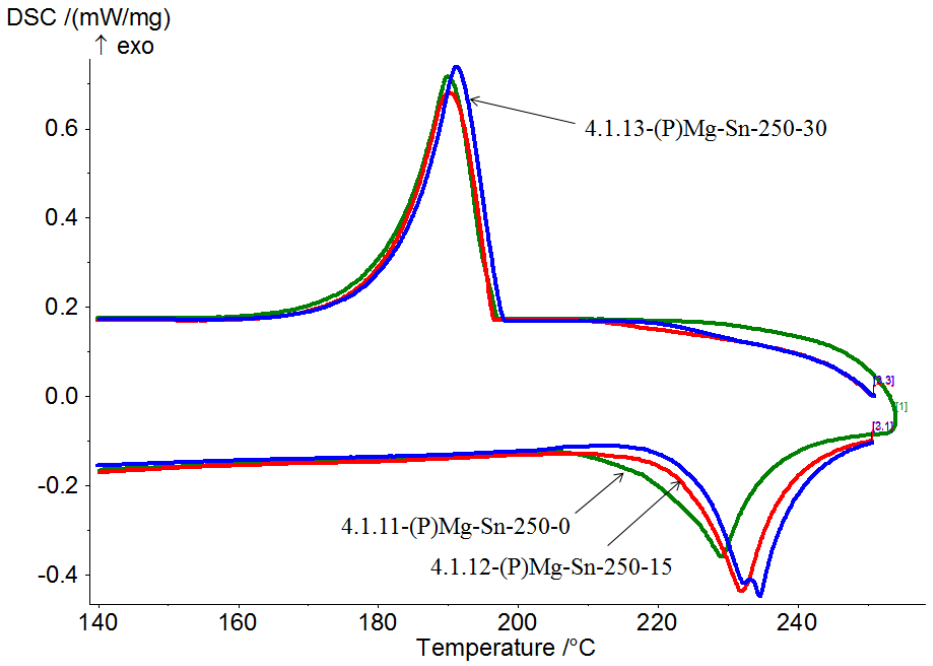

Figure 4.1.5: DSC thermal profiles for Zn Plated Pure Mg with Sn filler metal at 250°C (Hold times: 0, 15, and 30 minutes respectively)

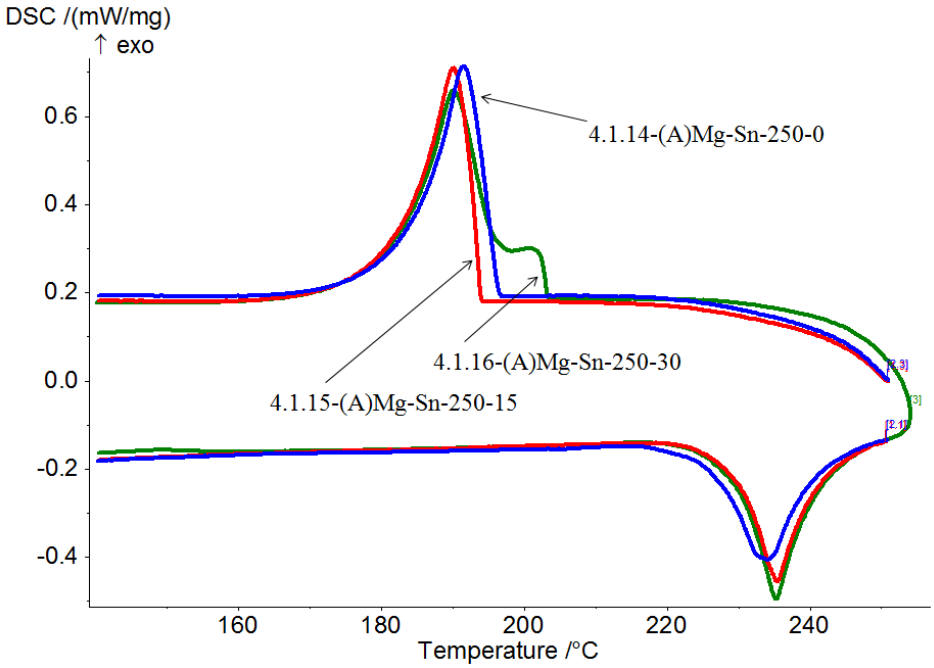

Figure 4.1.6: DSC thermal profiles for Zn Plated Mg Alloy with Sn filler metal at 250°C (Hold times: 0, 15, and 30 minutes respectively)

In sample 4.1.16, there does appear to be a solidification onset at higher temperature before consistent solidification peaks are observed suggesting certain amount of unreacted Sn. Comparing the DSC thermal profiles of Figures 4.1.1 and 4.1.2 with 4.1.5 and 4.1.6, it is clear that the formation of a stable solidification behavior is more rapid at 250°C. This increased temperature allows full melting of the filler metal and a more rapid metallurgical bond including dissolution of the base metal into the liquid filler metal.

SEM micrographs for the same set can be referred to from Figures 4.1.7 and 4.1.8. Continued diffusion of Sn into the Mg base metal slows down due to rapid intermetallic formation at the faying surfaces delaying isothermal solidification as evident from the DSC thermal profiles as well. This intermetallic layer is evident from the SEM images in Figure 4.1.7 and 4.1.8. A gradual and clear growth of intermetallics can be seen in increasing order with increasing hold time. Mg Alloy system appears to be behaving in a similar manner with respect to the intermetallic growth and; it is evident that a bond formation is a success. Evidence of Mg-Sn eutectic liquid is present at the particle boundaries of the powder Sn filler joint.

In all previous samples, symmetry was used to evaluate the microstructural evolution. In order to keep using this symmetry joint (half joint); it is of utmost importance to evaluate and compare results of full joint to half joint samples. Thus, complete geometry testing cells were prepared and experimented upon. These tests are summarized in Table 4.1.3. Zn Plated Pure Mg/Sn (4.1.17-(P)Mg-Sn-250-0-F) and Zn Plated Mg Alloy/Sn (4.1.19-(A)Mg-Sn-250-0-F) were heated once up to 250°C and then reheated to study if there is a shift in melting onset to prove metallurgical interaction.

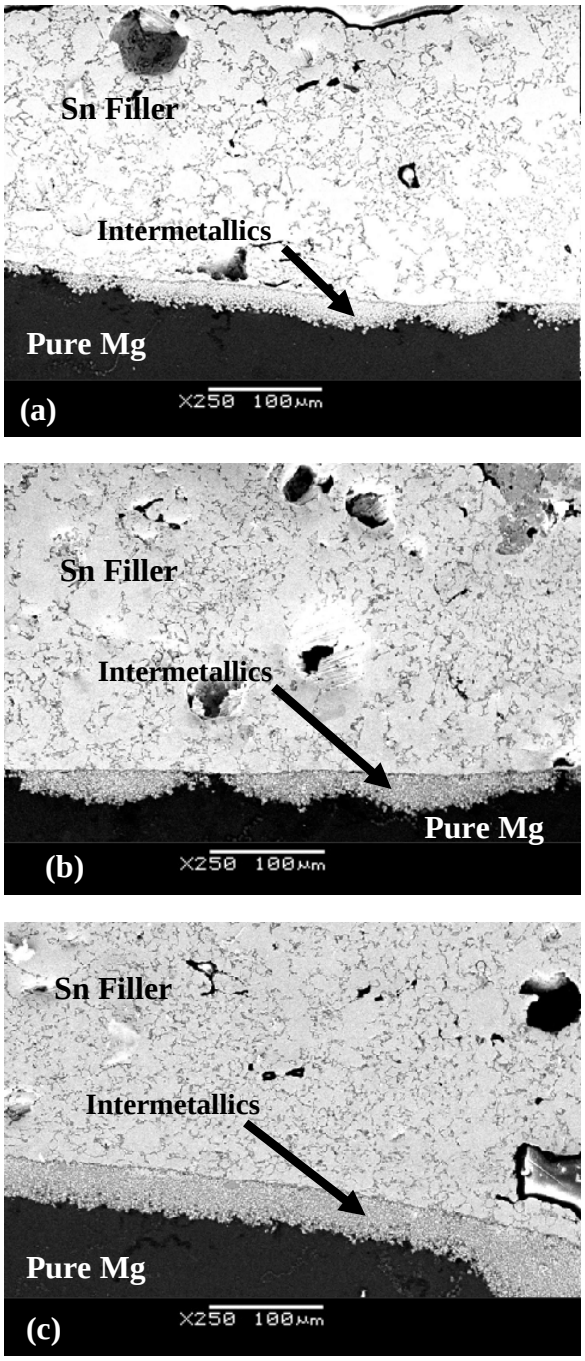

Figure 4.1.7: SEM Micrographs for samples (a) 4.1.11-(P)Mg-Sn-250-0, (b) 4.1.12-(P)Mg-Sn-250-15 and (c) 4.1.13-(P)Mg-Sn-250-30

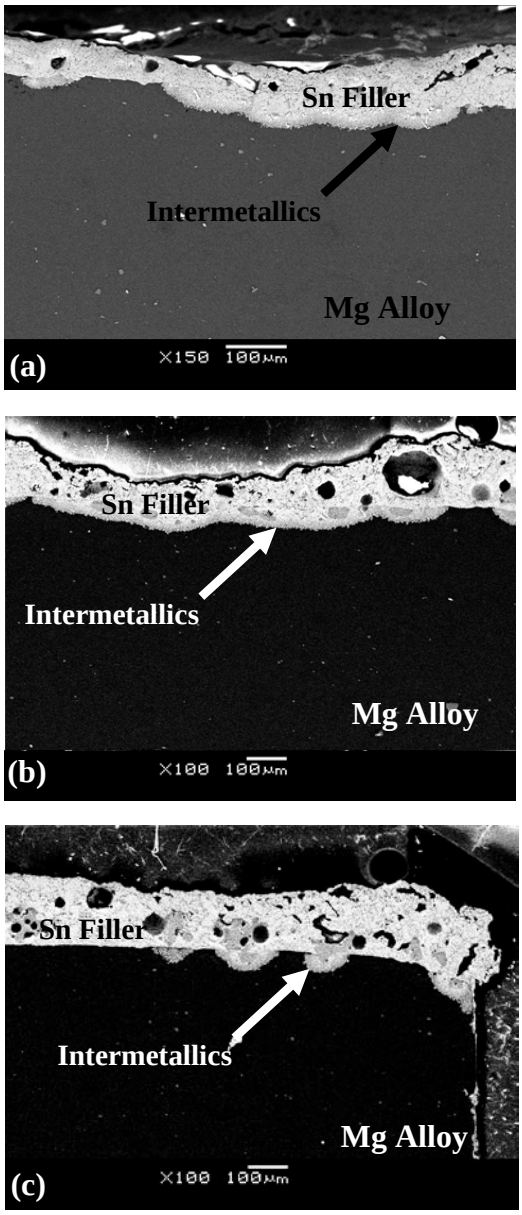

Figure 4.1.8: SEM Micrographs for samples (a) 4.1.14-(A)Mg-Sn-250-0, (b) 4.1.15-(A)Mg-Sn-250-15 and (c) 4.1.16-(A)Mg-Sn-250-30

Table 4.1.3: Experiments with Sn Filler metal Full Cell at 250°C

Sample ID.	Base Metal	Maximum Testing Temperature	Hold Time
4.1.17-(P)Mg-Sn-250-0-F	Zn Plated Pure Mg	Full Cell	No Hold
4.1.18-(P)Mg-Sn-250-0-FR	Reheat 4.1.17	Full Cell	No Hold
4.1.19-(A)Mg-Sn-250-0-F	Zn Plated Mg Alloy	Full Cell	No Hold
4.1.20-(A)Mg-Sn-250-0-FR	Reheat 4.1.19	Full Cell	No Hold

The DSC thermal profiles for Pure Mg and Mg Alloy Full cell samples can be referred from Figure 4.1.9. Complete melting of the filler metal can be noted with an increase in the area under the melting peak for both Pure Mg sample (4.1.17-(P)Mg-Sn-250-0-F) and Mg Alloy (4.1.19-(A)Mg-Sn-250-0-F) samples during reheats (4.1.18-(P)Mg-Sn-250-0-FR & 4.1.20-(A)Mg-Sn-250-0-FR). Solidification peak onsets for first heats and reheats are consistent for both Pure Mg and Mg Alloy samples at ~195°C. With information presented here, it can be observed that metallurgical interactions occur and liquid widening stabilizes during the first heat cycle. Thus, DSC thermal profiles point to the fact that successful bonding occurs for both samples.

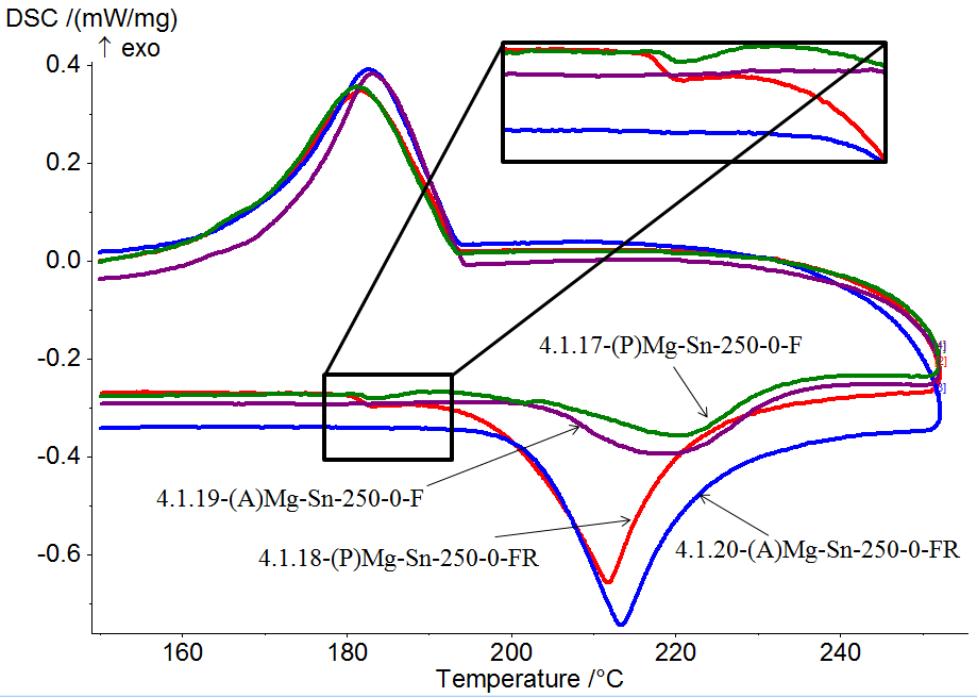

Figure 4.1.9: DSC thermal profiles for Zn Plated Pure Mg with Sn filler metal ; Full Cell at 250°C

It should also be further noted from sample 4.1.17-(P)Mg-Sn-250-0-F that ternary melting onset (~183°C) is observed on first melting cycle suggesting to interactions between Zn from Zn plated Mg proving the effectiveness of the Zn layer which helps reducing the oxide layer and promote good metallurgical bond at temperatures as low as ~183°C. The reheat thermal profiles of Figure 4.1.9 also indicate a melting point downshift of the filler metal from ~231°C indicative of pure Sn melting, to ~ 203°C indicative of a Sn-Mg eutectic filler composition. Note that the ternary melting observed initially is present upon reheat. This indicates that the initial Zn coating facilitated initial melting and shifts filler metal to a low overall composition. The SEM images for samples from Tables 4.1.3 can be referred to from Figure 4.1.10.

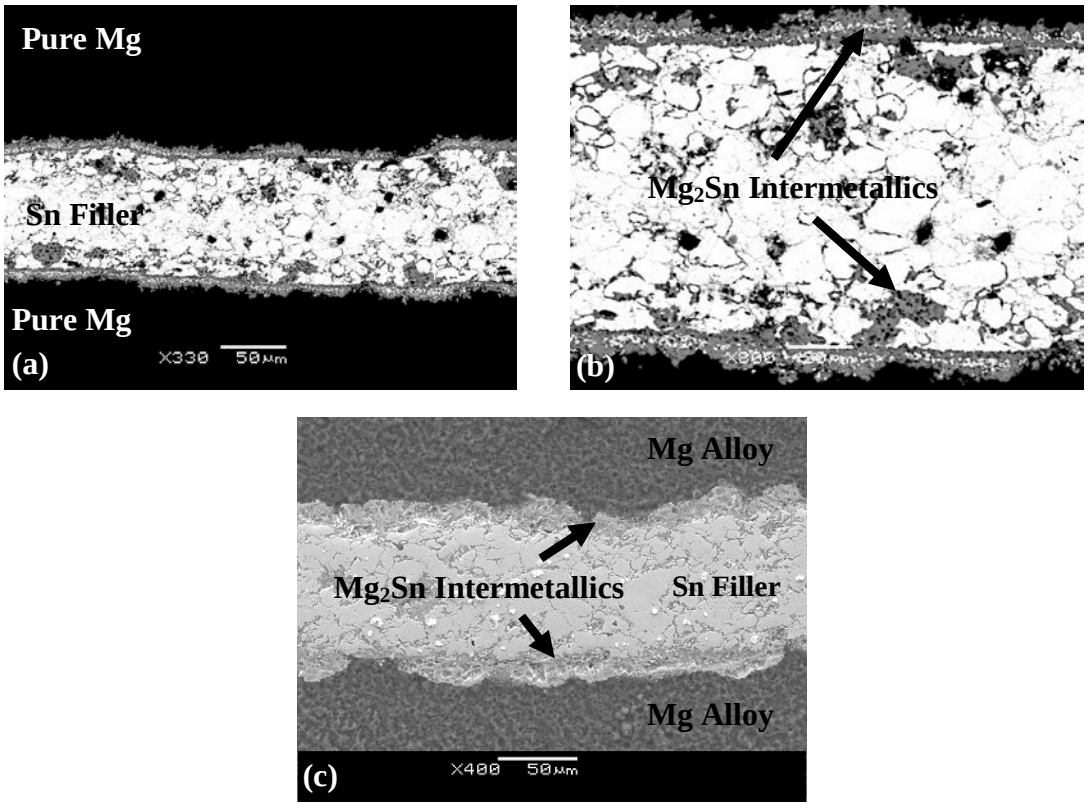

Figure 4.1.10: SEM Micrographs for samples (a & b) 4.1.17-(P)Mg-Sn-250-0-F; 4.1.18-(P)Mg-Sn-250-0-FR and (c) 4.1.19-(A)Mg-Sn-250-0-F; 4.1.20-(A)Mg-Sn-250-0-FR

SEM results confirm the DSC profile results, revealing a complete joint formation in the samples. Microstructure noted in Full Cell samples is symmetric at the bond centre line and consistent with the Half Cell microstructure observation from Figure 4.1.7 and 4.1.8. Thus samples tested hereon are all half cell joints. An excellent example of the joint produced in this study is noted from Zn Plated Pure Mg/Sn Filler sample at 250°C as can be referred to from Figure 4.1.10a. Intermetallic (Mg_2Sn) formation is noted at the base metal boundary with some Mg_2Sn growth into the filler metal layer. Mg_2Sn is also depressed throughout the filler layer which arises from the eutectic solidification reaction $L > (\beta Sn) + Mg_2Sn$.

Comparing the results found for Pure Mg and Mg Alloy samples at 235°C, 250°C (Half Cell) and 250°C (Full Cell), it can be noted that metallurgical interactions between the Sn filler metal and both type of base metals is evident regardless of the peak heating temperature. A more gradual equilibrium is reached at 235°C than at 250°C. Also, the peak solidification onset temperature approaches ~195°C regardless of the heating temperature and with increasing hold time at the respective temperatures. A ternary filler metal composition with a melting point at ~183°C also develops as is evident in DSC thermal profile of sample 4.1.17-(P)Mg-Sn-250-0-F. Significant growth of intermetallic layer at the interface is evident at 235°C, and 250°C however, in combination with consistent solidification thermal profiles suggest a stable system. Stable exothermic energy of solidification peaks further confirms that the intermetallic layer prevents or slows down further isothermal solidification. The Full Cell joint microstructure is symmetric

Thus, in order to determine if the intermetallic layer could be destabilized such that Sn diffusion and isothermal solidification could be accelerated, experiments were performed at 350°C and 450°C. From the binary Mg-Sn phase diagram, the

solubility of Mg in liquid Sn increases from approximately 2.1 wt% to 12 wt% in going from 203°C to 450°C. The purpose was to determine if this increase solubility led to increased dissolution of Mg_2Sn. These experiments are summarized in Table 4.1.4. Subsequently, the DSC thermal profiles can be referred from Figure 4.1.11 & 4.1.12.

Consistent solidification peak onset at ~195°C for Pure Mg samples while at ~198°C for Mg Alloy samples is noticed and is comparable with previous results for samples at 235°C and 250°C. A notable feature for DSC thermal profiles in Figures 4.1.12 and 4.1.13 are the exothermic peaks on heating curves noticed at temperatures above 300°C for Mg Alloy samples heated to 350°C and 450°C respectively. Pure Mg sample exhibits the exothermic peak on the heating curve only above 350°C. The exothermic peaks in the Mg Alloy samples are thought to occur due to an increased Zn and Al content in the base metal. Previous work on other reactive liquid phase systems [18, 25] has indicated that liquid formation often triggers an exothermic reaction by enhancing contact between reactants (in this case between Sn and Mg). However, the actual melting event is often not recorded as a separate peak on the DSC thermal profile. It is proposed that a melting event in the region of the Mg-Zn eutectic reaction (i.e. 340°C), but modified by the presence of Sn and, in the case of the Mg Alloy also by presence of Al, facilitates an increase rate of Mg_2Sn formation. This leads to the exothermic peaks above 300°C. The presence of Al and additional Zn in the alloy sample leads to melting and Mg_2Sn formation at lower temperatures. No solidification peak for any additional phases is noted in thermal profiles for both systems at 350°C and 450°C respectively during cooling. This indicates that dissolution of Zn or Al in the filler metal liquid is minor resulting in a Mg-Sn eutectic freezing event.

Table 4.1.4: Experiments with Sn Filler metal at 350°C and 450°C

Sample ID.	Base Metal	Maximum Testing Temperature	Hold Time
4.1.21-(P)-Mg-Sn-350-0	Zn Plated Pure Mg	350°C	0 min
4.1.22-(P)-Mg-Sn-450-0	Zn Plated Pure Mg	450°C	0 min
4.1.23-(A)-Mg-Sn-350-0	Zn Plated Mg Alloy	350°C	0 min
4.1.24-(A)-Mg-Sn-450-0	Zn Plated Mg Alloy	450°C	0 min

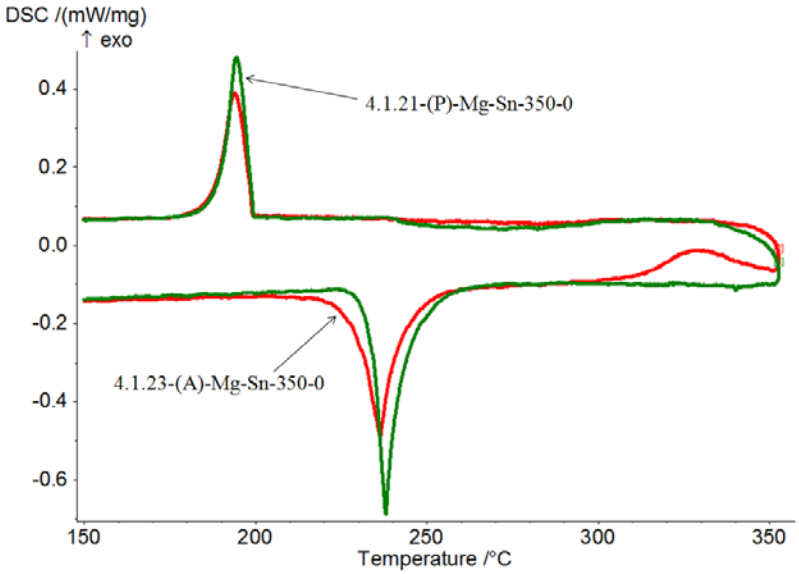

Figure 4.1.11: DSC thermal profiles for Zn Plated Pure Mg and Mg Alloy with Sn filler metal at 350°C

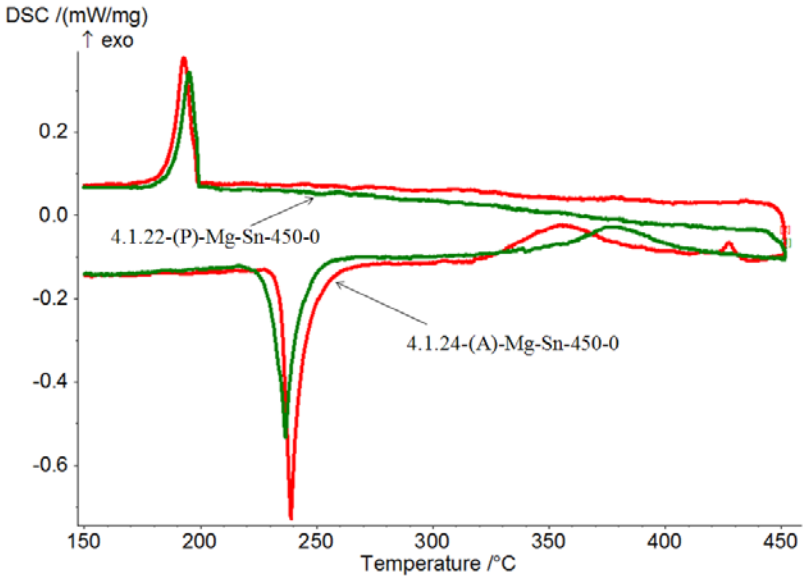

Figure 4.1.12: DSC thermal profiles for Zn Plated Pure Mg and Mg Alloy with Sn filler metal at 450°C

The SEM images for Pure Mg and Mg Alloy samples at 350°C and 450°C respectively can be referred from Figure 4.1.13. Debonding is noticed in samples at 350°C while 450°C samples for both Pure Mg and Mg Alloy system appears to have a good bond. Good bonding could be attributed to Mg-Zn forming liquid phase above ~342°C. Significant intermetallic growth can be seen in both systems at 350°C and 450°C. Mg_2Sn intermetallic is found in the joint microstructure however, evidence of any other phases as a result of Zn in the system is not conclusive. This may be due to Zn being in small quantities and not present in the cross sections evaluated. Therefore, further study to determine the role of Zn in joining Mg-Mg is presented in subsequent sections.

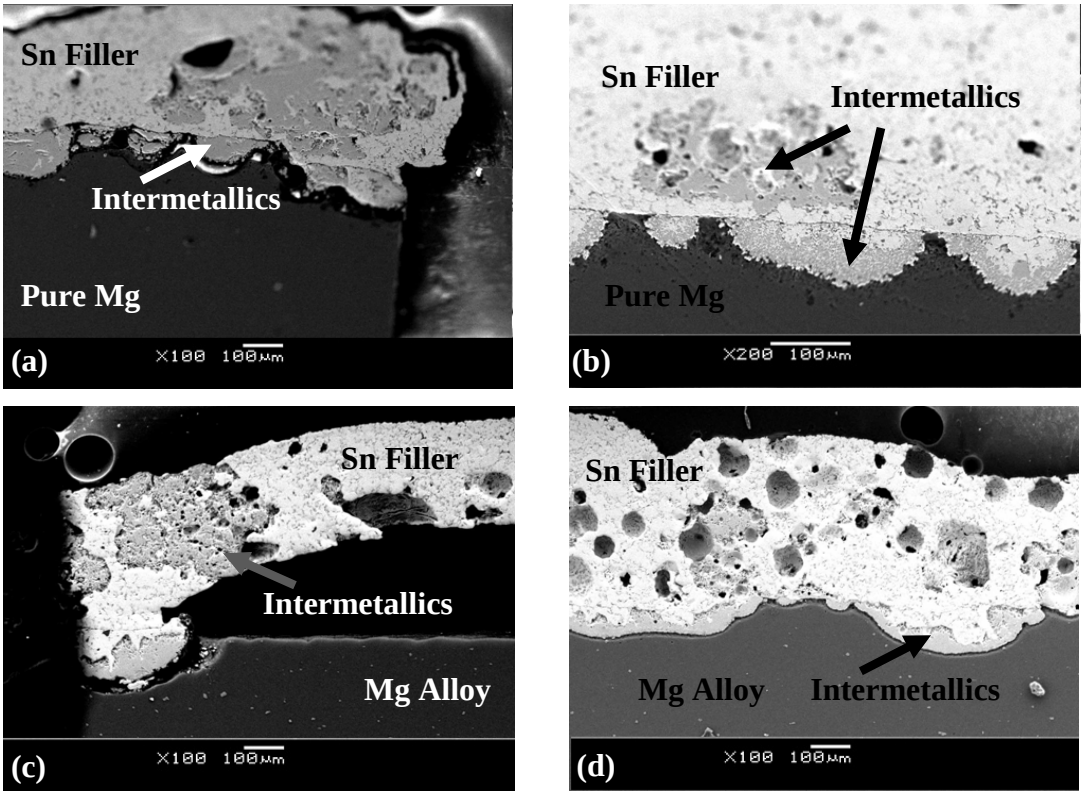

Figure 4.1.13: SEM Micrographs for samples (a) 4.1.21-(P)-Mg-Sn-350-0, (b) 4.1.22-(P)-Mg-Sn-450-0, (c) 4.1.23-(A)-Mg-Sn-350-0 and (d) 4.1.24-(A)-Mg-Sn-450-0

4.2 Experimental Results for Joining Mg using Sn-9Zn Eutectic Filler Metal

In continuation with the previous section, further experiments were carried out using a Sn-Zn based filler metal. In order to understand how the magnesium system interacts with the Sn-9Zn filler metal, initial experiments were carried out at a temperature (202°C), slightly above the melting temperature of Sn-9Zn filler metal (198.5°C). Table 4.2.1 summarizes the experiments performed near the melting temperature of the filler metal.

Table 4.2.1: Experiments using Sn-9Zn Filler metal at 202°C and 235°C

Sample ID.	Base Metal	Maximum Testing Temperature	Hold Time
4.2.1-(P)Mg-Sn9Zn-202-0	Zn Plated Pure Mg	202°C	0 min
4.2.2-(P)Mg-Sn9Zn-202-1	Zn Plated Pure Mg	202°C	1 min
4.2.3-(P)Mg-Sn9Zn-202-5	Zn Plated Pure Mg	202°C	5 min
4.2.4-(P)Mg-Sn9Zn-202-15	Zn Plated Pure Mg	202°C	15 min
4.2.5-(P)Mg-Sn9Zn-202-60	Zn Plated Pure Mg	202°C	60 min
4.2.6-(P)Mg-Sn9Zn-235-0	Zn Plated Pure Mg	235°C	0 min
4.2.7-(P)Mg-Sn9Zn-235-1	Zn Plated Pure Mg	235°C	1 min
4.2.8-(P)Mg-Sn9Zn-235-5	Zn Plated Pure Mg	235°C	5 min
4.2.9-(P)Mg-Sn9Zn-235-15	Zn Plated Pure Mg	235°C	15 min
4.2.10-(P)Mg-Sn9Zn-235-60	Zn Plated Pure Mg	235°C	60 min
4.2.11-(A)Mg-Sn9Zn-202-0	Zn Plated Mg Alloy	202°C	0 min
4.2.12-(A)Mg-Sn9Zn-202-1	Zn Plated Mg Alloy	202°C	1 min
4.2.13-(A)Mg-Sn9Zn-202-5	Zn Plated Mg Alloy	202°C	5 min
4.2.14-(A)Mg-Sn9Zn-202-15	Zn Plated Mg Alloy	202°C	15 min
4.2.15-(A)Mg-Sn9Zn-202-60	Zn Plated Mg Alloy	202°C	60 min
4.2.16-(A)Mg-Sn9Zn-235-0	Zn Plated Mg Alloy	235°C	0 min
4.2.17-(A)Mg-Sn9Zn-235-1	Zn Plated Mg Alloy	235°C	1 min
4.2.18-(A)Mg-Sn9Zn-235-5	Zn Plated Mg Alloy	235°C	5 min
4.2.19-(A)Mg-Sn9Zn-235-15	Zn Plated Mg Alloy	235°C	15 min
4.2.20-(A)Mg-Sn9Zn-235-60	Zn Plated Mg Alloy	235°C	60 min

In order to keep the results comparable with the previous section, the experiments were also performed near the melting temperature of Sn at 235°C. The

DSC thermal profiles for specimens summarized in Table 4.2.1 can be referenced through Figures 4.2.1 – 4.2.4.

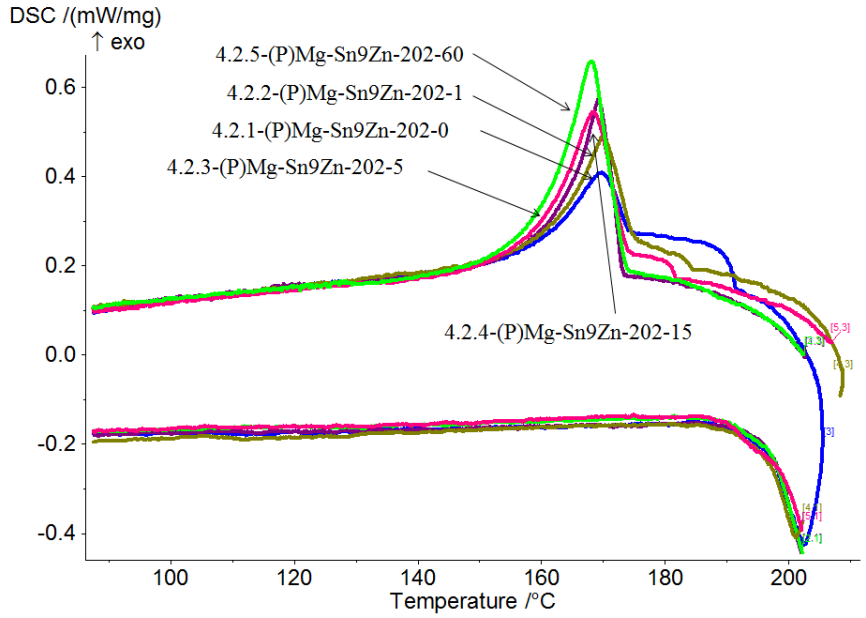

Figure 4.2.1: DSC thermal profiles for Zn Plated Pure Mg with Sn-9Zn filler metal at 202°C (Hold times: 0, 1, 5, 15, and 60 minutes respectively)

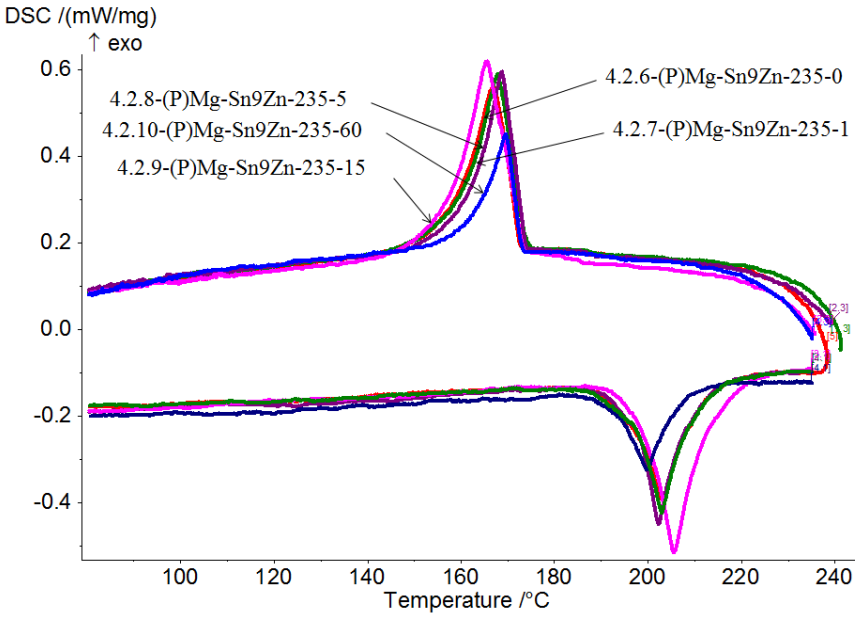

Figure 4.2.2: DSC thermal profiles for Zn Plated Pure Mg with Sn-9Zn filler metal at 235°C (Hold times: 0, 1, 5, 15, and 60 minutes respectively)

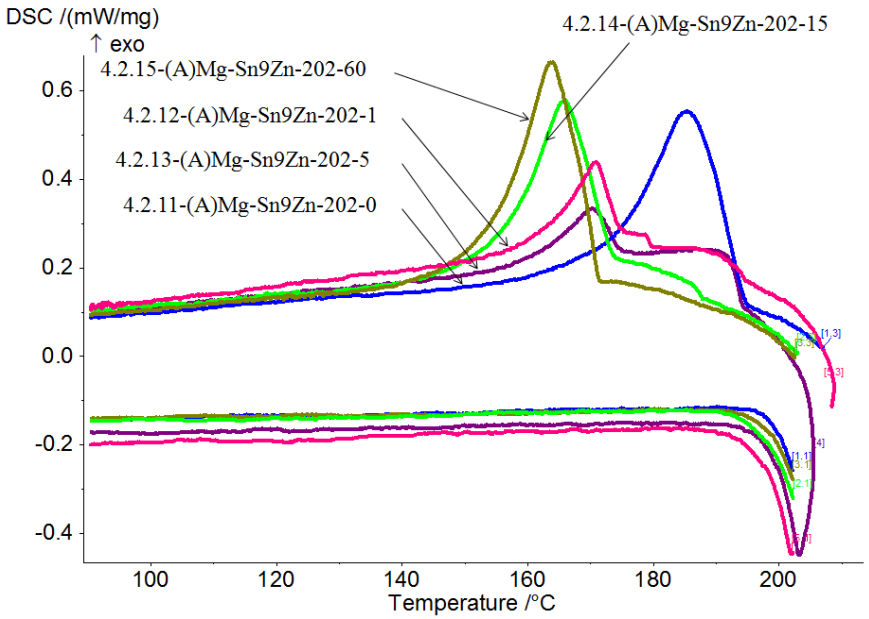

Figure 4.2.3: DSC thermal profiles for Zn Plated Mg Alloy with Sn-9Zn filler metal at 202°C (Hold times: 0, 1, 5, 15, and 60 minutes respectively)

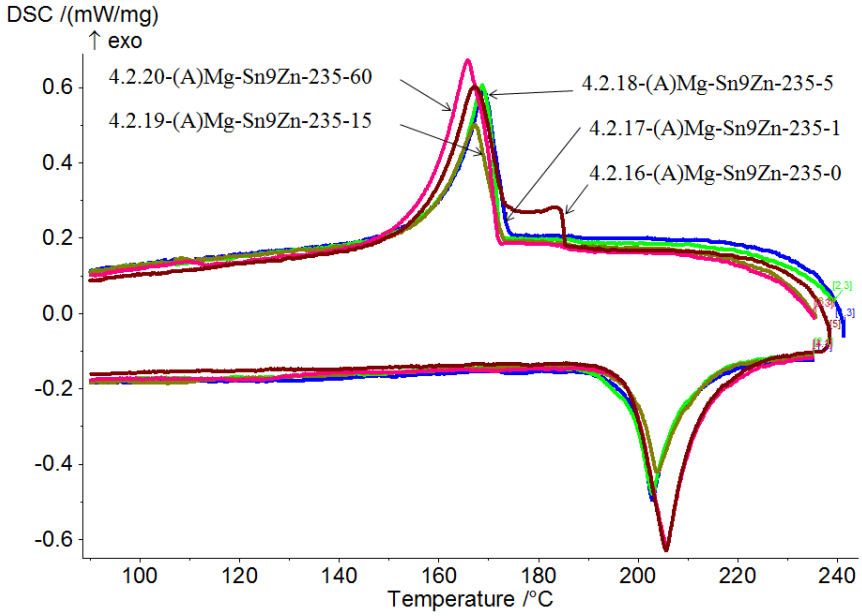

Figure 4.2.4: DSC thermal profiles for Zn Plated Mg Alloy with Sn-9Zn filler metal at 235°C (Hold times: 0, 1, 5, 15, and 60 minutes respectively)

A gradual shift to a lower solidification onset temperature is noted in the samples heated to 202°C (Figures 4.2.1 & 4.2.3). Zn plated Mg Alloy samples appear

to shift at a slower rate than Zn plated Pure Mg samples. However, both Pure Mg sample (4.2.5-(P)Mg-Sn9Zn-202-60) as well as Mg Alloy sample (4.2.15-(A)Mg-Sn9Zn-202-60) with 60 min hold have very close solidification onset temperatures of ~174°C and ~172°C respectively. A slower rate is also noted initially in the Mg Alloy sample (4.2.16-(A)Mg-Sn9Zn-235-0) at 235°C as compared to the Pure Mg samples (Figure 4.2.2). Samples at 235°C in general obtain a consistent solidification onset temperature independent of the hold time suggesting a very fast initial reaction. A solidification peak onset temperature for the Pure Mg samples (Figure 4.2.2) is observed to be ~173°C while that for Mg Alloy samples (Figure 4.2.4) is observed to be ~172°C suggesting a similar filler metal composition and solidification phenomenon for both base metals.

The SEM micrographs in correspondence with DSC thermal profiles 4.2.1-(P)Mg-Sn9Zn-202-0 to 4.2.5-(P)Mg-Sn9Zn-202-60 in Figure 4.2.1 can be referred from Figures 4.2.5a to 4.2.5e. There appears to be a systematic progression of evolving microstructure which can be observed to have a significant increase in the intermetallic layer in an increasing order as the hold time for Pure Mg samples at 202°C increases from 0 min to 60 min. The Mg Alloy system was noted to behave in a similar fashion as the Pure Mg system with respect to the intermetallic growth with increasing time. Microstructures for Mg Alloy samples at 0 min & 60 min can be referred from Figure 4.2.6a and 4.2.6b. Samples at 235°C (not shown here) were also observed to have intermetallic growth at the faying surfaces consistent with results found in samples at 202°C. EDX analysis confirmed that the intermetallic phase is Mg_2Sn. A detailed joint microstructure can be referred to from Figure 4.2.7. As can be seen from the figure, β-Sn matrix is in coexistence with Mg_2Sn phase and Zn rich phase which represents to close proximity what a ternary eutectic structure would be.

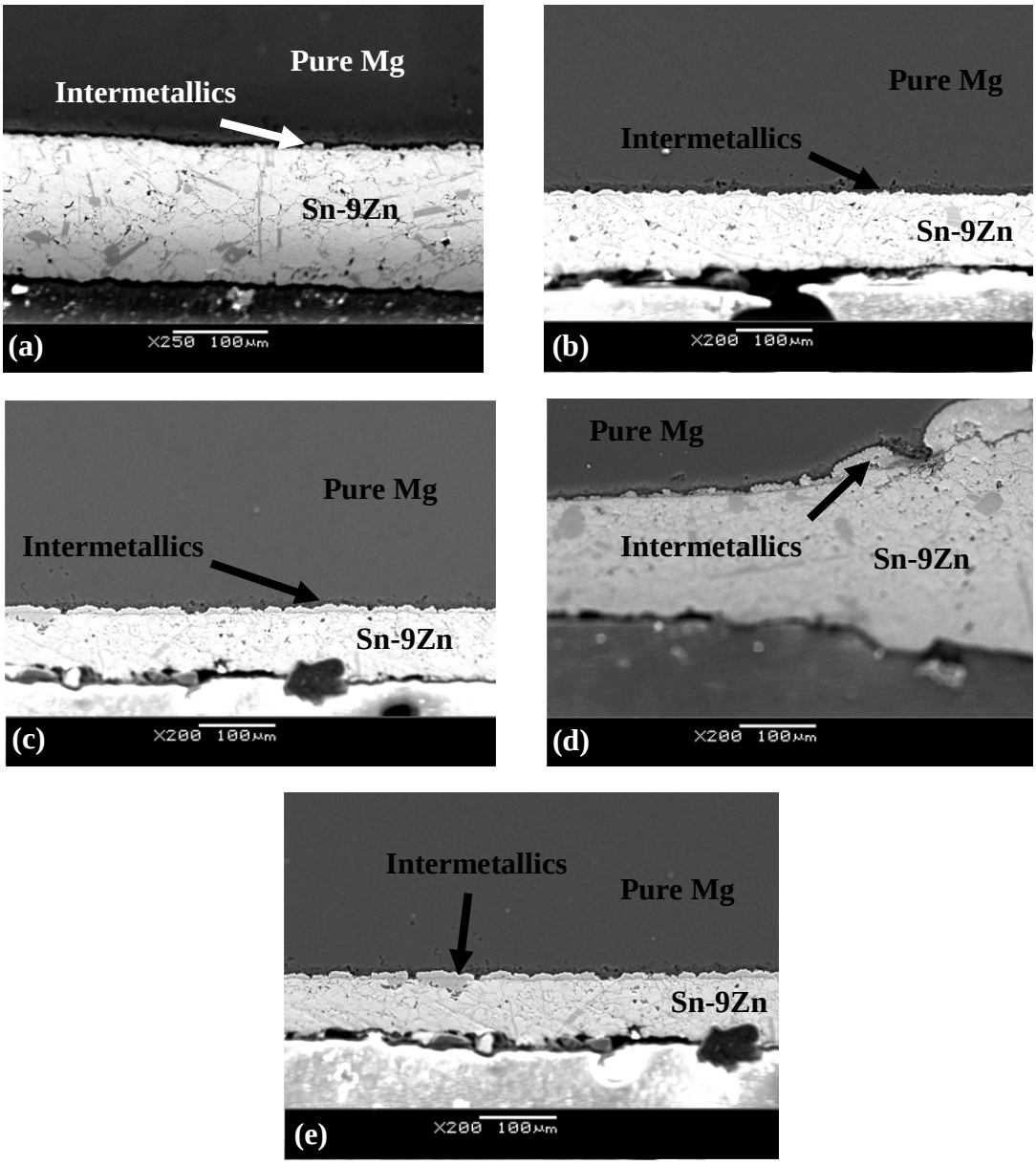

Figure 4.2.5: SEM Micrographs for samples (a) 4.2.1-(P)Mg-Sn9Zn-202-0, (b) 4.2.2-(P)Mg-Sn9Zn-202-1, (c) 4.2.3-(P)Mg-Sn9Zn-202-5, (d) 4.2.4-(P)Mg-Sn9Zn-202-15 and (e) 4.2.5-(P)Mg-Sn9Zn-202-60

In order to further evaluate the joint evolution and to keep the experimental results consistent to be comparable to the use of Sn filler metal as described in the previous section, further testing was carried out at 250°C. The increase in temperature, which is approx. 50°C over the melting temperature of Sn-9Zn filler

metal, is expected to result in more rapid formation of a homogenous joint. These experimental tests are summarized in Table 4.2.2. The experiments involved testing the filler metal at 250°C with hold times at 0, 15 and 30 minutes respectively at the peak temperature. The tests were repeated using Mg Alloy base metal and similar conditions to Pure Mg base metal as described above. DSC thermal profiles for Pure Mg and Mg Alloy samples with Sn-9Zn filler metal at 250°C and hold times of 0, 15 and 30 min respectively can be referred from Figure 4.2.8 and 4.2.9.

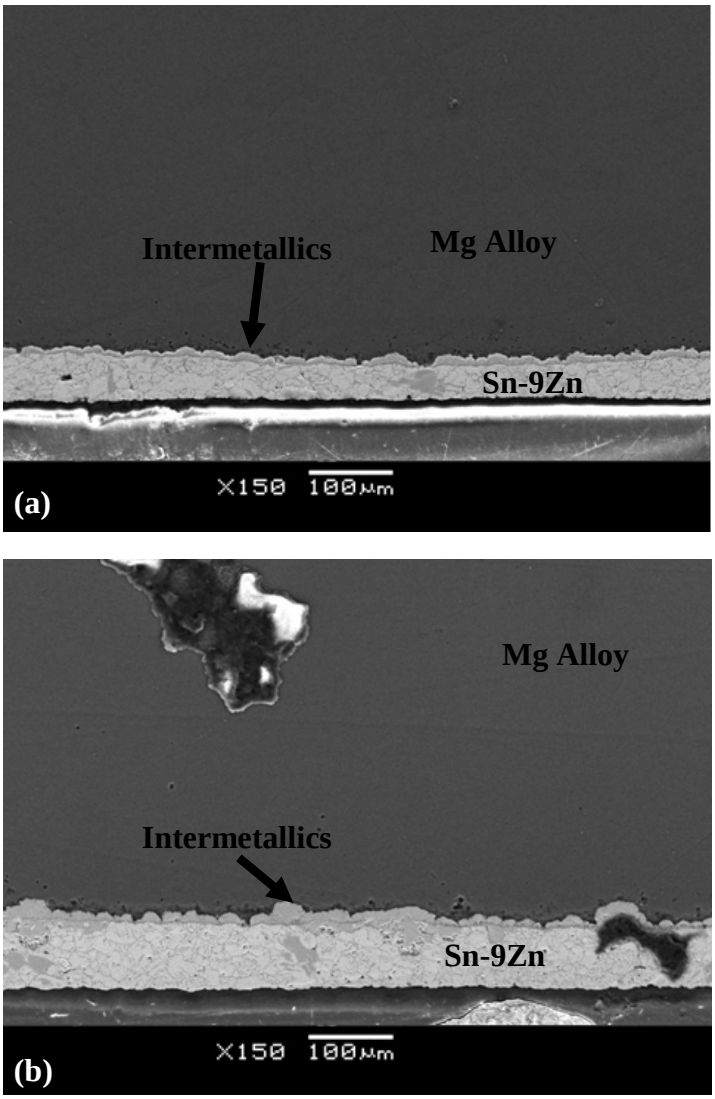

Figure 4.2.6: SEM Micrographs for samples (a) 4.2.11-(A)Mg-Sn9Zn-202-0 and (b) 4.2.15-(A)Mg-Sn9Zn-202-60

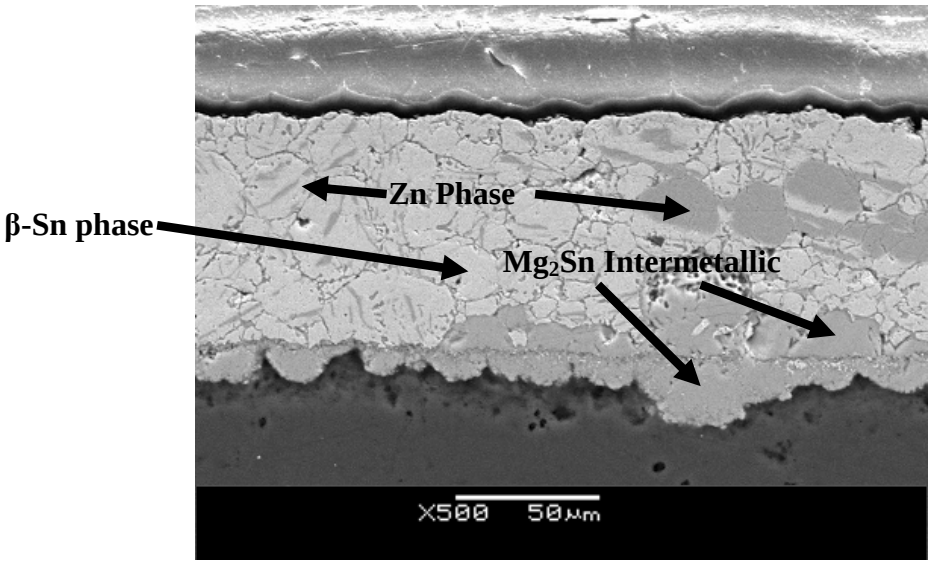

Figure 4.2.7: Approximate ternary joint microstructure at 235°C

Table 4.2.2: Experiments using Sn-9Zn Filler metal at 250°C

Sample ID.	Base Metal	Maximum Testing Temperature	Hold Time
4.2.21-(P)Mg-Sn9Zn-250-0	Zn Plated Pure Mg	250°C	0 min
4.2.22-(P)Mg-Sn9Zn-250-15	Zn Plated Pure Mg	250°C	15 min
4.2.23-(P)Mg-Sn9Zn-250-30	Zn Plated Pure Mg	250°C	30 min
4.2.24-(A)Mg-Sn9Zn-250-0	Zn Plated Mg Alloy	250°C	0 min
4.2.25-(A)Mg-Sn9Zn-250-15	Zn Plated Mg Alloy	250°C	15 min
4.2.26-(A)Mg-Sn9Zn-250-30	Zn Plated Mg Alloy	250°C	30 min

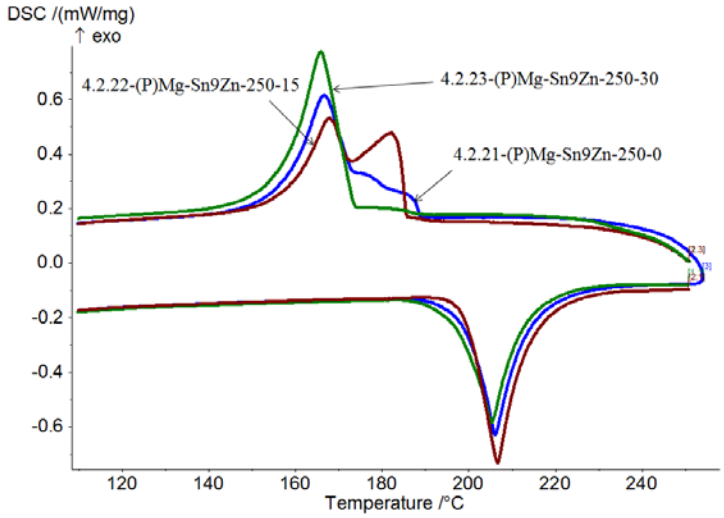

Figure 4.2.8: DSC thermal profiles for Zn Plated Pure Mg with Sn-9Zn filler metal at 250°C (Hold times: 0, 15, and 30 minutes respectively)

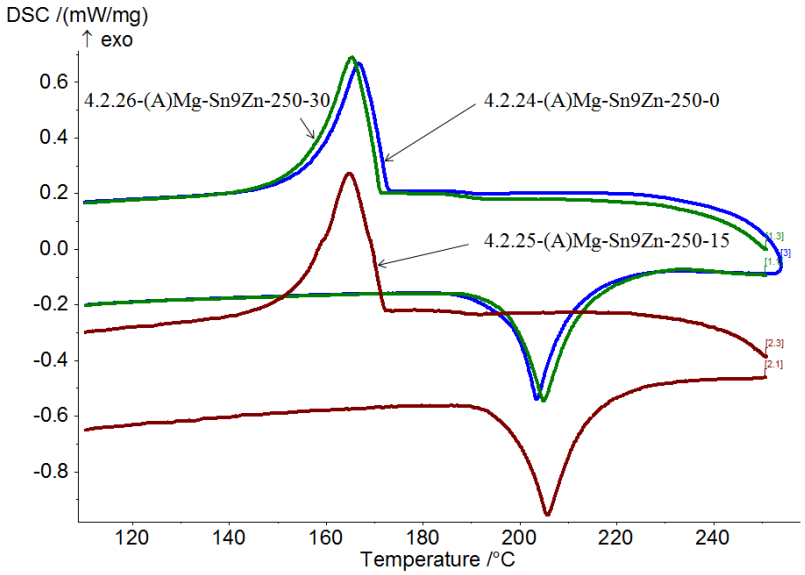

Figure 4.2.9: DSC thermal profiles for Zn Plated Mg Alloy with Sn-9Zn filler metal at 250°C (Hold times: 0, 15, and 30 minutes respectively)

A gradual shift to a lower solidification onset temperature is evident in Pure Mg samples at 250°C (Figure 4.2.8). Although, Pure Mg samples appear to react quickly at 202°C and 235°C as compared to Mg Alloy samples; Pure Mg samples have a slower solidification and gradual shift than Mg Alloy samples at 250°C. The solidification peak onset temperature for Pure Mg samples at 250°C is observed to be ~174°C while that for Mg Alloy samples at 250°C is observed to be ~172°C regardless of the hold times. This is consistent with results found for samples heated up to 202°C and 235°C.

The SEM micrographs for Pure Mg samples with Sn-9Zn filler metal at 250°C and 0, 15 and 30 min hold respectively can be referred to from Figure 4.2.10a to 4.2.10c. Similar to Pure Mg samples at 202°C and 235°C, a significant increase in the intermetallic layer can be seen. It should also be noted that intermetallic growth at various locations other than the faying surfaces can also be found. Although the specimen in Figure 4.2.10b appears to be debonded, it could be attributed to polishing

effects or cross section examination near a non reaction zone (sample edges). Similar to what was found in the SEM microstructures of the Pure Mg system, the Mg Alloy system referred to from the Figures 4.2.11a to 4.2.11c can also be said to have significant Mg_2Sn intermetallic growth at the faying surfaces. A detailed joint microstructure can be referred to from Figure 4.2.12. As can be seen from the figure, β-Sn matrix is in coexistence with Mg_2Sn phase and Zn rich phase which represents to close proximity what a ternary eutectic structure would be.

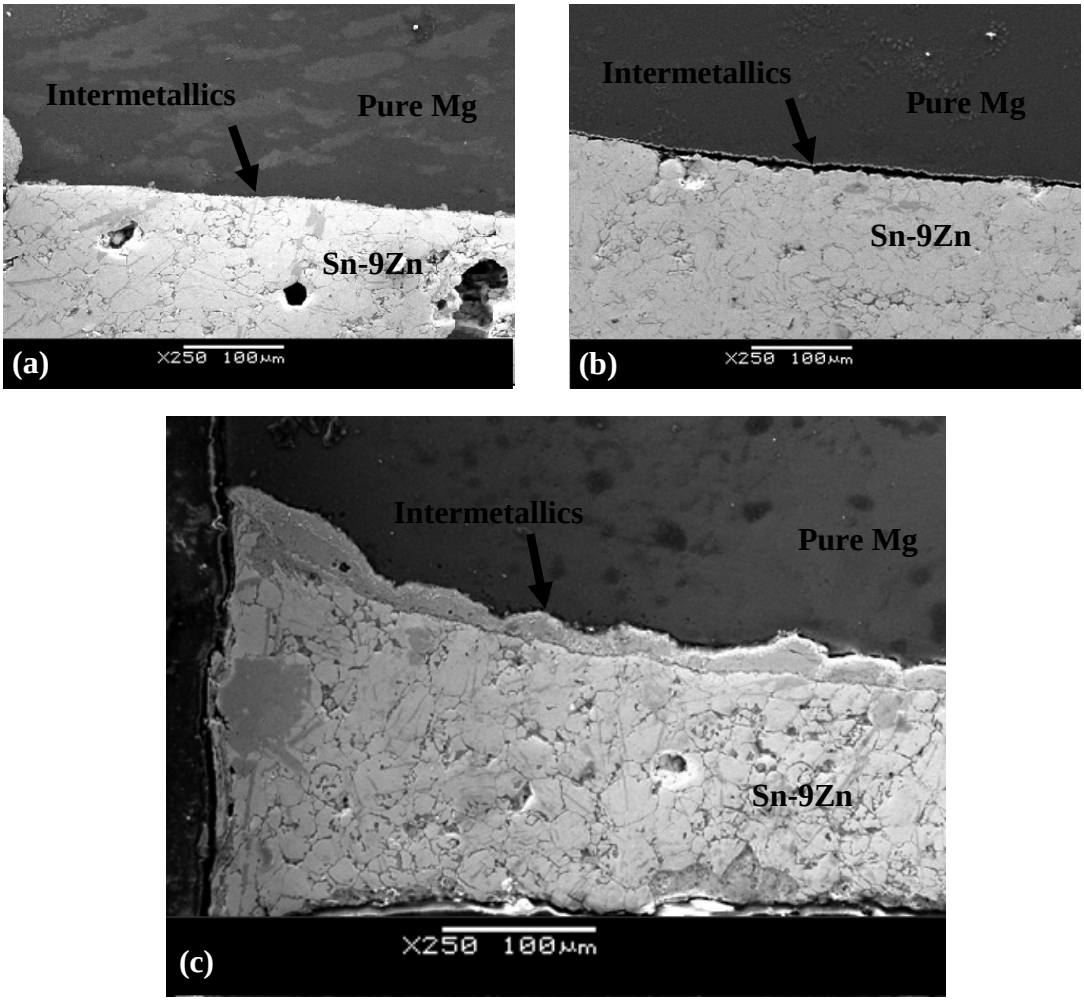

Figure 4.2.10: SEM Micrographs for samples (a) 4.2.21-(P)Mg-Sn9Zn-250-0 (b) 4.2.22-(P)Mg-Sn9Zn-250-15 and (c) 4.2.23-(P)Mg-Sn9Zn-250-30

Comparing the results found for Pure Mg and Mg Alloy samples at 202°C, 235°C and 250°C, it can be noted that metallurgical interactions between the Sn-9Zn filler metal and both type of base metals is evident regardless of the peak heating temperature. A more gradual equilibrium is reached at 202°C than 235°C and 250°C. Also, the peak solidification onset temperature approaches ~172°C regardless of the heating temperature and with increasing hold time at the respective temperatures. A ternary filler metal composition with a melting point at approximately 183°C develops in the Mg and Mg Alloy Sn-9Zn couples. This is confirmed by the reheat curve of Figure 4.2.13 where the onset temperature of the filler was measured as 183°C.

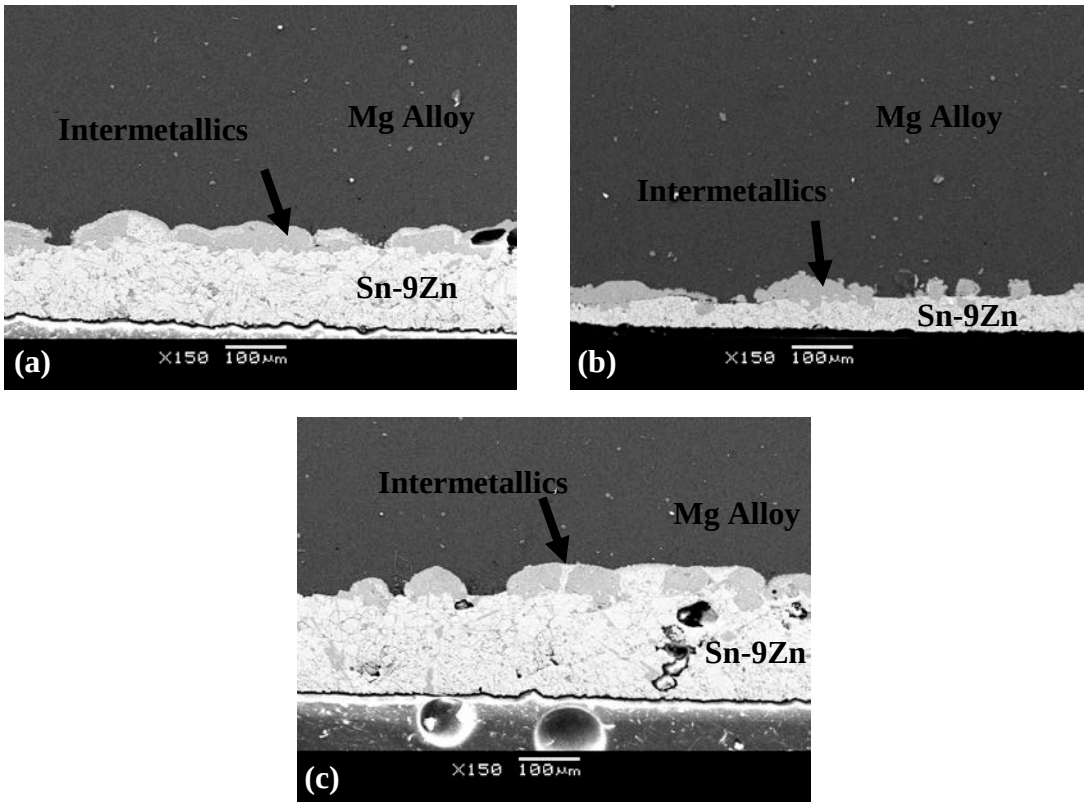

Figure 4.2.11: SEM Micrographs for samples (a) 4.2.24-(A)Mg-Sn9Zn-250-0, (b) 4.2.25-(A)Mg-Sn9Zn-250-15 and (c) 4.2.26-(A)Mg-Sn9Zn-250-30

Significant growth of intermetallic layer at the interface is evident at 202°C, 235°C and 250°C however, in combination with a consistent solidification thermal profiles suggest a stable system. Stable exothermic energy of solidification peaks further confirms that the intermetallic layer prevents or slows down further isothermal solidification. Therefore, an attempt to destabilize the intermetallic layer and promote faster isothermal solidification, experiments was performed at 350°C and 450°C respectively (Table 4.2.3).

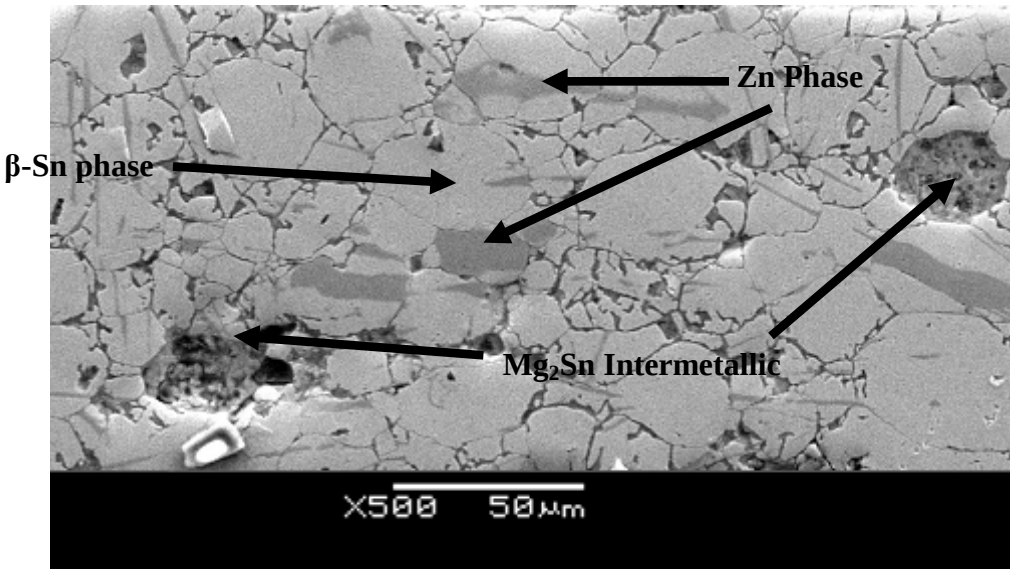

Figure 4.2.12: Approximate ternary joint microstructure at 250°C with 30 min hold

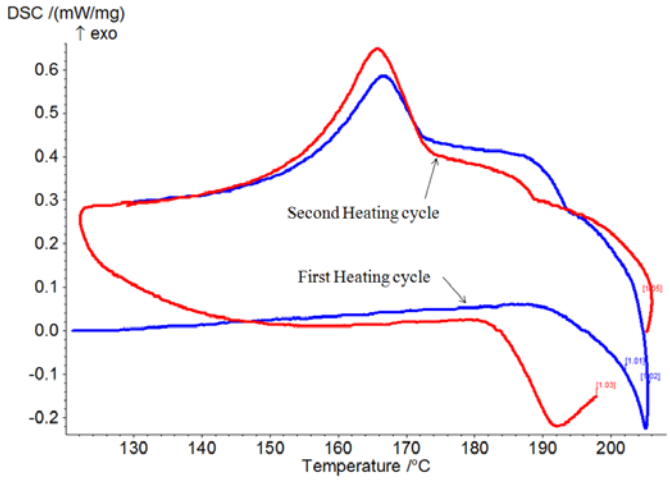

Figure 4.2.13: First and Second heating cycle of Pure Mg/ Sn-9Zn couple cyclic sample DSC Thermal profile

The DSC thermal profiles for experiments performed at 350°C and 450°C can be seen from Figures 4.2.14 and 4.2.15. It should be noted that there are exothermic reaction peaks present on the heating curve for both 350°C and 450°C samples. The Sn-9Zn couple DSC thermal profiles heated to 350°C are similar to that seen for the couples made with Pure Sn filler metal. A broad exothermic peak occurs in the Mg Alloy couple while heating but not in the Pure Mg couple. However, samples heated to 450°C indicate different behavior, with a large exothermic peak during heating. There is also some indication of liquid present at solidification onset of ~330°C during cooling from 450°C which is assumed to be a Mg-Zn eutectic reaction in the samples. Samples at 350°C show no such solidification event. Similar to samples at 202°C, 235°C and 250°C; the samples at 350°C and 450°C also exhibit solidification peak onset at ~170°C which is attributed to the bulk freezing of the filler metal.

Table 4.2.3: Experiments using Sn-9Zn Filler metal at temperature over 350°C

Sample ID.	Base Metal	Max. Testing Temperature	Hold Time
4.2.27-(P)Mg-Sn9Zn-350-0	Zn Plated Pure Mg	350°C	0 min
4.2.28-(A)Mg-Sn9Zn-350-0	Zn Plated Mg Alloy	350°C	0 min
4.2.29-(P)Mg-Sn9Zn-450-0	Zn Plated Pure Mg	450°C	0 min
4.2.30-(A)Mg-Sn9Zn-450-0	Zn Plated Mg Alloy	450°C	0 min

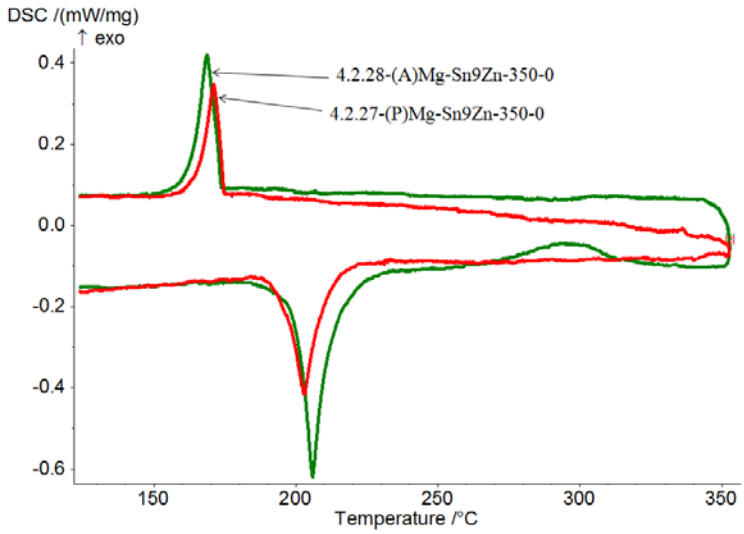

Figure 4.2.14: DSC thermal profiles with Sn-9Zn filler metal for at 350°C for Zn Plated Pure Mg and Zn Plated Mg Alloy

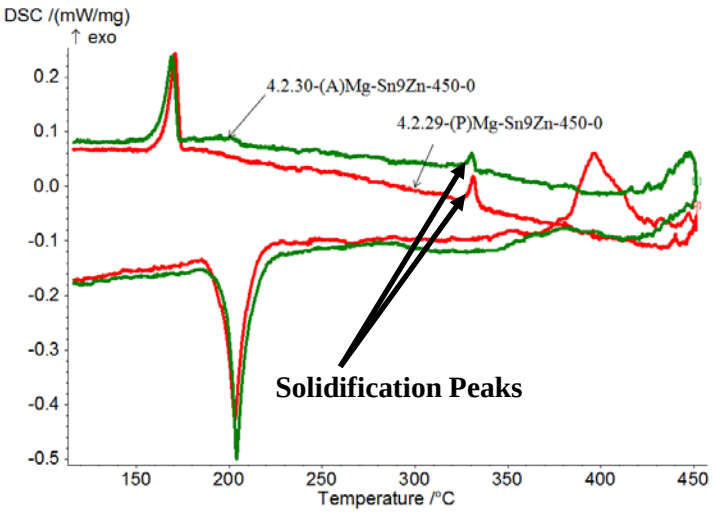

Figure 4.2.15: DSC thermal profiles with Sn-9Zn filler metal for at 450°C for Zn Plated Pure Mg and Zn Plated Mg Alloy

The SEM images for Pure Mg and Mg Alloy samples at 350°C and 450°C respectively can be referred from Figure 4.2.16 and 4.2.17. Mg_2Sn intermetallic growth can be seen in systems at 350°C and 450°C. Mg_7Zn_3 intermetallic can be seen in Pure Mg samples however was absent in Mg Alloy sample at 350°C. Debonding was observed at 350°C while samples at 450°C were found to have good bonding which can be attributed to the Mg-Zn eutectic phase formation. As can be referred to from Figure 4.2.17a and Figure 4.2.17b, a distinct eutectic microstructure which is approximately 49Mg– 51Zn weight % (Mg-Zn Eutectic) can be seen between the Mg substrate and Mg_2Sn intermetallic layer.

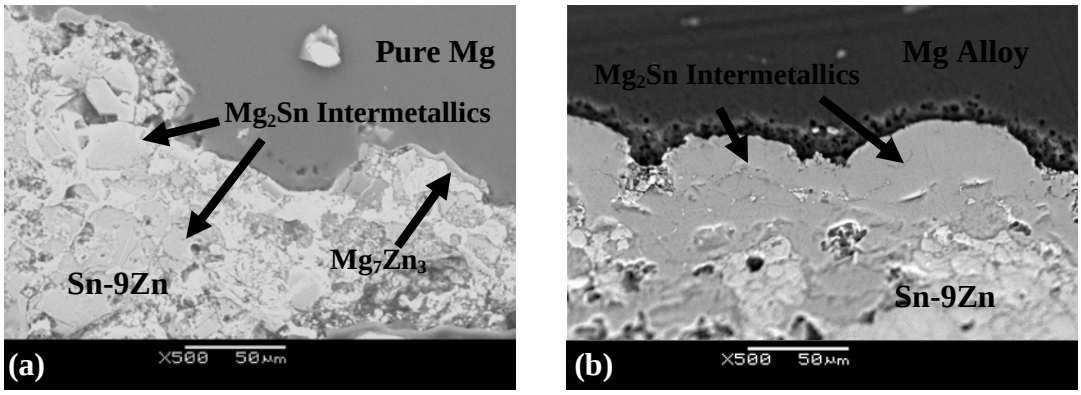

Figure 4.2.16: SEM Micrographs for samples (a) 4.2.27-(P)Mg-Sn9Zn-350-0 and (b) 4.2.28-(A)Mg-Sn9Zn-350-0

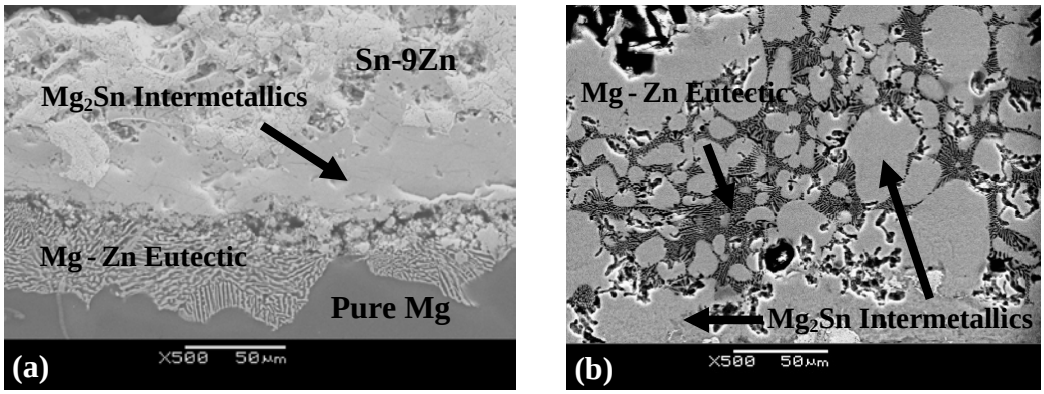

Figure 4.2.17: SEM Micrographs for samples (a) 4.2.29-(P)Mg-Sn9Zn-450-0 and (b) 4.2.30-(A)Mg-Sn9Zn-450-0

4.3 Experimental results for Joining Mg using Wide Gap Filler Metal

It is clear from Sections 4.1 and 4.2 that complete isothermal solidification of the Sn or Sn-Zn filler metal does not occur even at temperature as high as 450°C. This is due to the growth of the continuous Mg_2Sn intermetallic layer. This layer acts as a barrier, preventing further diffusion of Sn (or Zn) into the Mg base. One possible solution to this problem is to implement a "wide gap" TLPB approach. This involves placing powders with the substrate composition into the filler metal powder mixture. This base metal powder acts as an additional "sink" for isothermal solidification.

In order to evaluate the feasibility of this approach, Zn plated Pure Mg was selected as base metal material with Sn-9Zn as a filler metal. To create wide gap joint simulation; Mg powder was added to the Sn-9Zn filler powder mixture in increments of 10wt% and test samples were prepared by the procedure outlined in Chapter 3. Summary for the samples used for experiments can be referred to from Table 4.3.1. Samples were tested at 250°C, 350°C and 450°C respectively at each filler metal composition without any hold time at the peak heating temperature. The DSC thermal profiles for the samples outlined in Table 4.3.1 can be referred to from Figures 4.3.1 – 4.3.4.

Table 4.3.1: Experiments with Wide Gap filler metal on Zn Plated Pure Mg base metal

Sample ID.	Filler Metal Composition	Maximum Testing Temperature	Hold Time
4.3.1-(P)Mg-Sn9Zn-250-0	Sn9Zn	250°C	0 min
4.3.2-(P)Mg-Sn9Zn-350-0	Sn9Zn	350°C	0 min
4.3.3-(P)Mg-Sn9Zn-450-0	Sn9Zn	450°C	0 min
4.3.4-(P)Mg-10Mg90(Sn9Zn)-250-0	10Mg:90(Sn9Zn)	250°C	0 min
4.3.5-(P)Mg-10Mg90(Sn9Zn)-350-0	10Mg:90(Sn9Zn)	350°C	0 min
4.3.6-(P)Mg-10Mg90(Sn9Zn)-450-0	10Mg:90(Sn9Zn)	450°C	0 min
4.3.7-(P)Mg-20Mg80(Sn9Zn)-250-0	20Mg:80(Sn9Zn)	250°C	0 min
4.3.8-(P)Mg-20Mg80(Sn9Zn)-350-0	20Mg:80(Sn9Zn)	350°C	0 min
4.3.9-(P)Mg-20Mg80(Sn9Zn)-450-0	20Mg:80(Sn9Zn)	450°C	0 min
4.3.10-(P)Mg-30Mg70(Sn9Zn)-250-0	30Mg:70(Sn9Zn)	250°C	0 min
4.3.11-(P)Mg-30Mg70(Sn9Zn)-350-0	30Mg:70(Sn9Zn)	350°C	0 min
4.3.12-(P)Mg-30Mg70(Sn9Zn)-450-0	30Mg:70(Sn9Zn)	450°C	0 min

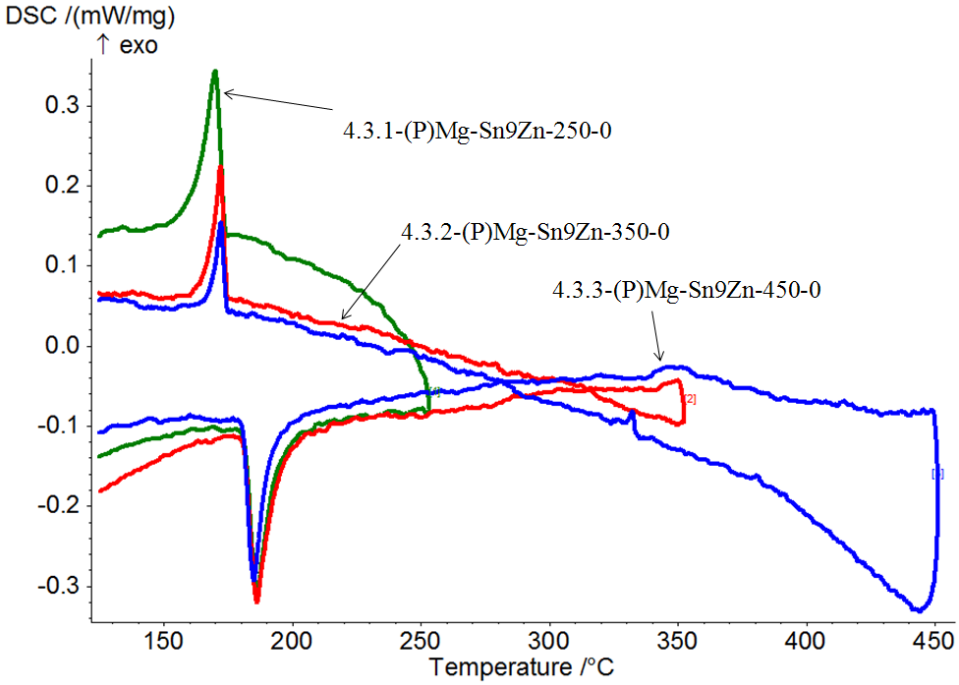

Figure 4.3.1: DSC thermal profiles for samples with Sn-9Zn filler composition

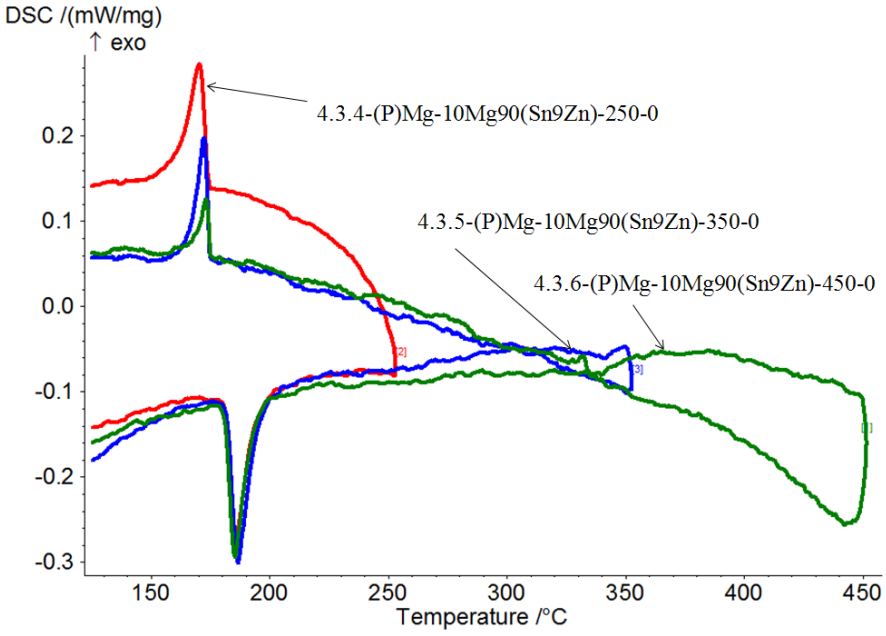

Figure 4.3.2: DSC thermal profiles for samples with 10Mg:90(Sn-9Zn) wt% filler composition

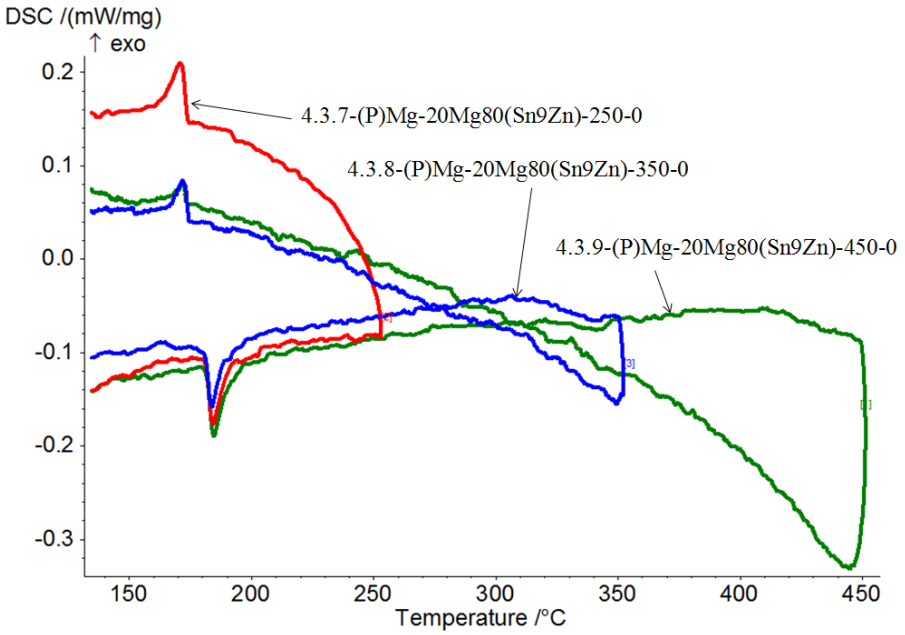

Figure 4.3.3: DSC thermal profiles for samples with 20Mg:80(Sn-9Zn) wt% filler composition

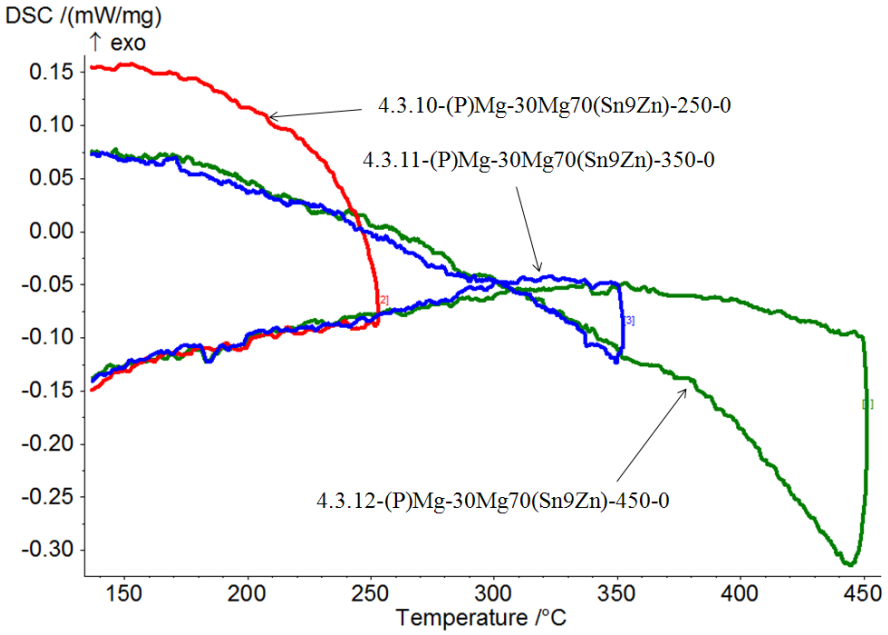

Figure 4.3.4: DSC thermal profiles for samples with 30Mg:70(Sn-9Zn) wt% filler composition

Solidification onset at ~170°C is noted for all samples from Table 4.3.1 regardless of the filler metal composition. Solidification onset temperature is consistent with previous Sn-9Zn experiments from Section 4.2. Comparing the melting peak and the solidification peak for each sample in Figures 4.3.1 – 4.3.3; a progressive reduction in liquid volume fraction is observed. Small solidification liquid peaks are seen in samples heated to 450°C. It is of utmost importance to notice that although a melting peak is clearly observed in sample 4.3.9-(P)Mg-20Mg80(Sn9Zn)-450-0; no obvious solidification peak is found during cooling indicating completion of isothermal solidification at 450°C with no hold at peak heating temperature.

A decrease in the initial melting liquid peak is obvious as Mg powder wt% in the filler metal increases. This is due to the lower volume fraction of melting phase. No significant events occur at 30wt%Mg-70wt%(Sn-9Zn) either during heating or cooling. This suggests that either the liquid volume fraction is insignificant to emit a signal strong enough to be detected by the DSC or solid state diffusion reacts all of Sn-9Zn in the filler to form intermetallics before melting occurs. Regardless of the filler metal composition, decrease in liquid volume fraction on solidification with increase in temperature is evident. The above results indicate that adding Mg powder to the filler metal can cause complete isothermal solidification (i.e. 20% Mg heated to 450°C) even without a hold time at peak heating temperatures.

In order to evaluate the dependency of wide gap filler metal joints with respect to hold times; 10wt%Mg-90wt%(Sn-9Zn) filler composition was tested at 250°C, 350°C and 450°C. The samples were heated three times to the peak temperature to simulate increase in time at the joining temperature. Summary of the samples tested can be found from Table 4.3.2 and the DSC thermal profiles from Figures 4.3.5 – 4.3.7.

Table 4.3.2: Cyclic temperature profile experiments with wide gap filler metal

Sample ID.	Filler Metal Composition	Maximum Testing Temperature
4.3.13-(P)Mg-10Mg90(Sn9Zn)-250-CYL	10Mg:90(Sn9Zn)	250°C
4.3.14-(P)Mg-10Mg90(Sn9Zn)-350-CYL	10Mg:90(Sn9Zn)	350°C
4.3.15-(P)Mg-10Mg90(Sn9Zn)-450-CYL	10Mg:90(Sn9Zn)	450°C

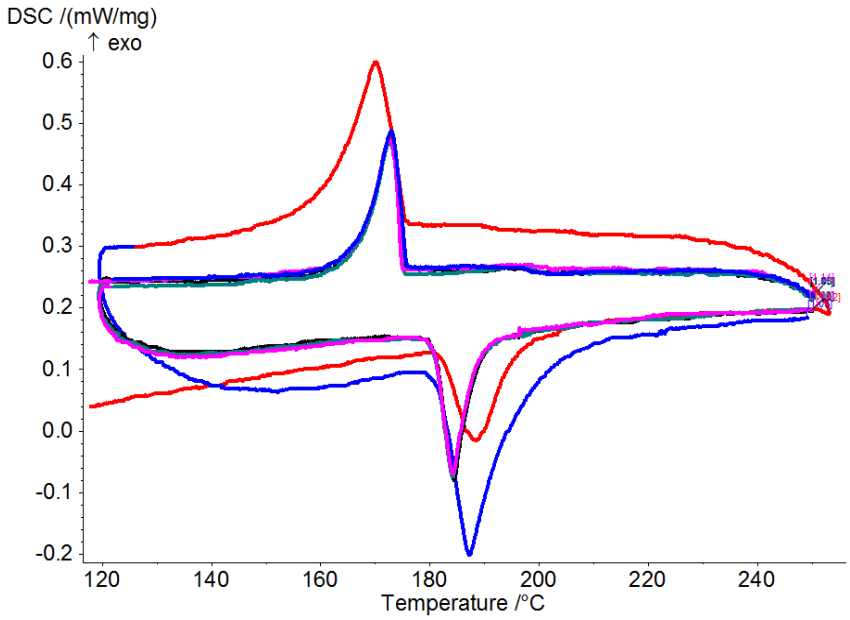

Figure 4.3.5: DSC thermal profile for sample with 10Mg:90(Sn-9Zn) wt% filler composition at 250°C

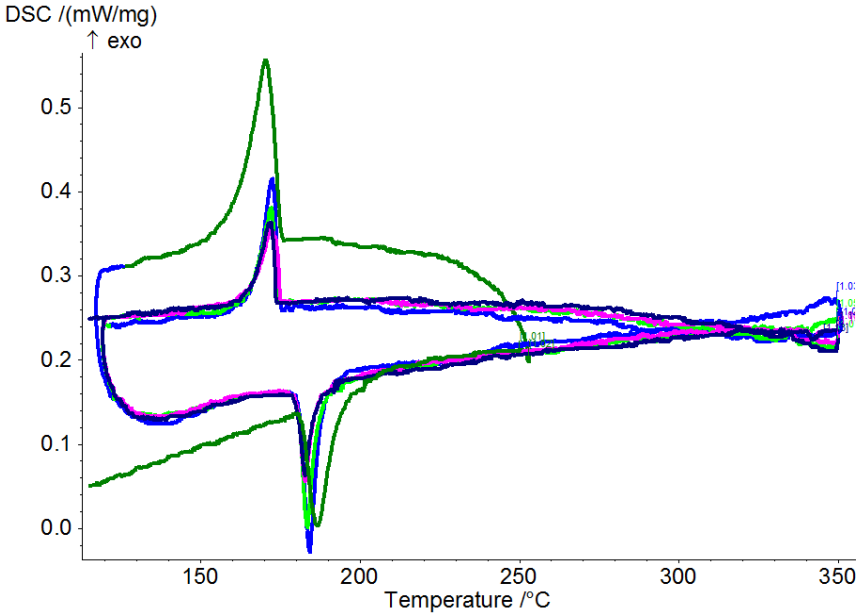

Figure 4.3.6: DSC thermal profile for sample with 10Mg:90(Sn-9Zn) wt% filler composition at 350°C

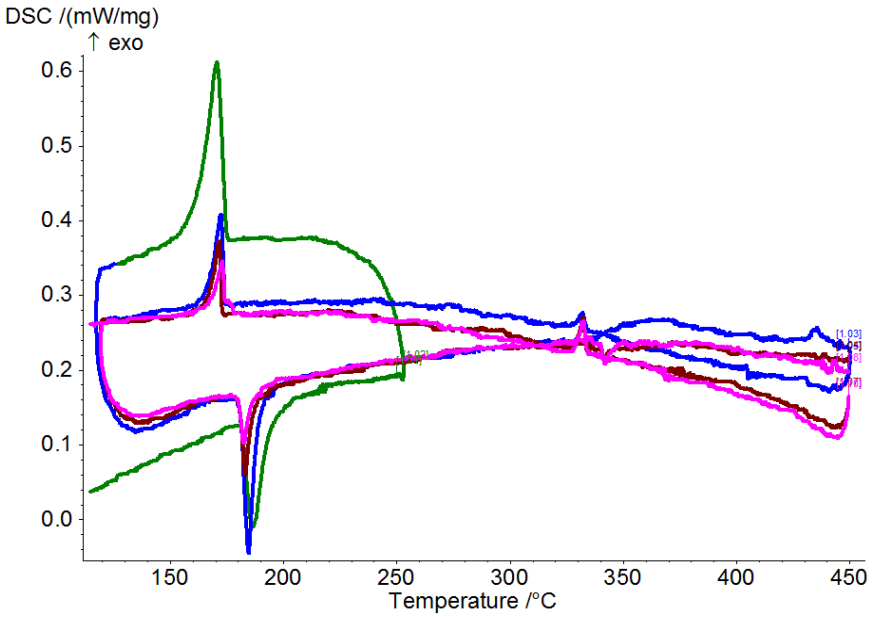

Figure 4.3.7: DSC thermal profile for sample with 10Mg:90(Sn-9Zn)wt % filler composition at 450°C

A minor reduction in liquid volume fraction is noted for the sample heated to 250°C. The reduction appears to occur during the first heating and cooling cycle stabilizing thereafter to have no further significant isothermal solidification with respect to increase in hold time. All samples with filler metal composition of 10Mg:90(Sn-9Zn) have a solidification peak onset at ~175°C irrespective of the hold time. Sample heated to 350°C does exhibit reduction in the solidification peak with respect to increase in hold times. No liquid peaks other than at ~175°C can be noted. Sample heated to 450°C also exhibits a reduction in the solidification peak with respect to hold times however, other liquid peaks on solidification thermal profile can be noted. SEM micrographs for samples in Table 4.3.2 can be referred from Figure 4.3.8a to 4.3.8c.

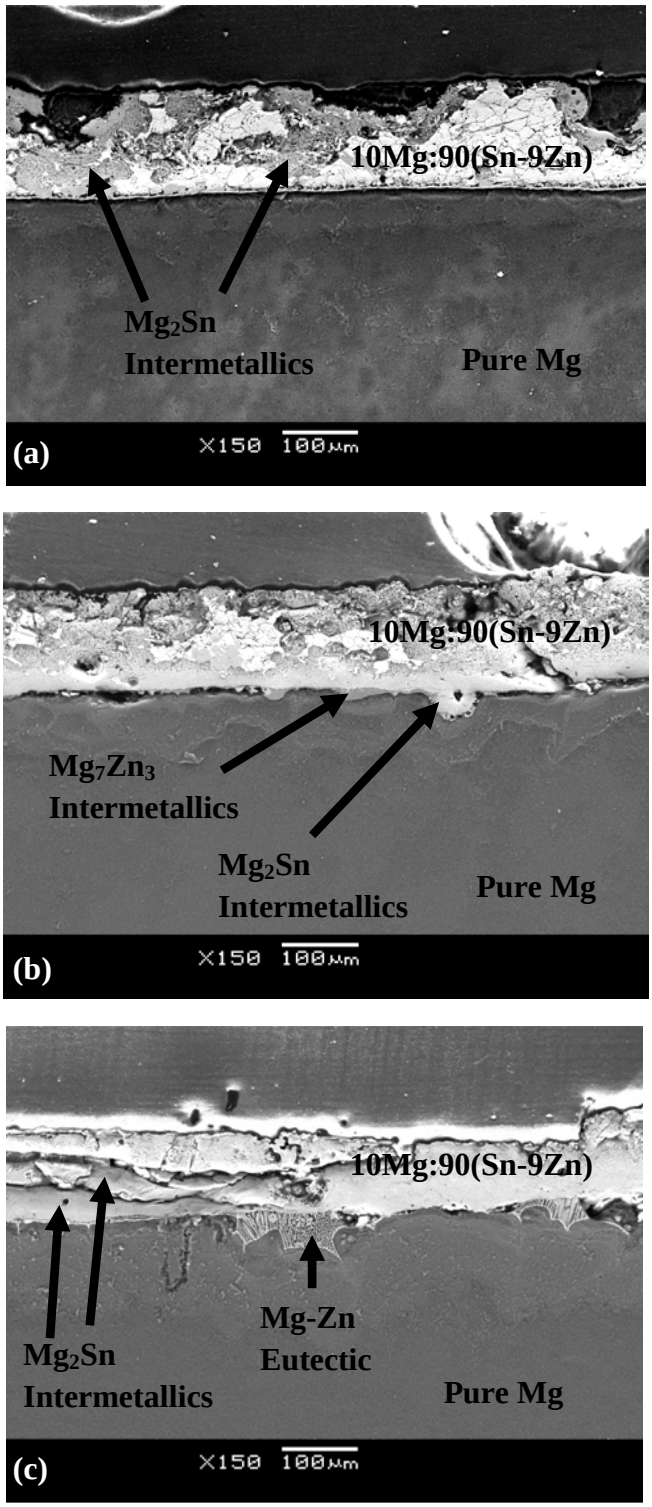

Figure 4.3.8: SEM Micrographs for samples (a) 4.3.13-(P)Mg-10Mg90(Sn9Zn)-250-CYL, (b) 4.3.14-(P)Mg-10Mg90(Sn9Zn)-350-CYL and (c) 4.3.15-(P)Mg-10Mg90(Sn9Zn)-450-CYL

Mg_2Sn intermetallic phase is observed in all samples irrespective of the heating temperature. However, Mg_7Zn_3 phase is only noted in the sample heated to 350°C. No eutectic microstructure is seen which is consistent to the thermal profile observed from Figure 4.3.6. Mg-Zn eutectic microstructure can be seen from Figure 4.3.8c which also corresponds to the 450°C thermal profile referred from Figure 4.3.7. The above results indicate that the use of a wide gap approach is successful in increasing the rate of isothermal solidification. The exact time required to cause complete solidification for a given Mg content is beyond the scope of this thesis.

4.4 Experimental Results for Mg using with Zn rich Filler Metal

In order to evaluate the significance of Zn in the filler metal composition, a number of experiments were conducted. Based on the 450°C results of Section 4.2, it was proposed that an increasing percentage of Zinc promotes Mg-Zn eutectic formation and thus improves braze joint formation. Also, it would aid in the investigation of the compositions and reactions in presence of Zinc at the temperatures of 350°C and 450°C.

In line with the previous statements, as Zinc was thought to play a very significant role, further testing was carried out first without any Sn present in the system keeping the filler metal composition at 50Mg:50Zn wt%. These tests were performed at 350°C & 450°C respectively first to keep consistent with the other testing temperature presented in this study and due to the eutectic temperature of Mg-Zn at approximately 340°C. Subsequent tests were performed by adding 5% and 10% Sn-9Zn to the system. The experiment set is summarized in Table 4.4.1. The DSC thermal profiles can be referred from Figures 4.4.1 & 4.4.2.

Table 4.4.1: Experiments with Zn rich filler metal and Zn Plated Pure Mg base metal

Sample ID.	Filler Metal Composition	Maximum Testing Temperature	Hold Time
4.4.1-(P)Mg-50Mg50Zn-350-30	50Mg : 50Zn	350°C	30 min
4.4.2-(P)Mg-47.5Mg47.5Zn5(Sn9Zn)-350-30	47.5Mg : 47.5Zn: 5(Sn9Zn)	350°C	30 min
4.4.3-(P)Mg-45Mg45Zn10(Sn9Zn)-350-30	45Mg : 45Zn: 10(Sn9Zn)	350°C	30 min
4.4.4-(P)Mg-50Mg50Zn-450-30	50Mg : 50Zn	450°C	30 min
4.4.5-(P)Mg-47.5Mg47.5Zn5(Sn9Zn)-450-30	47.5Mg : 47.5Zn: 5(Sn9Zn)	450°C	30 min
4.4.6-(P)Mg-45Mg45Zn10(Sn9Zn)-450-30	45Mg : 45Zn: 10(Sn9Zn)	450°C	30 min

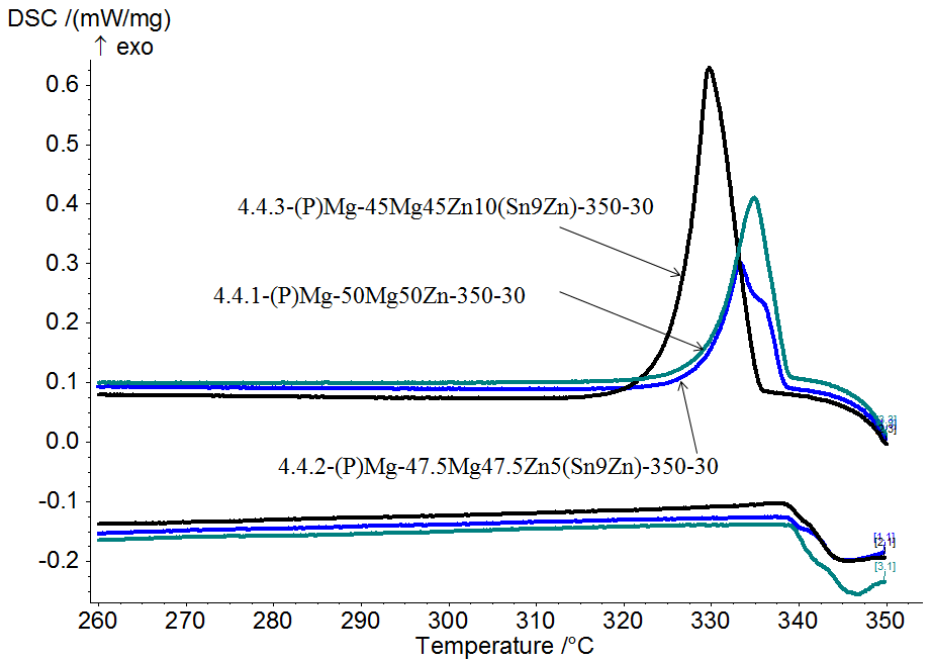

Figure 4.4.1: DSC thermal profiles for Zn Plated Pure Mg with 50Mg:50Zn; 47.5Mg:47.5Zn:5(Sn-9Zn); 45Mg:45Zn:10(Sn-9Zn) filler metals at 350°C

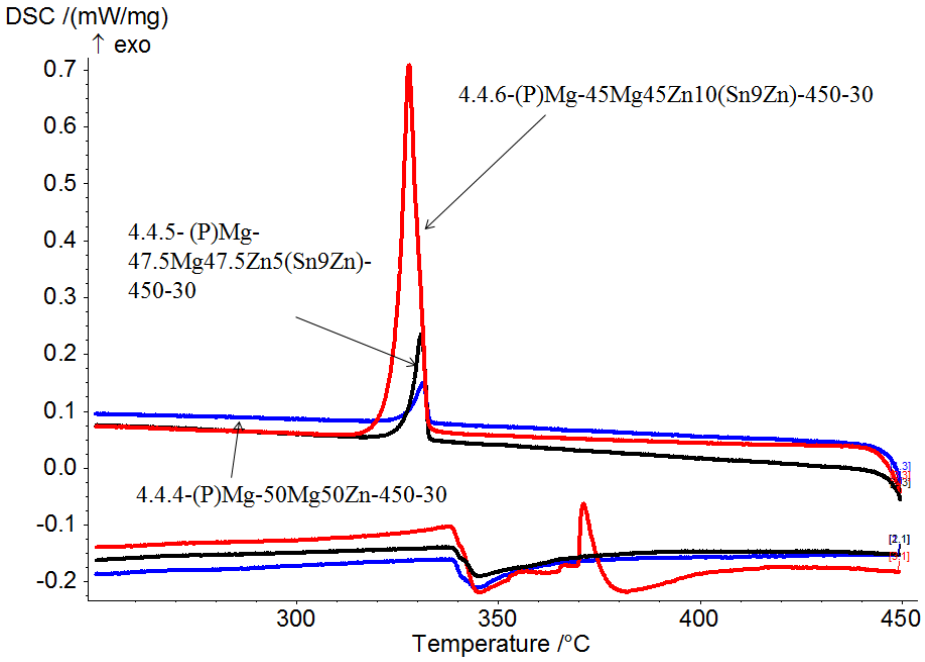

Figure 4.4.2: DSC thermal profiles for Zn Plated Pure Mg with 50Mg:50Zn; 47.5Mg:47.5Zn:5(Sn-9Zn); 45Mg:45Zn:10(Sn-9Zn) filler metals at 450°C

As can be noted from Figure 4.4.1, the onset of melting occurs at ~341°C which corresponds to the Mg-Zn eutectic temperature. A distinct solidification peak is observed during cooling. The peak is noted to increase in magnitude and becomes sharper with an increase in Sn content. Also, a shift to a lower solidification temperature is noted which corresponds to the Mg-Zn-Sn ternary phase diagram predicting a lower melting temperature with slight increase of Sn in a Mg-Zn system. Thermal profiles heated to 450°C show a similar trend, with a melting peak onsetting at ~341°C. However, the couple with the highest Sn content in the filler metal (i.e. 4.4.6-(P)Mg-45Mg45Zn10(Sn9Zn)-450-30) also exhibits a distinct exothermic reaction at about 370°C on the heating curve. All samples cooled from 450°C exhibit a distinct solidification peak onset at ~330°C. This corresponds to a Mg-Zn eutectic, if one accounts for little undercooling. The sample with the highest Sn content indicates a significantly higher magnitude in its solidification peak indicating a larger volume of liquid formation.

The samples were examined in SEM and micrographs are presented in Figures 4.4.3 – 4.4.5. All samples evaluated at 350°C (Figure 4.4.3) were observed to have a distinct Mg_7Zn_3 intermetallic phase as well as another phase which corresponds to roughly maximum solubility of Magnesium in Zinc. The samples at 450°C however, have a significant eutectic microstructure present. The amount of eutectic microstructure appears to be increasing with increase in Sn-9Zn content. This observation is in line with the increase in volume fraction as noted on solidification peaks of samples heated to 450°C (Figure 4.4.2). Increase in diffusion into the base metal is noted with increase in the Sn-9Zn content. Further evaluation can be found in subsequent discussion section.

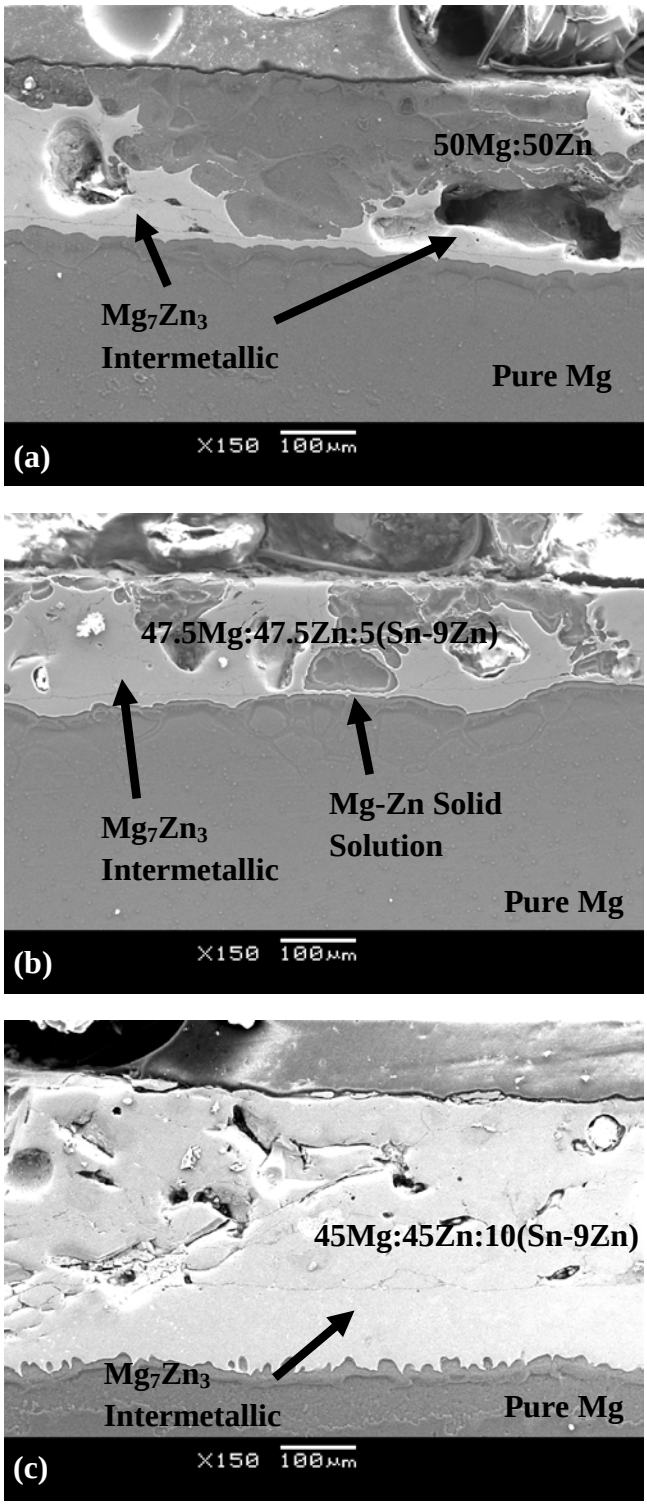

Figure 4.4.3: SEM Micrographs for samples (a) 4.4.1-(P)Mg-50Mg50Zn-350-30; (b) 4.4.2-(P)Mg-47.5Mg47.5Zn5(Sn9Zn)-350-30 and (c) 4.4.3-(P)Mg-45Mg45Zn10(Sn9Zn)-350-30

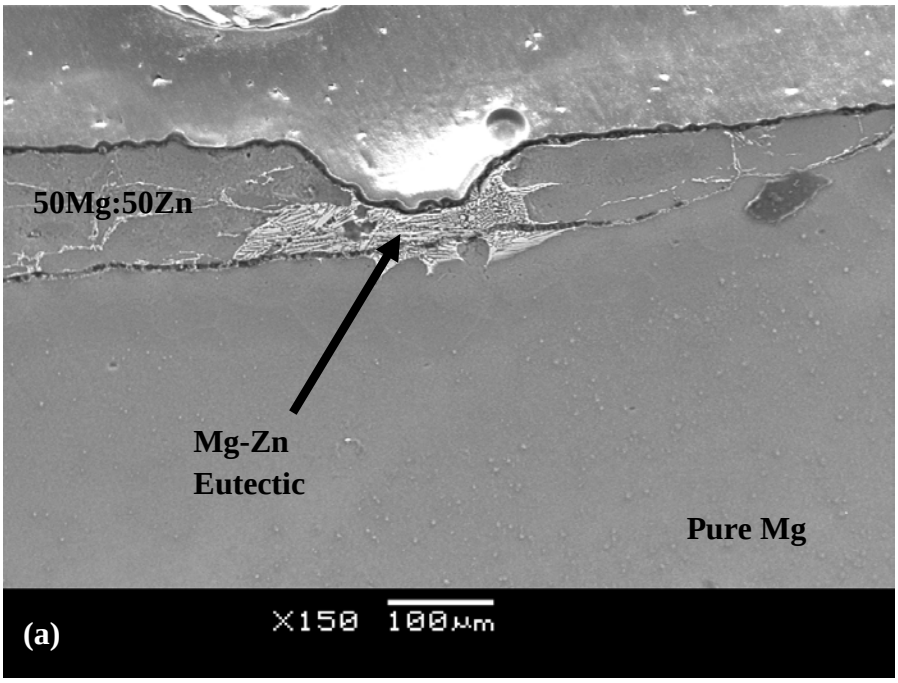

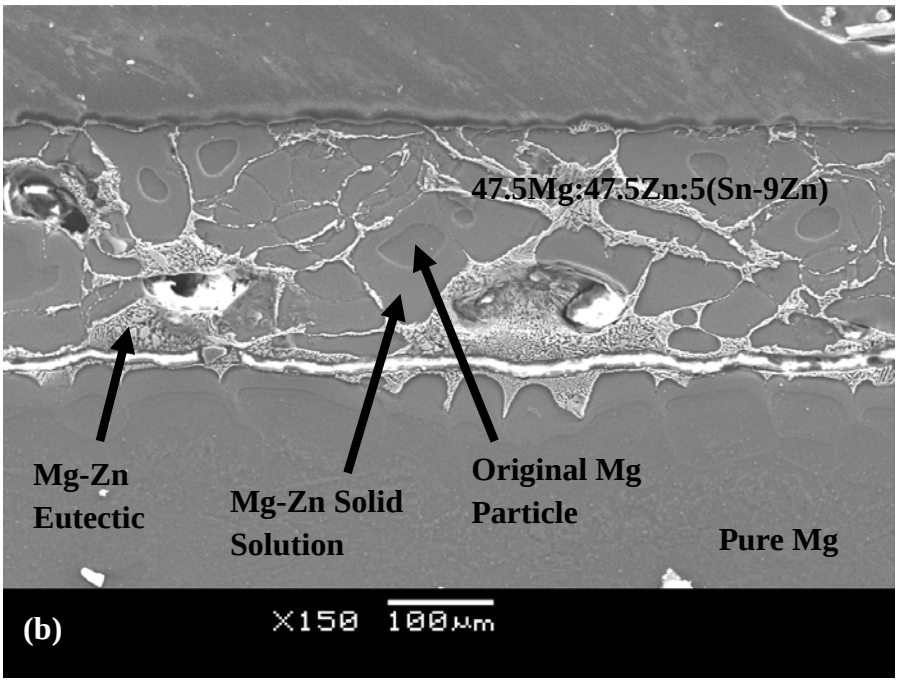

Figure 4.4.4: SEM Micrographs for samples (a) 4.4.4-(P)Mg-50Mg50Zn-450-30 and (b) 4.4.5-(P)Mg-47.5Mg47.5Zn5(Sn9Zn)-450-30

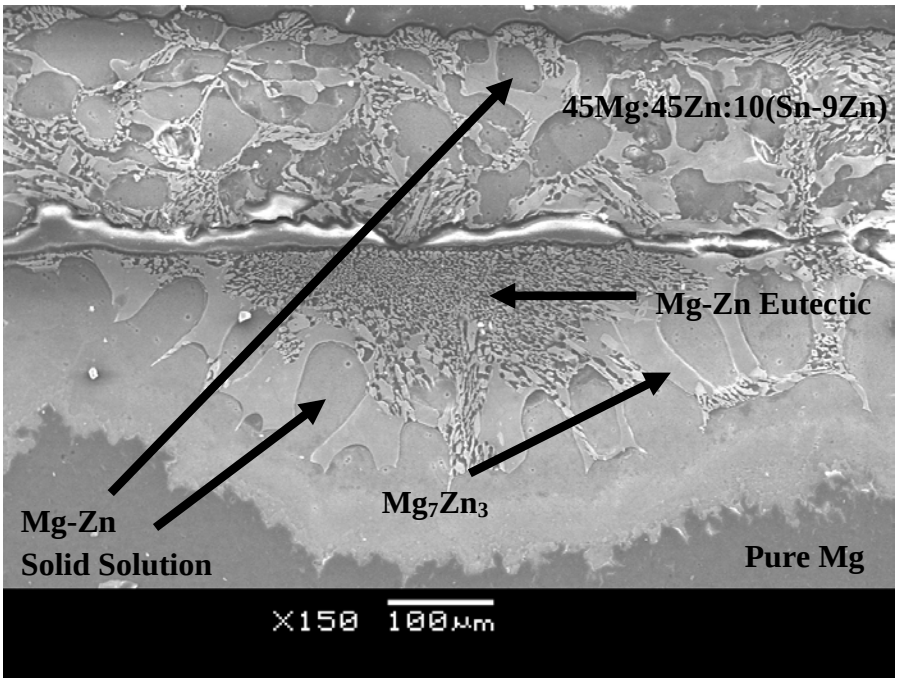

Figure 4.4.5: SEM Micrograph for sample 4.4.6-(P)Mg-45Mg45Zn10(Sn9Zn)-450-30

5.0 Discussion

a) Joining Mg using Sn Filler Metal

Joining of Magnesium to Magnesium was carried out successfully using Sn filler metal as can be referred from Section 4.1. A binary Mg-Sn couple can be assumed if the presence of the thin Zn immersion coating is ignored. An explanation for the results observed in Section 4.1 can begin with reference to the binary Mg-Sn phase diagram (Figure 5.1). If equilibrium was established between the Mg and Sn phases in the brazed joint, initial melting would be expected to onset at ~203.5°C due to the eutectic reaction.

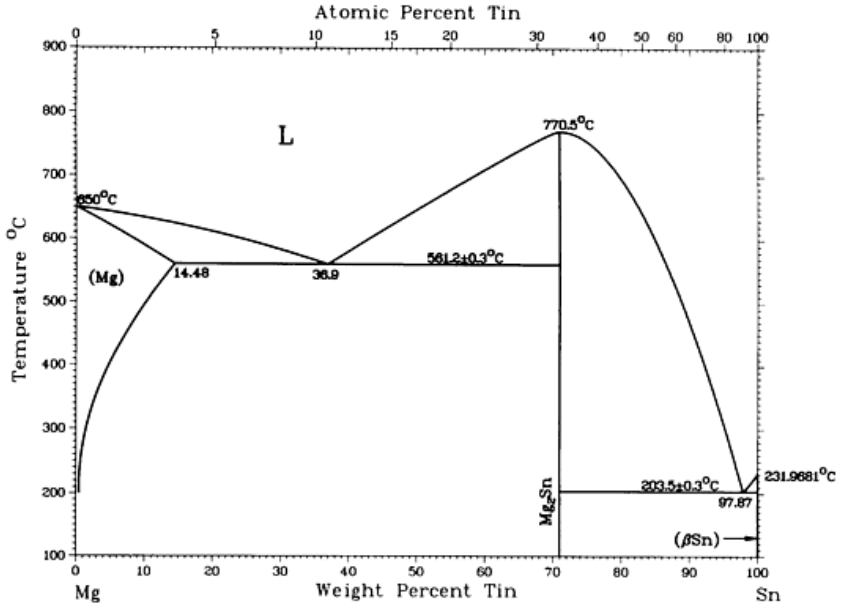

Figure 5.1: Mg-Sn binary phase diagram [33]

The actual initial melting onsets for the Mg/Sn couples were measured to be in the range of 217°C to 226°C indicating incomplete metallurgical contact between the phases at the start. This is further supported by the cooling traces of Figures 4.1.1

and 4.1.2 heated to only 235°C, where the solidification onset temperatures for filler metal begin at higher temperatures (i.e. 222°C to 227°C). This is indicative of the freezing of a Sn rich hypereutectic filler composition. Only after hold times of 60 minutes does the solidification temperature drop to the lower temperature of ~198°C expected from an undercooled filler metal with Mg-Sn eutectic composition. Samples heated to the higher peak temperature of 250°C (Figures 4.1.5 and 4.1.6) indicate a more rapid development of a low solidification temperature and therefore the development of a Mg-Sn eutectic filler metal composition. The reheat samples of Figure 4.1.9 indicate an onset melting temperature of ~203°C, consistent with the melting point of the Mg/Sn binary eutectic. The heating trace of Figure 4.1.9 also indicates that the Zn immersion coating does initiate a small ternary Mg-Zn-Sn eutectic melting event. However, once a fully developed liquid filler metal layer is established, the Zn content is minimal to have any impact on the melting behaviour.

Referring to the Mg-Sn binary phase diagram, heating the Mg/Sn binary couple further to 350°C and 450°C is expected to increase the liquid volume fraction at the joint interface due to an increased solubility of Mg in the liquid. A schematic of joint evolution as it is heated up to 450°C and cooled back to room temperature can be seen from Figure 5.2.

During the heating stage, due to solid state diffusion, Mg_2Sn intermetallics are expected to form before first occurrence of any liquid at the joint interface. As the joint is further heated, Mg-Sn eutecitc liquid appears at ~203.5°C (if complete equilibrium is established) followed by full melting of the filler metal as Sn melts at ~232°C. The joint geometry is expected to have a center liquid zone with intermetallics present on either side. With increasing peak temperatures from 235°C to 250°C, 350°C and 450°C the composition of the liquid will change to a higher Mg value, with the possibility of an increased liquid fraction.

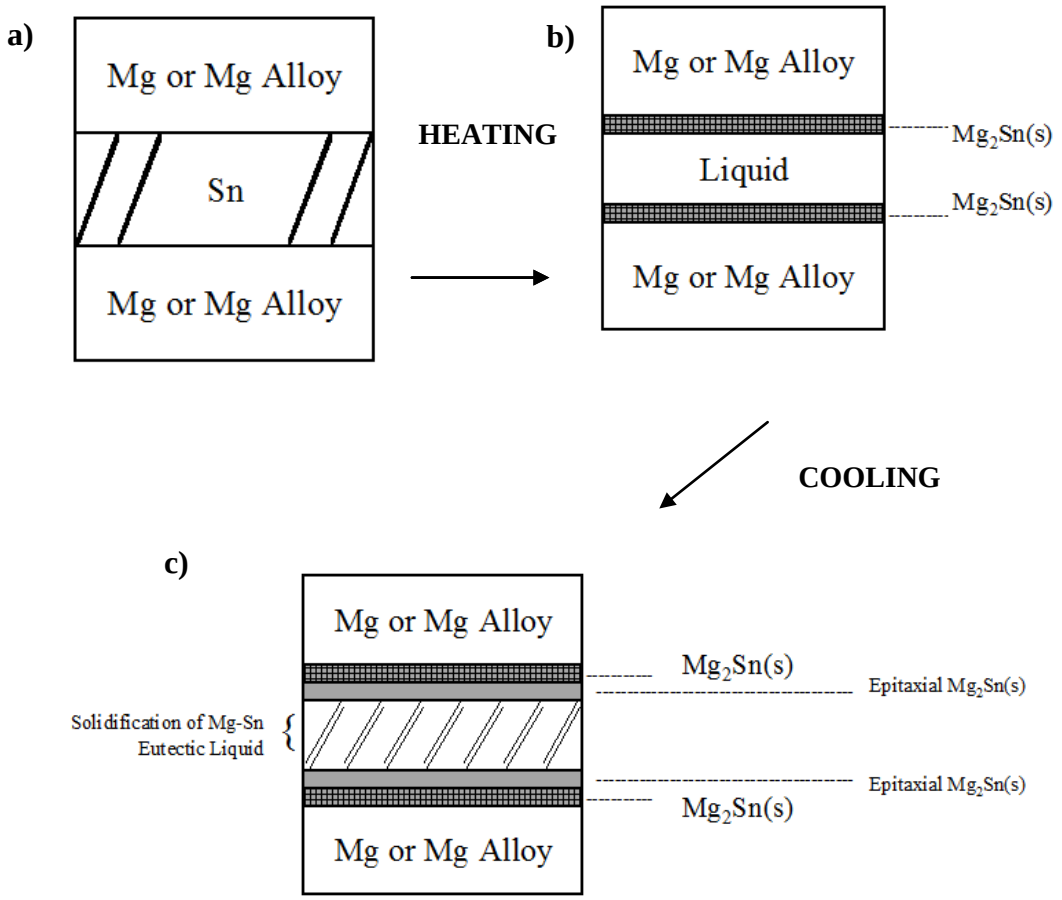

Figure 5.2: a) Unheated Sn filler metal joint; b) Sn filler metal behaviour as the joint assembly is heated up to 450°C and c) Sn filler metal behaviour as the joint assembly is cooled from 250°C, 350°C or 450°C

Inspection of the Mg-Sn phase diagram indicates that epitaxial growth of Mg_2Sn during cooling from higher temperatures is possible (see Figure 5.2c). However, no direct evidence of this process was identified in the DSC trace or polished cross sections. For all peak temperatures, the only solidification event observed was the Mg/Sn eutectic event. Complete isothermal solidification was not found with respect to increase in temperature or increase in time. Incomplete isothermal solidification can be attributed to very slow diffusion through the Mg_2Sn intermetallic layer at the faying surfaces.

b) Joining Mg using Sn-9Zn Eutectic Filler Metal

An explanation of the melting, solidification behaviour and microstructural evolution in the Mg/Sn-9Zn couples of Section 4.2 can begin with reference to the binary Sn-Zn and Mg-Zn phase diagrams in Figures 5.3 and 5.4, and the ternary Mg-Sn-Zn liquidus projection in Figure 5.5.

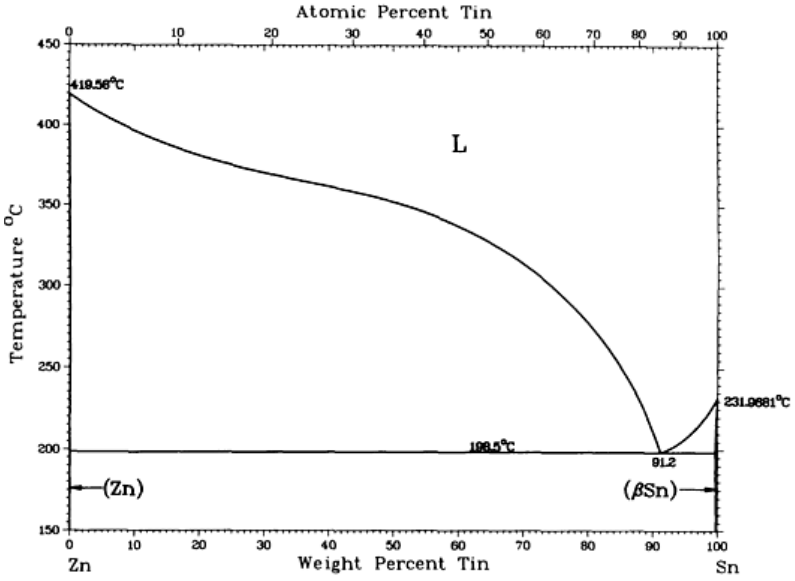

Figure 5.3: Sn-Zn binary phase diagram [33]

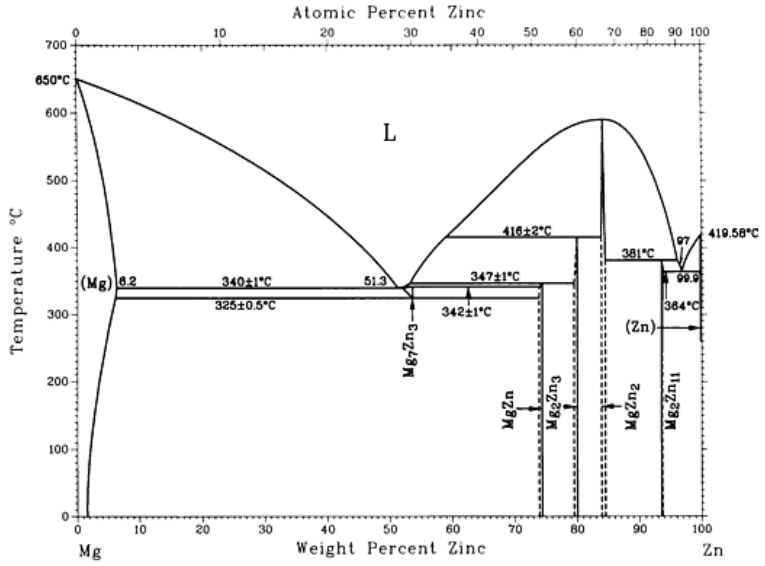

Figure 5.4: Mg-Zn binary phase diagram [33]

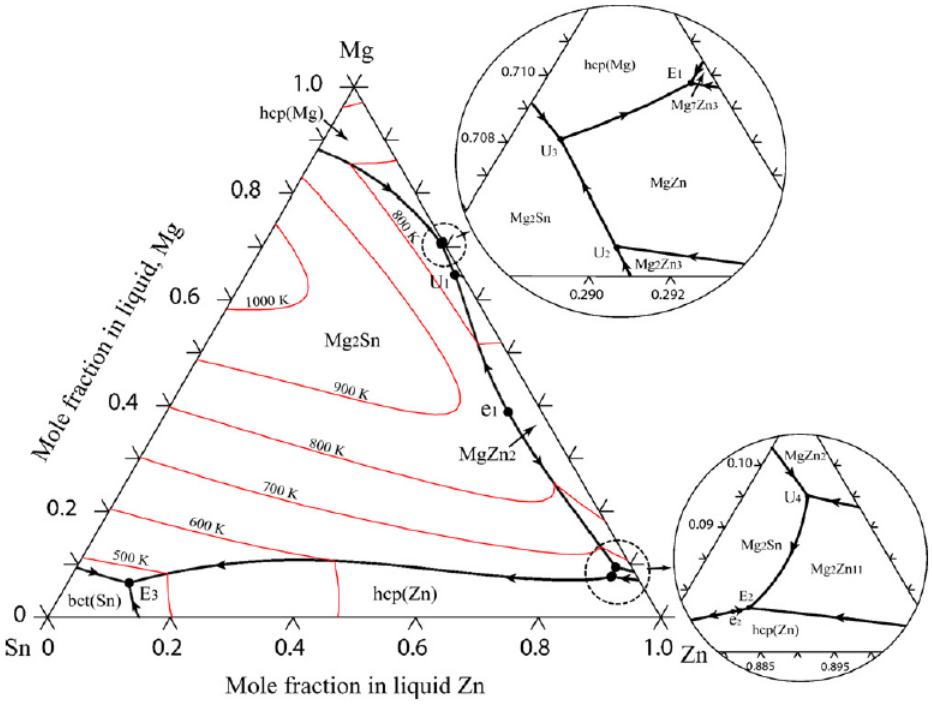

Figure 5.5: Mg-Sn-Zn ternary phase diagram [58]

The pre-alloyed Sn-9 wt% Zn eutectic filler powder used in these experiments has a melting point of 198.5 °C. In addition, as Figure 5.5 indicates, interaction with the Mg base metal could result in the formation of a termary Mg-Sn-Zn eutectic (E_3) with a melting point 186°C [58].

The behaviour of the Mg/Sn-9Zn braze couple has some similarities with the Mg/Sn couple. Heating to the relatively low temperature of 202°C, results in a gradual shift in the filler metal composition toward the Mg-Sn-Zn eutectic composition. This is evidenced by the higher onset temperatures of solidification during cooling in the traces of Figures 4.2.1 and 4.2.3. Heating to higher temperature (i.e. 235°C to 250°C) leads to a rapid development of a filler metal which exhibits a lower solidification temperature during cooling indicative of a Mg-Sn-Zn composition.

Using FactSage [59] software, an isothermal section of the ternary Mg-Sn-Zn phase diagram at 250 °C was produced (Figure 5.6). Superimposed on this diagram is a tie line from Pure Mg to the Sn-9 wt% Zn filler composition. The production of vertical sections using FactSage software was beyond the scope of this project. However Meng et al. [58] produced a vertical section at 3 wt% Zn over the Sn rich corner of the pseudo-binary Mg-Sn phase diagram as can be referred from Figure 5.7.

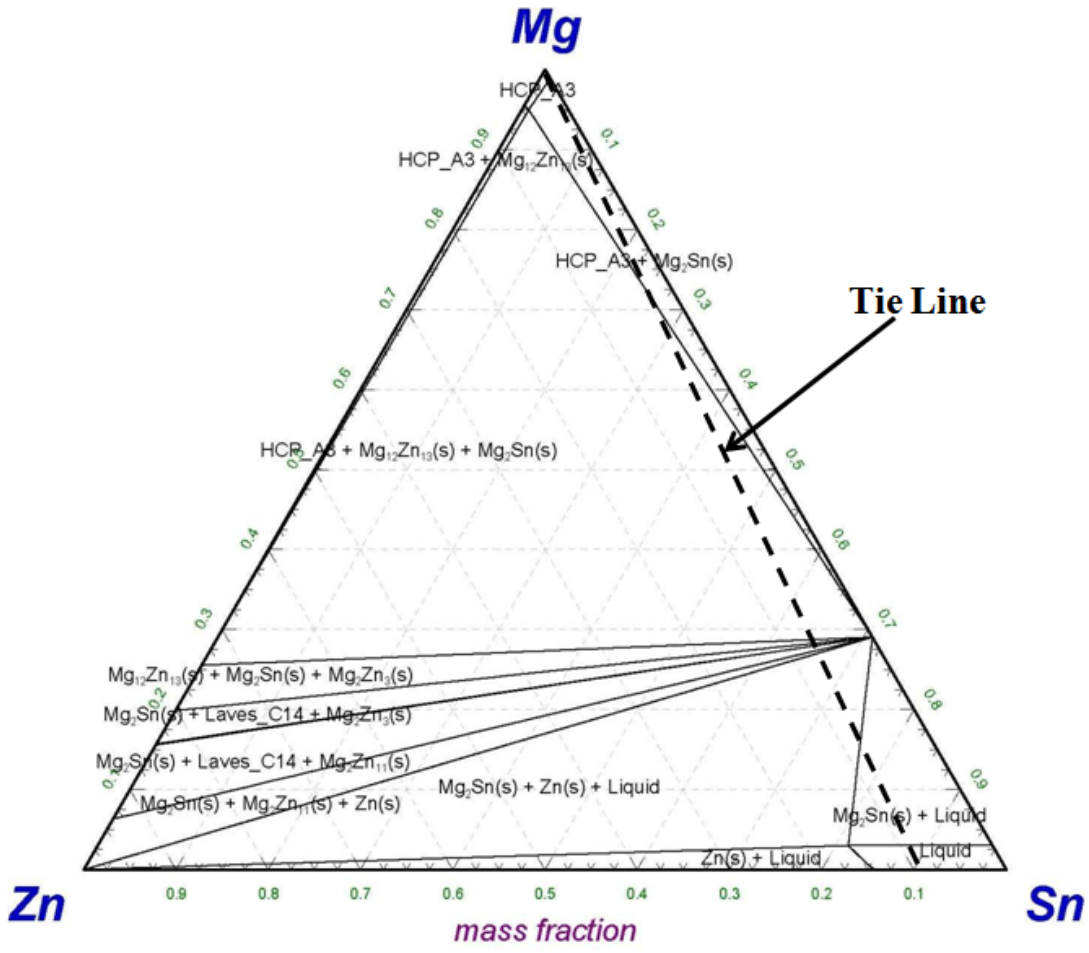

Figure 5.6: Mg-Sn-Zn Ternary Phase diagram isotherm at 250°C (Generated using FactSage Software [59]**)**

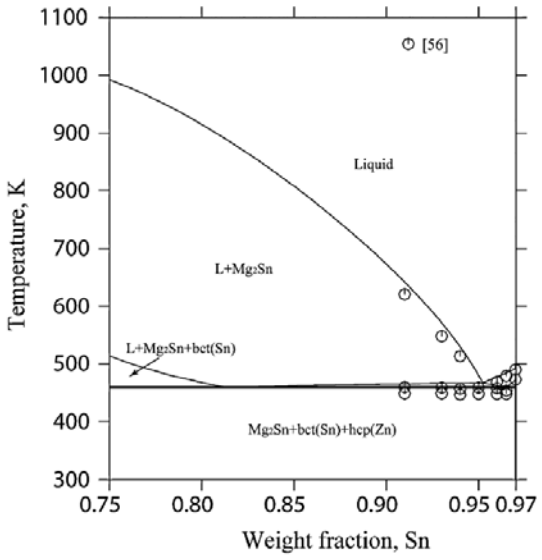

Figure 5.7: Calculated vertical section at the 3 wt% Zn in Mg-Sn-Zn ternary system with experimental data [58]

Based on these phase diagram prediction, the expected diffusion couple that would develop at 250°C is depicted in Figure 5.8. The filler metal liquid layer would be Sn rich and in equilibrium with Mg_2Sn layer. All of the microstructural evidence of Section 4.2 supports this microstructural feature, an example of which is reproduced here in Figure 5.9.

The tie line construction of Figure 5.6 indicates that a series of Mg_xZn_y intermetallic phases are also thermodynamically feasible within the diffusion couple which forms between Pure Mg and a Sn rich, Zn containing liquid phase. These phases would grow between the Mg base metal and Mg_2Sn layers. In Figure 5.8 these various possible phases are combined into an Intermetallic Compound (IMC) zone. None of the experimental Mg (or Mg alloy)/Sn-9Zn couples of Section 4.2 that were heated to 250°C exhibited an IMC layer. This is due to the slow growth rate of these layers at 250°C.

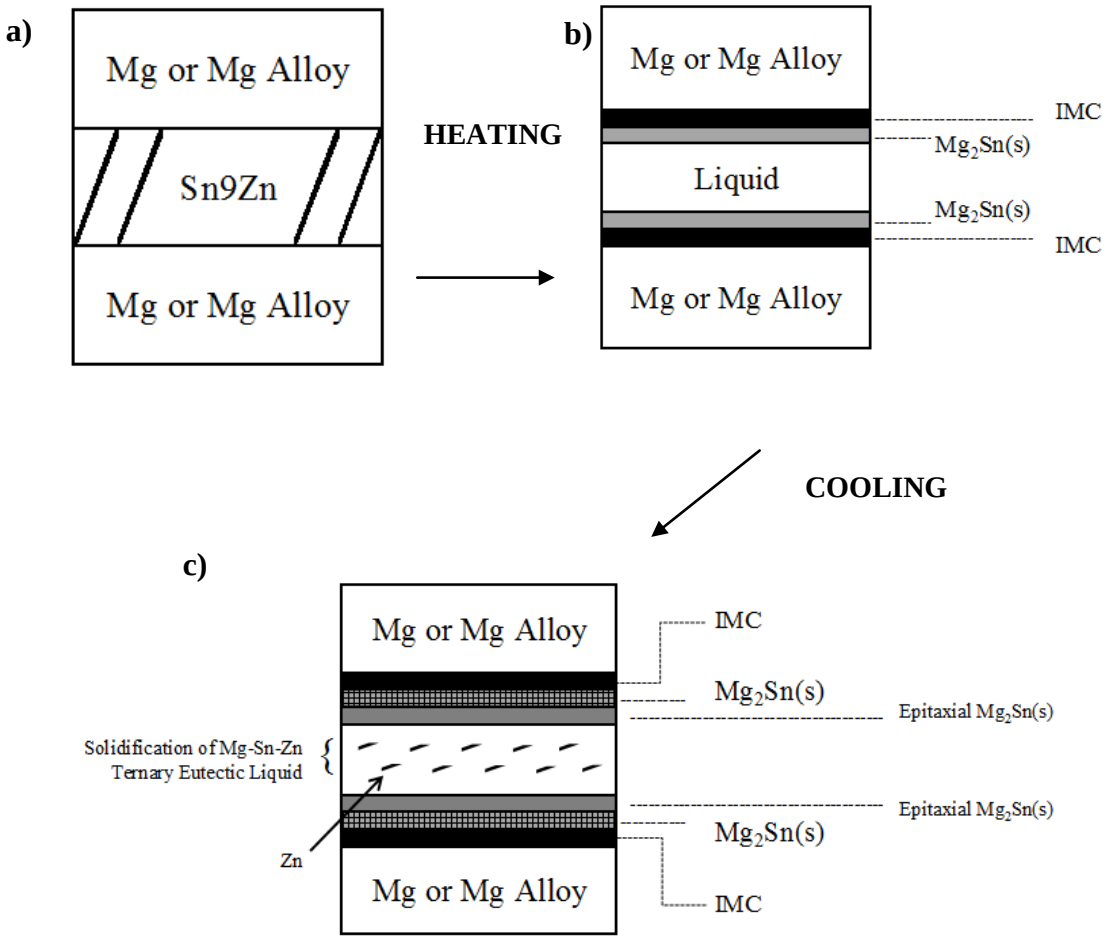

IMC = Mg_7Zn_3(s), MgZn(s), Mg_2Zn_3(s), $MgZn_2$(s) or Mg_2Zn_{11}(s)

Figure 5.8: a) Unheated Sn-9Zn filler metal joint; b) Sn-9Zn filler metal behaviour as the joint assembly is heated up to 250°C and c) Sn-9Zn filler metal behaviour as the joint assembly is cooled from 250°C

During cooling from 250°C, epitaxial Mg_2Sn growth can be expected, followed by Mg-Sn-Zn ternary eutectic composition solidification (see the vertical section of the ternary diagram of Figure 5.7). It is during this stage that Zinc solidifies into needle like solid plates. DSC and SEM images for samples at 202°C, 235°C and 250°C from Section 4.2 provide conclusive proof of the ternary solidification process (see Figure 5.9 for example).

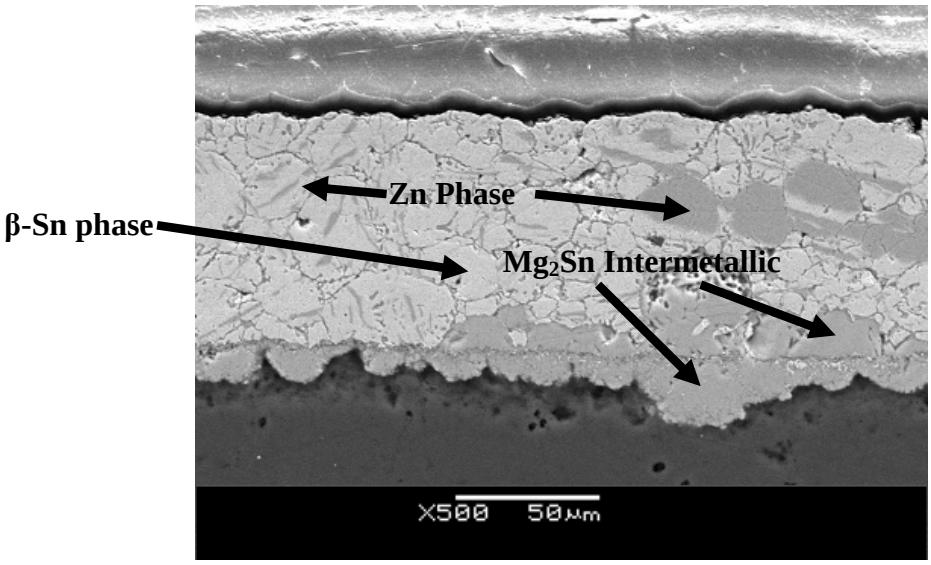

Figure 5.9: Approximate ternary joint microstructure at 235°C

In order to assess the joint evolution to promote further interactions with the Mg substrate, and perhaps destabilize the Mg_2Sn intermetallic layer, samples were further heated to 350°C and 450°C. FactSage was used to produce isothermal sections of the Mg-Sn-Zn ternary phase diagram at 350°C and 450°C as indicated in Figures 5.10 and 5.11 respectively. A tie line construction similar to that of Figure 5.6 is also superimposed on these figures. The primary differences in the phase equilibria predictions upon heating to 350°C are; increasing solubilities of Mg in the Sn rich liquid phase, increasing solubilities of Sn in the Mg base metal and the introduction of Mg-Zn eutectic liquid phase within the region of the IMC portion of the diffusion couple.

The concept joint while heating further to 350°C can be referred to in Figure 5.12. As the entire assembly is heated past ~325°C to ~340°C, Mg_7Zn_3 intermetallic along with other intermetallics including MgZn, Mg_2Zn_3, $MgZn_2$ or Mg_2Zn_{11} are expected to be noted depending on favourable metallurgical conditions for each intermetallic composition. The phases are expected to grow at the Mg_2Sn and Mg

interface boundary. As the assembly crosses the threshold temperature of ~340°C; first Mg-Zn eutectic liquid formation can be expected (see Figure 5.12b).

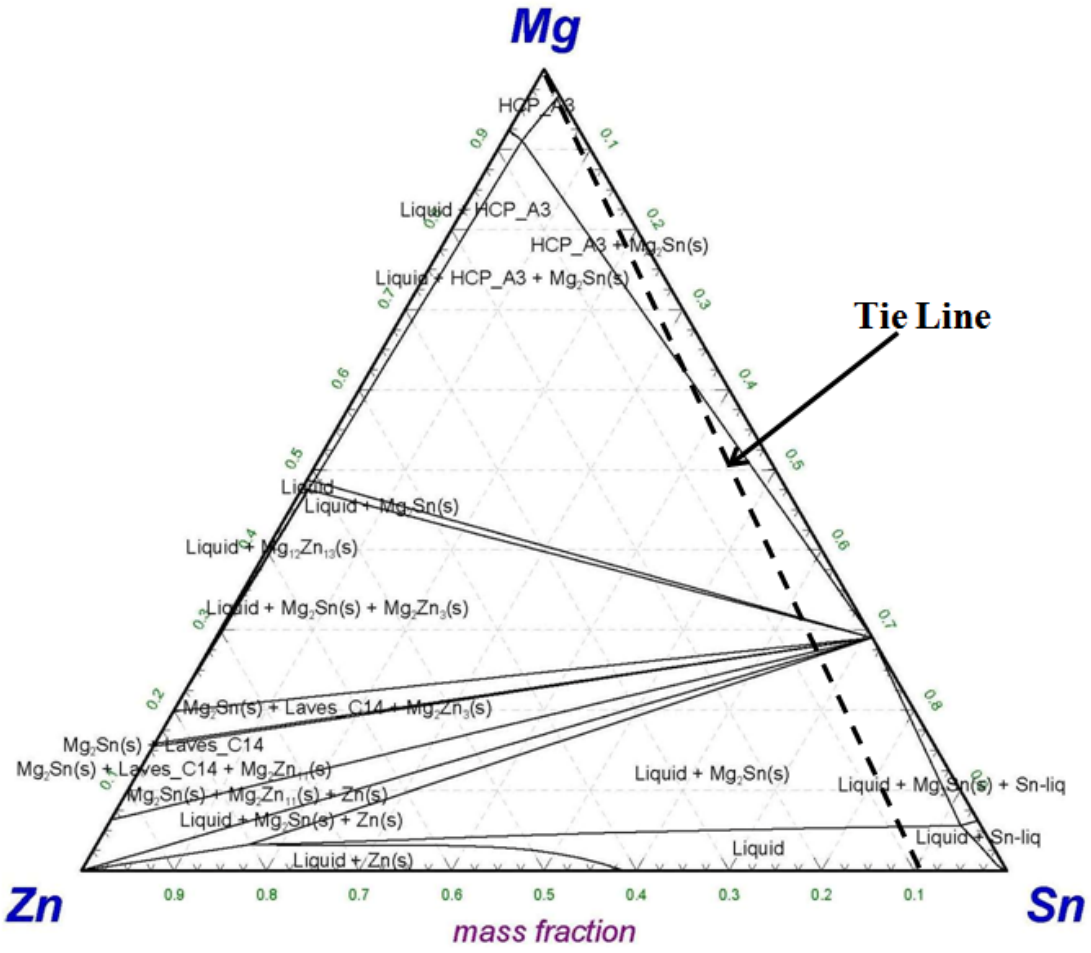

Figure 5.10: Mg-Sn-Zn Ternary Phase diagram isotherm at 350°C(Generated using FactSage Software [59]**)**

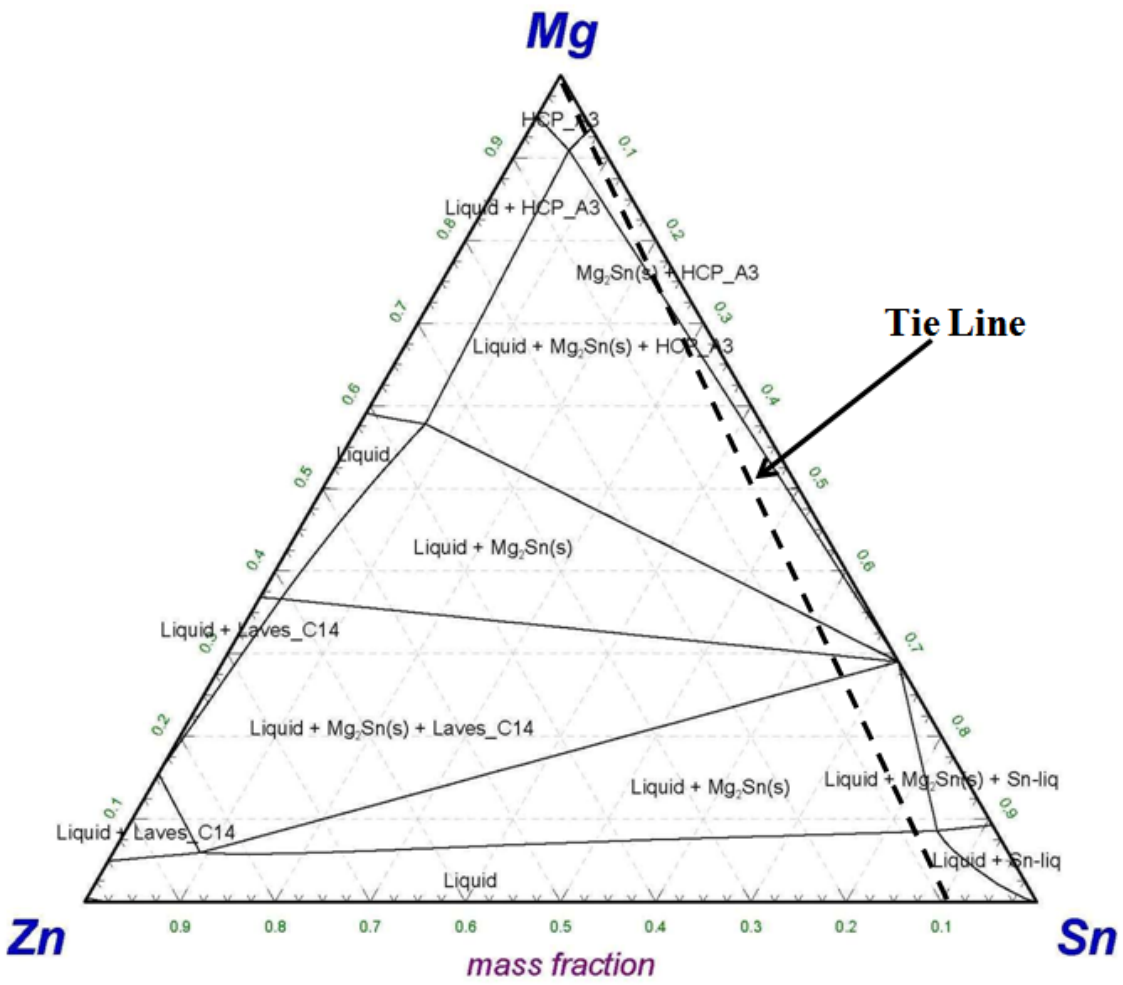

Figure 5.11: Mg-Sn-Zn Ternary Phase diagram isotherm at 450°C (Generated using FactSage Software [59]**)**

The results for the Mg Alloy/Sn-9Zn couples from Section 4.2 show no evidence of the formation of Mg_xZn_y, layers or Mg-Zn eutectic liquid phase formation while heating up to 350°C. The Pure Mg/Sn-9Zn does show some isolated evidence of Mg-Zn liquid phase formation, but only in the form of a solidification event upon cooling from 350°C. No initial melting at a temperature of 340°C, corresponding to the Mg-Zn eutectic temperature is observed in the DSC trace during initial heating of this sample.

a)

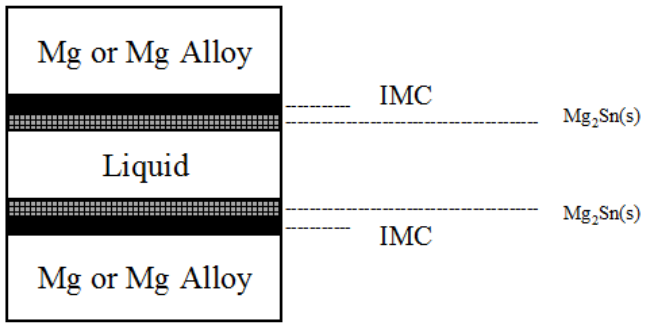

IMC = $Mg_7Zn_3(s)$, $MgZn(s)$, $Mg_2Zn_3(s)$, $MgZn_2(s)$ or $Mg_2Zn_{11}(s)$

b)

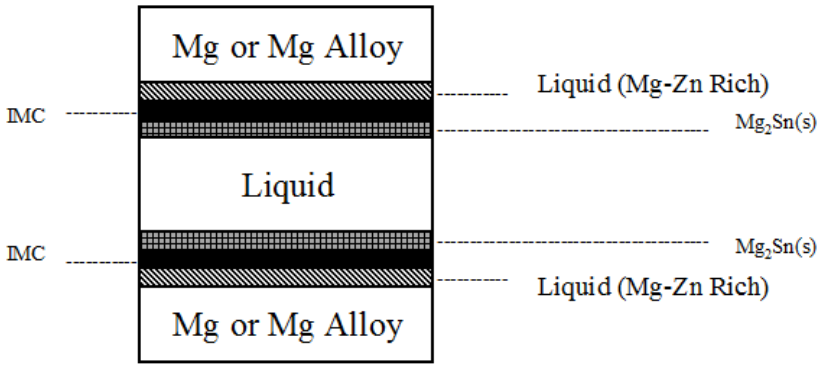

IMC = $Mg_2Zn_3(s)$, $MgZn_2(s)$ or $Mg_2Zn_{11}(s)$

Figure 5.12: a) Sn-9Zn filler metal behaviour as the joint assembly is heated to ~330°C and b) Sn-9Zn filler metal behaviour as the joint assembly is heated to ~350°C

Strictly speaking, the above thermodynamic predictions are only directly applicable to the Pure Mg/Sn-9Zn couples, since the use of the base metal alloy introduces a fourth element (i.e. Al) into the phase equilibria process. Even in the case of the Pure Mg/Sn-9Zn couple, (ignoring the Zn from the immersion coating), the source of Zn is from the filler metal. The continuous Mg_2Sn intermetallic layer formed between the Mg base metal and filler liquid phase may inhibit the diffusion of Zn to the Mg interface. This could explain why the IMC layer and Mg-Zn eutectic phases are slow to form at both 250°C and 350°C. The presence of Al in the Mg substrate may further delay the formation of Mg-Zn phases. As indicated in the 450°C isothermal ternary diagram of Figure 5.11, further heating to 450°C means

more dissolution of Mg base metal into the liquid Mg-Zn zone and a further increase in Sn solubility in the Mg base metal. Another important difference at 450°C is the absence of a number of Mg-Zn intermetallic phases including MgZn, Mg_2Zn_3, and Mg_2Zn_{11}. Only $MgZn_2$ (i.e. Laves C14) remains. This feature can be better understood by inspecting the binary Mg-Zn phase diagram of Figure 5.4 and the vertical section of the Mg-Sn-Zn phase diagram produced by Meng et al. [58] at a fixed Sn composition of 40wt% (Figure 5.13). All other Mg-Zn intermetallics are unstable above ≈400°C to 416°C. Based on this, the concept diffusion couple when the joint assembly is heated up to ~450°C is presented in Figure 5.14.

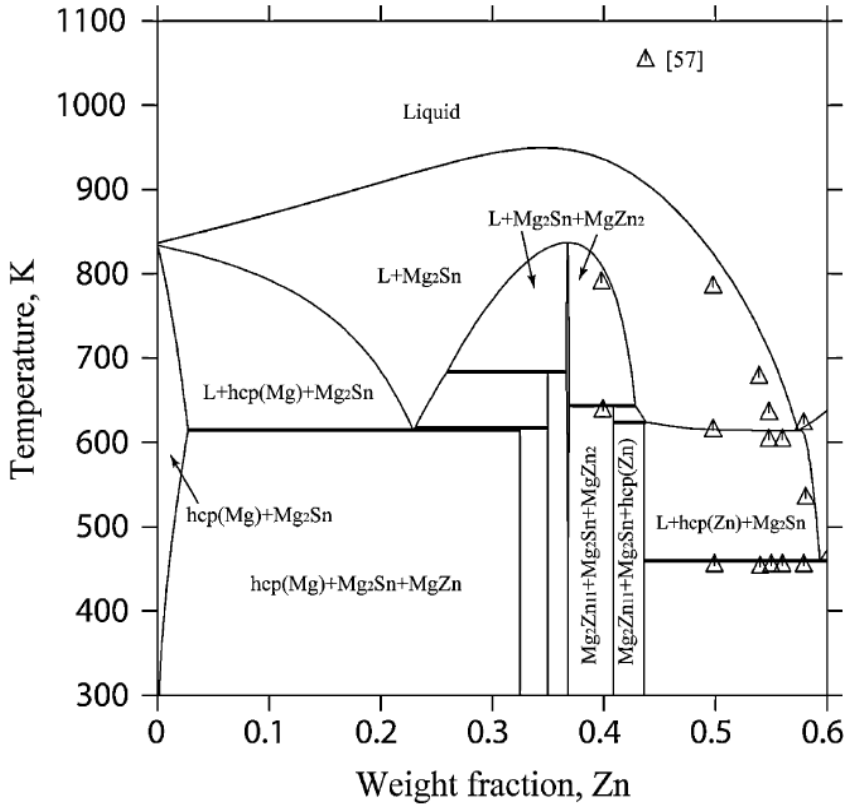

Figure 5.13: Calculated vertical section at the 40 wt% Sn in Mg-Sn-Zn ternary system with experimental data [58]

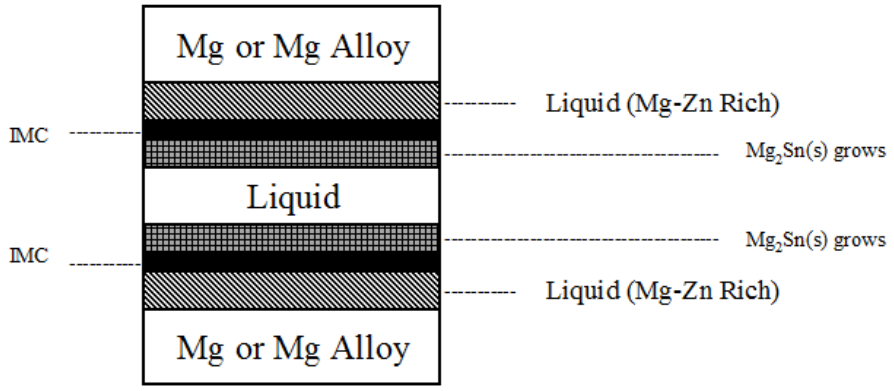

IMC = $MgZn_2$(s)

Figure 5.14: Sn-9Zn filler metal behaviour as the joint assembly is heated to ~450°C

As with the 350°C samples, no initial melting at 340°C is observed in the DSC trace during initial heating. However both, the microstructure of the post 450°C heated sample and the DSC cooling traces clearly show the solidification of a liquid phase according to the Mg-Zn eutectic reaction. This process is described schematically in Figure 5.15 and occurs for both the Pure Mg and Mg Alloy base metals. Note that during cooling it is also possible to re-develop the other Mg-Zn intermetallic phases through solid state reactions. No evidence of this solid-state reaction was present in the cooled 450°C samples.

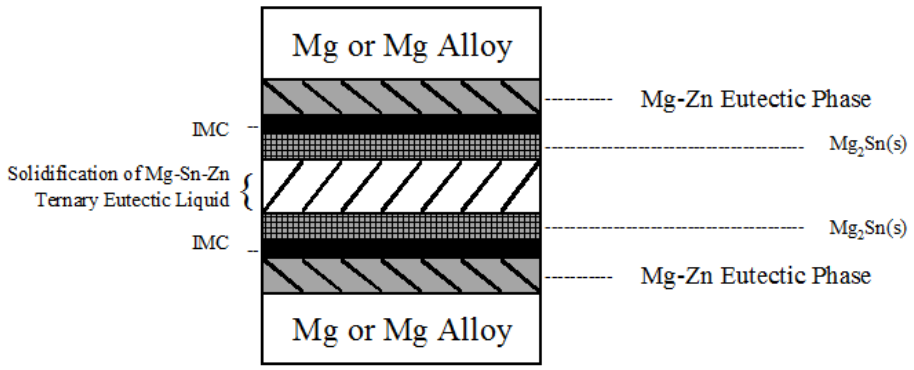

IMC = Mg_7Zn_3(s), MgZn(s), Mg_2Zn_3(s), $MgZn_2$(s) or Mg_2Zn_{11}(s)

Figure 5.15: Sn-9Zn filler metal behaviour as the joint assembly is cooled from 350°C and 450°C

The 350°C and 450°C experimental results indicate that a complex diffusion couple develops in the joint assemblies and that the behaviour is not entirely predicted by the ternary phase equilibria. To investigate the significance of the diffusion couple reactions present in the system and the temperatures of importance, three further sets of experiments were carried out at 375°C, 400°C and 425°C respectively. Table 5.1 summarizes the experiments performed while the thermal profiles can be referred to from Figure 5.16.

Consistent with the previous results, the DSC initial heating traces of Figure 5.16 show some broad exothermic baseline shifts above 340°C but no endothermic peak that would indicate Mg-Zn eutectic melting reaction. During cooling, all samples (except the Mg Alloy couple cooled from 350°C) exhibit a small exothermic solidification peak at ~330°C. The magnitude of this peak increases with an increase in maximum temperature heated to. The Mg Alloy couple heated to 375°C exhibits only a small solidification peak at 330°C, while the sample couple heated to 450°C exhibits several solidification peaks over the entire cooling trace down to 300°C.

Table 5.1: Experiments using Sn-9Zn Filler metal at temperatures 375°C, 400°C and 425°C

Sample ID.	Base Metal	Maximum Testing Temperature	Hold Time
5.1-(P)Mg-Sn9Zn-375-0	Zn Plated Pure Mg	375°C	0 min
5.2-(A)Mg-Sn9Zn-375-0	Zn Plated Mg Alloy	375°C	0 min
5.3-(P)Mg-Sn9Zn-400-0	Zn Plated Pure Mg	400°C	0 min
5.4-(A)Mg-Sn9Zn-400-0	Zn Plated Mg Alloy	400°C	0 min
5.5-(P)Mg-Sn9Zn-425-0	Zn Plated Pure Mg	425°C	0 min
5.6-(A)Mg-Sn9Zn-425-0	Zn Plated Mg Alloy	425°C	0 min

SEM images for the samples in Table 5.1 are depicted in Figure 5.17. Examination of Figure 5.17 a, c and e indicates a progression in the Pure Mg/Sn-9Zn diffusion couple microstructure. A prominent Mg_7Zn_3 intermetallic layer was found

at the Mg/Mg_2Sn interface in the Pure Mg couple cooled from 375°C. Despite the lack of a two phase Mg-Zn eutectic structure evident in the polished section of this cooled sample, a distinct solidification peak does occur in the DSC trace around 330°C. This can be understood with reference to the binary Mg-Zn phase diagram of Figure 5.4.

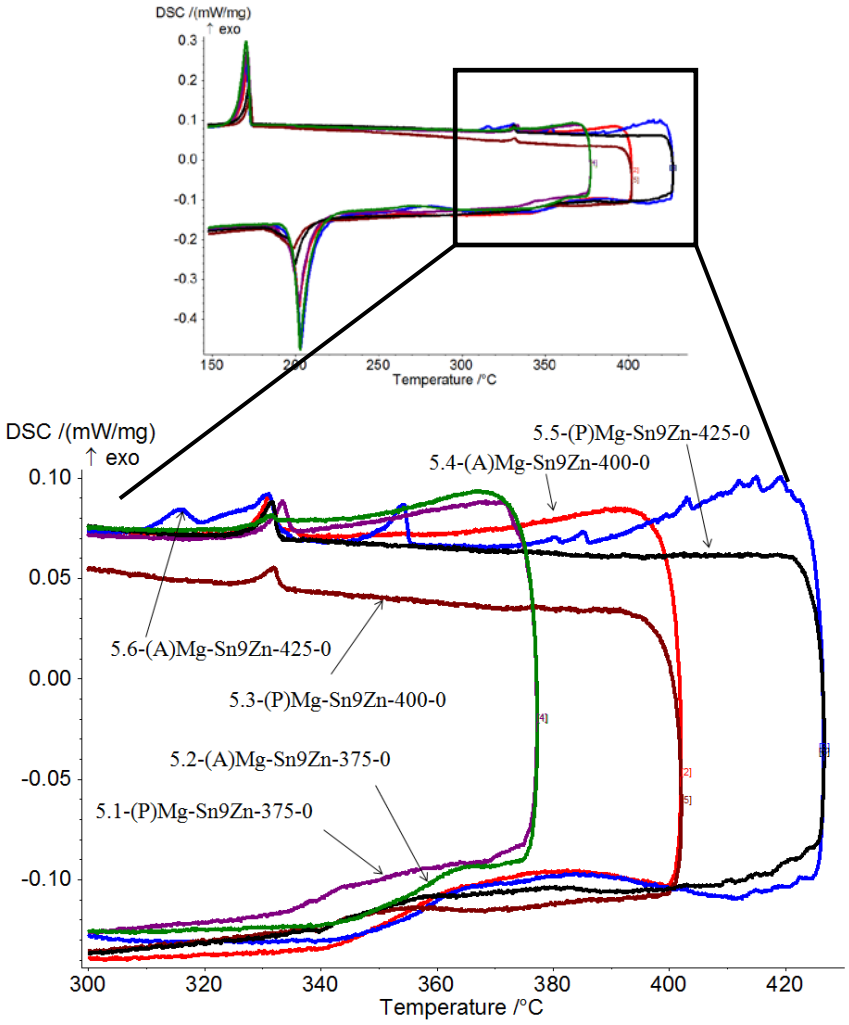

Figure 5.16: DSC Traces with Sn-9Zn filler metal at 375°C, 400°C and 425°C for Pure Mg and Mg Alloy

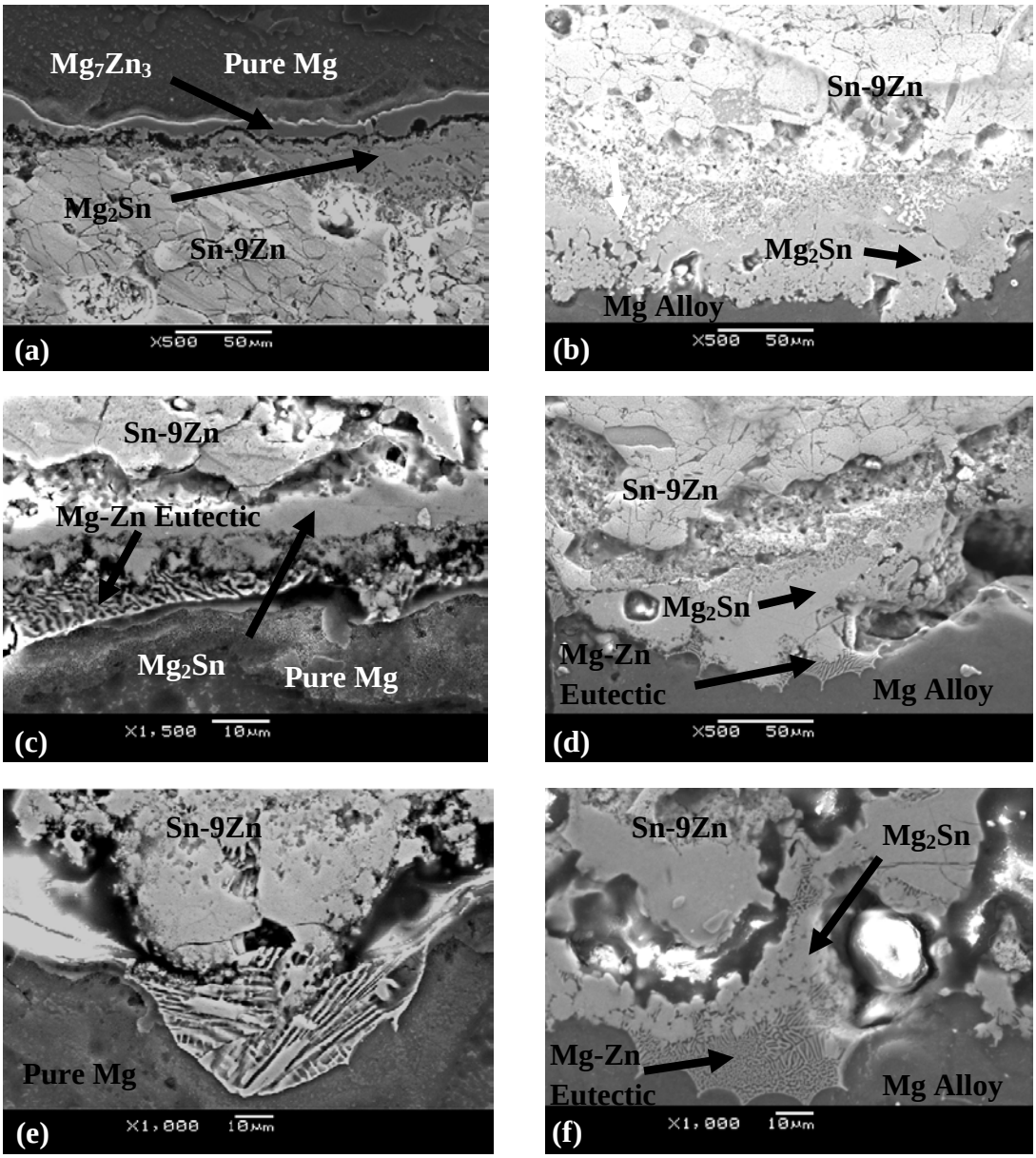

Figure 5.17: SEM Micrographs for samples (a) 5.1-(P)Mg-Sn9Zn-375-0, (b) 5.2-(A)Mg-Sn9Zn-375-0, (c) 5.3-(P)Mg-Sn9Zn-400-0, (d) 5.4-(A)Mg-Sn9Zn-400-0, (e) 5.5-(P)Mg-Sn9Zn-425-0 and (f) 5.6-(A)Mg-Sn9Zn-425-0

According to Meng et al. [58], Ghosh et al. [60] and Figure 5.4, a eutectoid reaction at a composition of 28.1 at% Zn occurs in the binary Mg-Zn system at 321°C to 325°C as:

$$MgZn + (Mg) \leftrightarrow Mg_7Zn_3 \qquad (5\text{-}1)$$

In addition, a peritectic and eutectic reaction takes place in the range of 340°C to 345°C as:

$$Mg_7Zn_3 \leftrightarrow (Mg) + L \quad (5\text{-}2)$$

$$Mg_7Zn_3 + MgZn \leftrightarrow L \quad (5\text{-}3)$$

with the peritectic reaction (5-2) occurring at a slightly lower temperature than the eutectic (5-3) reaction.

A further complication in the reactions listed above occurs when considering the ternary composition of the diffusion couple. With the addition of Sn, a ternary eutectic reaction is possible;

$$Mg_7Zn_3 + (Mg) + Mg_2Sn \leftrightarrow L \quad (5\text{-}4)$$

In addition, there are two ternary peritectic reactions;

$$Mg_7Zn_3 + Mg_2Sn \leftrightarrow MgZn + L \quad (5\text{-}5)$$

and;

$$MgZn + Mg_2Sn \leftrightarrow Mg_2Zn_3 + L \quad (5\text{-}6)$$

All of these ternary reactions take place at a temperature near that of the binary versions (i.e. ≈342°C), with the exception of (5-6) which takes place at 346°C. No mention of a ternary version of the eutectoid reaction (5-1) is present in the literature.

Based on the above evidence, it is clear that liquid formation around 342°C first requires the presence of the solid Mg_7Zn_3 intermetallic phase, which itself forms through the solid-state eutectoid reaction (5-1) at lower temperatures (≈ 321°C). This explains why melting at 340°C does not occur during initial heating. A metastable interface between the (Mg) and Mg_2Sn must exist which prevents the eutectoid reaction and the formation of Mg_7Zn_3 during heating. However, with further heating a

more well developed metallurgical interface forms, allowing the nucleation and growth of the Mg_7Zn_3 phase. At 375°C a liquid phase must be present, since a solidification peak develops upon cooling. The microstructure of this cooled sample (Fig. 5.17a) indicates that the solidification event must be according to the peritectic reaction (5-2) (or its ternary form (5-5)). Heating above 375°C, develops a liquid phase that, upon cooling, solidifies through the eutectic reaction (5-3) (or its ternary form (5-6)).

Both the DSC evidence of Fig. 5.16 and the microstructure of Fig. 17 b, d and f, indicate that a similar microstructural evolution occurs in the Mg Alloy/Sn-9Zn diffusion couple. The primary difference is a delay in the formation of Mg_7Zn_3 and the associated liquid phase formation until temperatures are as high as 400°C. This is likely due to the added presence of Al in the system which alters the complex phase equilibria necessary for the microstructural changes needed for liquid formation.

c) Joining Mg using Wide Gap Filler Metal

As indicated in Section 4.3, a wide gap TLPB approach was carried out by placing the base metal composition powder in the joint filler metal to promote faster isothermal solidification. Magnesium powder was placed in increments of 10wt% of the filler metal to create filler joint. The wide gap approach for joints heated up to 250°C can be schematically represented as can be seen from Figure 5.18. It is essentially the same process as joining magnesium with Sn-9Zn filler metal with addition of spherical particles to promote consumption of Sn-9Zn filler metal and achieve isothermal solidification over time. During the heating stage up to 250°C, before melting is observed, Mg_2Sn intermetallic is expected to form at the Mg/Sn-9Zn planar and spherical interfaces. Further heating allows Sn-9Zn liquid to form which increases in volume rapidly and quickly moves towards Mg-Sn-Zn ternary eutectic composition due to added combined surface area of planar and spherical interfaces and help Mg dissolve accelerating the liquid widening stage. Upon solidification, epitaxial Mg_2Sn growth is expected at the planar and spherical interfaces followed by a Mg-Sn-Zn ternary eutectic composition solidification.

Heating the entire joint assembly to 450°C adds more liquid volume due to Mg-Zn eutectic melting. Solidification behaviour for joint assemblies heated to 350°C and 450°C follow the same solidification behaviour of the planar joints described in Section 5b). A schematic of the wide gap joint during processing is represented in Figures 5.19 and 5.20. Adding additional magnesium in the joint filler metal promotes faster consumption of Sn-9Zn filler metal liquid phase. This ultimately leads to complete isothermal solidification of the joint.

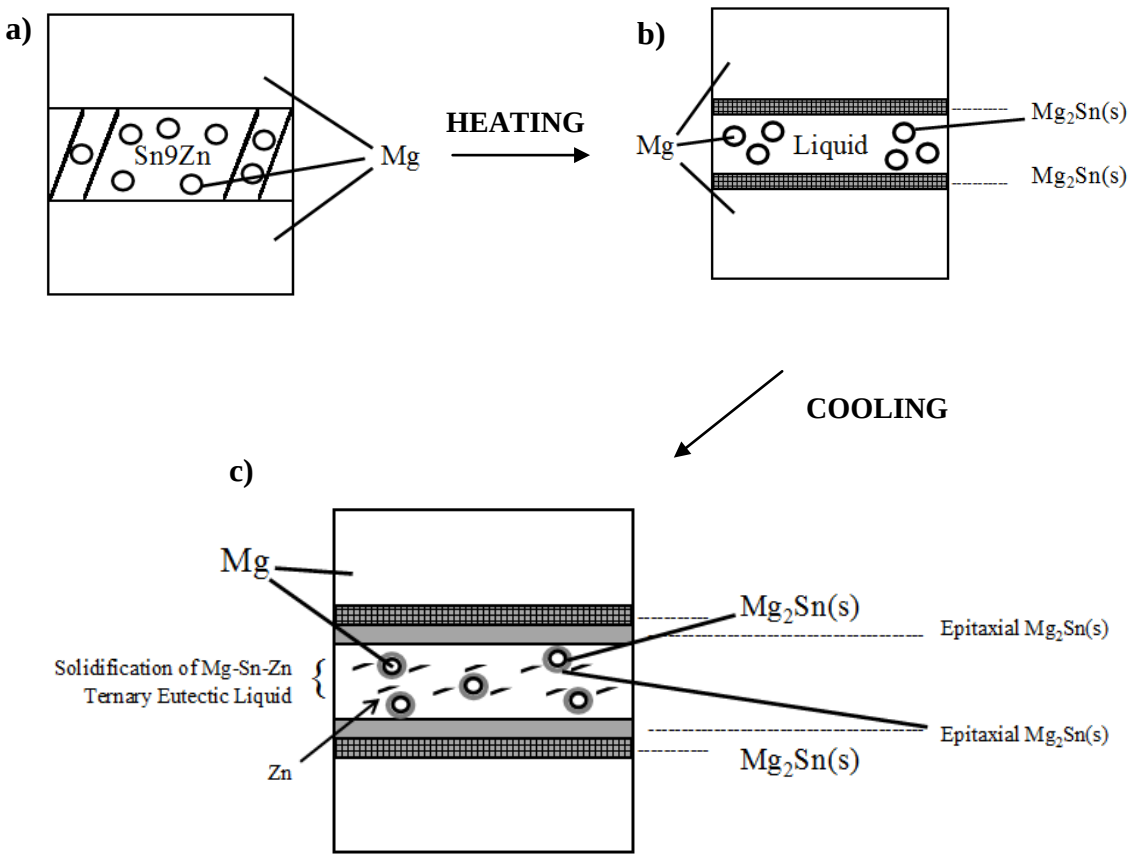

Figure 5.18: a) Unheated Sn-9Zn+Xwt% Mg filler metal joint; b) Sn-9Zn+Xwt% Mg filler metal behaviour as the joint assembly is heated up to 250°C and c) Sn-9Zn+Xwt% Mg filler metal behaviour as the joint assembly is cooled from 250°C

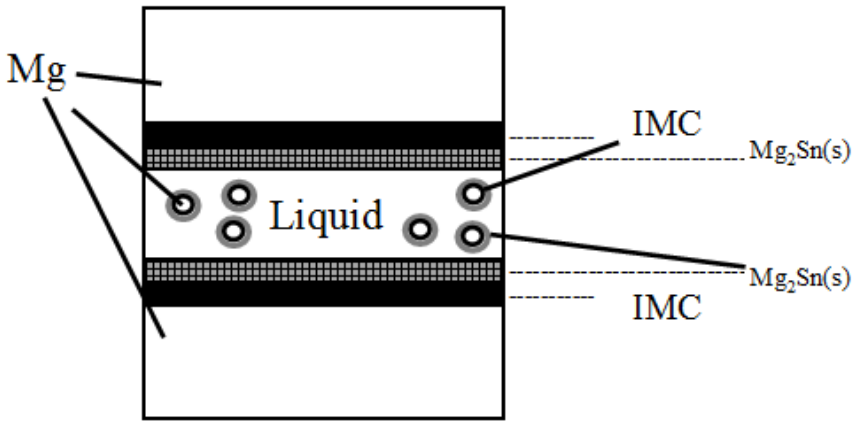

IMC = $Mg_7Zn_3(s)$, MgZn(s), $Mg_2Zn_3(s)$, $MgZn_2(s)$ or $Mg_2Zn_{11}(s)$

Figure 5.19: Sn-9Zn+Xwt% filler metal behaviour as the joint assembly is heated to ~330°C

a)

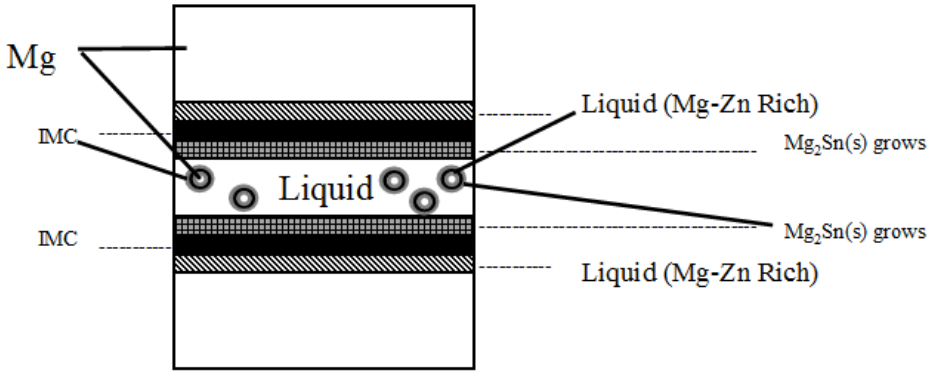

IMC = Mg_2Zn_3(s), $MgZn_2$(s) or Mg_2Zn_{11}(s)

b)

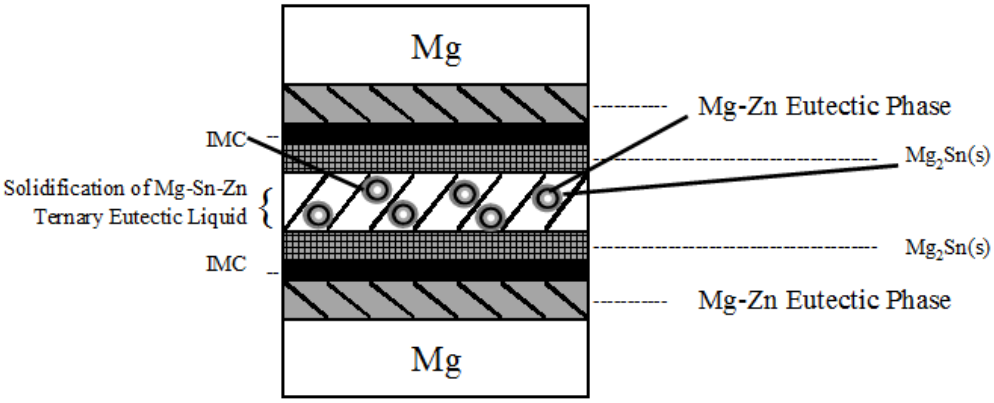

IMC = Mg_7Zn_3(s), MgZn(s), Mg_2Zn_3(s), $MgZn_2$(s) or Mg_2Zn_{11}(s)

Figure 5.20: a) Sn-9Zn+Xwt% filler metal behaviour as the joint assembly is heated to ~350°C and b) Sn-9Zn+Xwt% filler metal behaviour as the joint assembly is cooled from 350°C and 450°C

d) Joining Mg using Zn rich Filler Metal

The behaviour of the Pure Mg/Mg-Zn rich filler metal couples of Section 4.4 can be understood with reference to the schematic of Figure 5.21 for the case of a 50:50 wt% Mg:Zn filler mixture. Only the powder mixtures of the filler within the joint are depicted. The events shown here are identical at the filler / base metal planar faying surfaces). Because this is a binary mixture which places Pure Zn in direct contact with Pure Mg (i.e. with no complications due to Mg_2Sn formation), it is expected that a more rapid equilibrium interface will be developed. This should result in liquid phase formation around 342°C during initial heating. Melting upon initial heating is supported by the endothermic peaks in the DSC traces of Fig. 4.4.1 and 4.4.2. This melting process will first take place at the contact points between the Mg and Zn phases (Fig. 5.21b). However, the Zn is expected to undergo rapid dissolution, producing a liquid phase which spreads over the Mg particles (Fig. 5.21c). Diffusion of Zn into the Mg produces a solid-solution layer around the Pure Mg particles.

The DSC cooling trace for the Mg/Mg-Zn couple exhibits a solidification peak, further indicating a liquid phase. The microstructure of this sample heated to 350°C (Fig.4.4.3a) indicates the presence of Mg_7Zn_3 surrounding partially alloyed Mg particles. Therefore, like the samples of Section 4.2, cooling from 350°C produces the peritectic reaction (5-2) and the formation of solid Mg_7Zn_3. Mg-Zn solid solution zones and unreacted Mg particles are both evident in the microstructure of Figure 4.4.3a.

The bulk composition of the 50:50 Mg:Zn filler metal is very close to the eutectic composition. Despite this, it is clear from Fig. 4.4.3a that only limited melting and alloying between the Zn and Mg powders occur. This is due to the large particle sizes used, which slow the dissolution of the Mg particles into the Zn rich

liquid. At the same time Fig. 4.4.3a indicates that measureable dissolution of the Mg substrate by the Zn rich liquid occurs. This shifts the overall bulk composition of the filler metal region to a Mg rich hypoeutectic value, further preventing a full liquid filler metal layer.

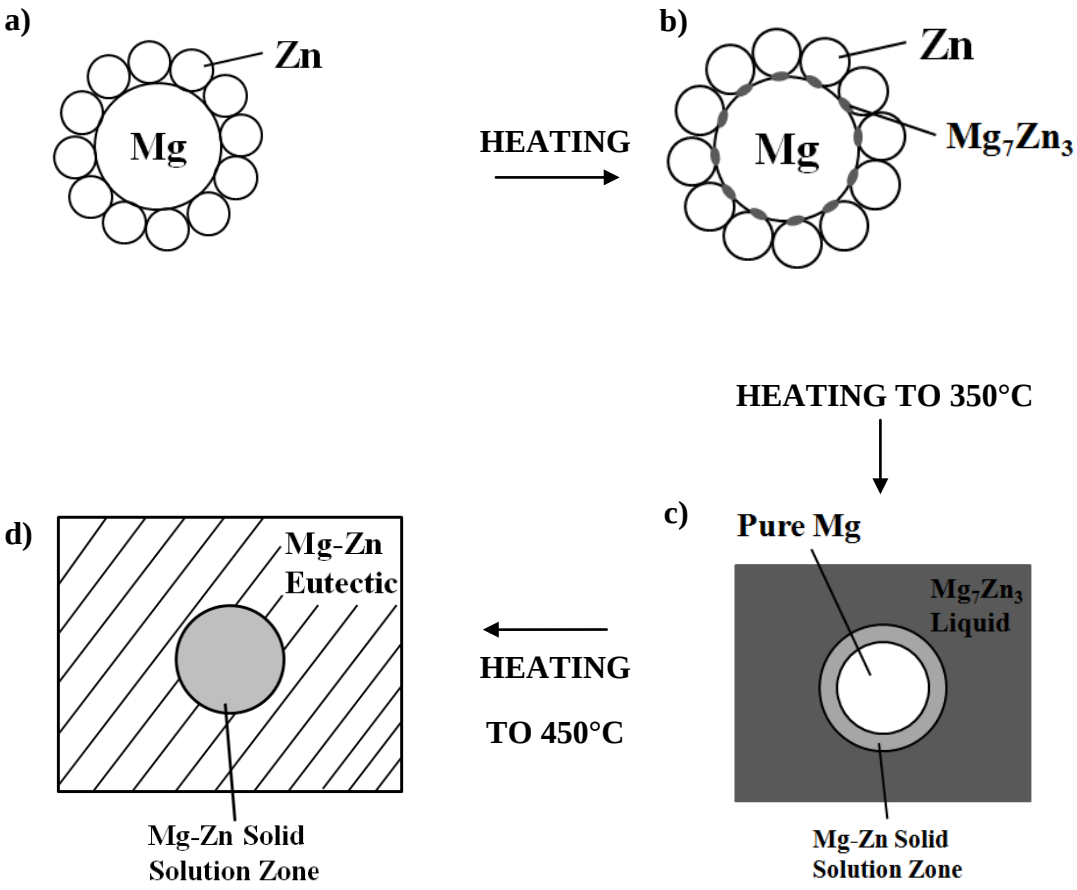

Figure 5.21: a) Filler metal Mg-Zn 50:50 wt% unheated; b) Filler metal behaviour as the joint assembly is heated to ~330°C; c) Filler metal behaviour as the joint assembly is heated to 350°C and d) Filler metal behaviour as the joint assembly is heated to 450°C

Heating the Mg/Mg-Zn couple to 450°C produces no further melting and the cooling trace exhibits a smaller solidification peak. The area under the solidification peak cooled from 350°C was measured as 20.14 J/g whereas the same peak cooled from 450°C was measured as 3.904 J/g. This indicates that the higher temperatures

produce more diffusional solidification as Zn diffuses further into the unreacted Mg powder and the Mg base metal. Fig. 4.4.4a indicates that the liquid that remains present at 450°C solidifies according to the eutectic reaction (5-3), which is similar to that exhibited for the samples of Section 4.2 when cooled from 450°C.

The presence of Sn-9Zn eutectic powder within the Mg and Zn filler metal mixture has a pronounced influence over the diffusion couple microstructural development. A schematic of joint evolution with the addition of Sn-9Zn powder is illustrated in Figure 5.22.

As the joint assembly is heated to ~250°C, Mg_2Sn intermetallics are expected at the boundaries of Mg and Sn-9Zn according to the results of Section 4.2. Contact between Sn-9Zn and Zn particles would result in interdiffusion, shifting the Sn-9Zn particle composition to towards zinc rich composition. No melting at the Sn-9Zn (or Sn rich ternary) temperatures of 186°C to 198°C was observed during the initial heating of the Mg/(Mg-Zn + Sn-9Zn) couples. This indicates that solid state diffusion and reaction between the Sn-9Zn and Mg and Zn powders was sufficient to "consume" the small amounts of Sn-9Zn powders added to the filler powder mixture, prior to reaching 174°C.

Further heating to ~350°C results in liquid formation similar to that seen in the Mg/Mg-Zn couple. The onset temperature of the endothermic melting peak for all of the Mg-Zn rich filler metal couples was measured between 339.2°C and 340.5°C. This is consistent with the predictions of Meng et al. [58] and Ghosh et al. [60] in that the presence of Sn and the ternary 3 phase reactions that develop, does not alter the temperatures at which the events take place.

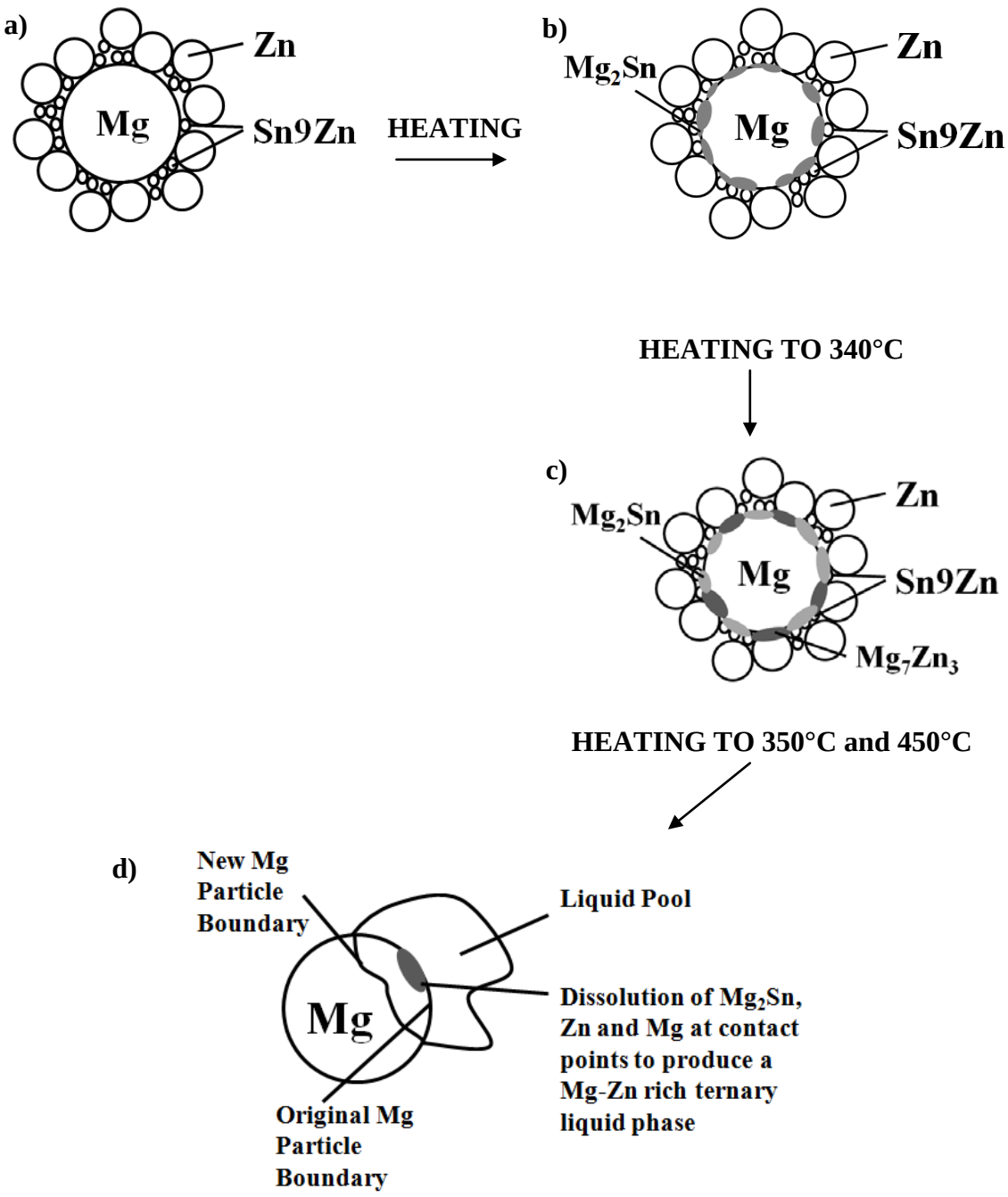

Figure 5.22: a) Filler metal Mg-Zn-(Sn-9Zn) 47.5:47.5:5wt% and 45:45:10wt% unheated; b) Filler metal behaviour as the joint assembly is heated to ~250°C; c) Filler metal behaviour as the joint assembly is heated to ~340°C and d) Filler metal behaviour as the joint assembly is heated to 350°C and 450°C

The cooling traces for the Mg/Mg-Zn couple with and without Sn-9Zn all exhibit a noticeable solidification peak. The Mg:Zn and Mg:Zn + 5% (Sn-9Zn) solidification peaks onset at a temperature of 338 °C, while the Mg-Zn + 10% (Sn-9Zn) onsets at 332°C. The area under the solidification peaks for the Mg:Zn couples with increasing Sn-9Zn and 350°C content are 20.14 J/g, 15.16 J/g and 38.9 J/g respectively. The microstructures of Fig. 4.4.3 all indicate that the solidification event is a peritectic reaction according to either equation (5-2) or (5-5), with Mg_7Zn_3 as the primary solid formed.

Fig. 4.4.3 also indicates that the addition of Sn-9Zn powder accelerates the alloying and dissolution of the Pure Mg particles in the filler metal (as schematically depicted in Fig. 5.22d). In the case of the filler containing 10% of Sn-9Zn, no Mg powder remained in the filler layer and this sample also exhibited the largest liquid formation, as indicated by the area under the solidification peak.

The microstructures of Fig. 4.4.4 and 4.4.5 indicate that, heating the Sn-9Zn containing couples to 450°C followed by cooling also results in a solidification process that occurs according to a eutectic reaction (presumably through the ternary reaction of equation (5-4)). Like the Mg/Mg-Zn couple, the solidification peak in the Mg/(Mg-Zn + 5% (Sn-9Zn)) cooled from 450°C, has a lower area under the curve (i.e. 9.2 J/g) compared to the same sample cooled from 350°C. This provides further evidence of diffusional solidification in this composition.

The area under the solidification peak for the Mg/(Mg-Zn + 10% (Sn-9Zn)) couple is the highest of all the samples at 41.31 J/g. This is consistent with the microstructure of this sample, which indicates a complex solidified structure indicative of a large volume fraction of liquid present at 450°C. This sample (Fig. 4.4.5) indicates that primary cellular grains of (Mg) grow from the Mg base metal

substrate. It also indicates that Mg_7Zn_3 solidifies in the intercellular region. This solidification mode eventually develops into a well developed eutectic solidification microstructure. In the original filler metal portion of the diffusion couple, a similar mixture of (Mg), Mg_7Zn_3 and eutectic appears but with a more dispersed character indicative of an equiaxed growth process.

A boundary is clearly visible in all of the diffusion couples of Fig. 4.4.3 through 4.4.5. It is believed that this demarks the original Mg substrate surface containing the Zn immersion coating. Overtime this coating may have oxidized allowing a semi-continuous MgO layer to form. This layer did not prevent metallurgical contact between the filler metal and Mg base metal. However, it was connected enough to remain as a physical feature within the diffusion couple.

6.0 Summary and Conclusion

During this work, Pure Mg and Mg Alloy base metal along with four filler metals (Sn, Sn-9Zn, Sn-9Zn+X wt%Mg and Mg:Zn:X(Sn-9Zn)) were used to evaluate the feasibility of forming Mg-Mg joints using soldering and brazing using Differential Scanning Calorimetry and microstructure characterization.

Successful joining of Magnesium to Magnesium was carried out first using Sn filler metal. A gradual shift in solidification onset to reach ~203.5°C and solidification of Sn rich hypereutectic filler composition was observed due to slow diffusion through the Mg_2Sn intermetallic layer when the samples were heated up to 250°C. In order to increase the liquid volume fraction due to increase in Mg solubility in liquid at the joint interface, the Mg/Sn binary couple was heated to 350°C and 450°C. No experimental evidence of Mg_2Sn epitaxial growth during cooling was identified in the DSC trace or polished cross sections. For all peak temperatures, the only solidification event observed was the Mg/Sn eutectic event and growth of Mg_2Sn intermetallics. Complete isothermal solidification was absent with respect to increase in time or temperature which can be attributed to very slow diffusion through the Mg_2Sn intermetallic layer. Zn immersion coating was found to have minimal impact on the melting behaviour of Mg/Sn binary diffusion couple due to the very small quantities.

Prealloyed Sn-9Zn was thus used in an attempt of lowering the joining temperature by promoting the formation of ternary Mg-Sn-Zn eutectic with a melting temperature of 179°C [59], 181°C [60], 183°C [61] or 186°C [58]. Similar to the Sn filler metal system, lower heating temperature (202°C) for the Sn-9Zn filler metal resulted in a gradual shift in the filler metal composition toward the Mg-Sn-Zn eutectic composition however, heating to higher temperature (235°C & 250°C) leads

to a rapid shift to a lower solidification temperature during cooling, indicative of a Mg-Sn-Zn composition which was conclusively proven through SEM images and DSC traces. Epitaxial Mg_2Sn growth, a series of Mg_xZn_y intermetallic phases as well as Mg-Sn-Zn ternary eutectic composition are thermodynamically possible while cooling the joint from a peak heating temperature of 250°C. However, Pure Mg and Mg Alloy couples did not exhibit any epitaxial Mg_2Sn growth or an IMC layer (Mg_7Zn_3(s), MgZn(s), Mg_2Zn_3(s), $MgZn_2$(s) or Mg_2Zn_{11}(s) (see Figure 5.8 for reference) in any experiments likely due to slow rate of growth rate of these layers.

Samples were then tested at 350°C and 450°C to possibly destabilize Mg_2Sn layer, promote Mg solubility in liquid as well as introduce Mg-Zn eutectic liquid within the region of the IMC portion of diffusion couple. Experimental results for Pure Mg/Sn-9Zn showed isolated evidence of Mg-Zn liquid in the form of a solidification event during cooling, while Mg Alloy/Sn-9Zn showed no evidence of eutectic liquid while cooling from peak heating temperature of 350°C. No evidence of Mg_xZn_y layers was observed for Pure Mg and Mg Alloy systems at 250°C and 350°C. This was due to the continuous Mg_2Sn intermetallic layer forming a diffusion barrier between the Mg base metal and the Zn containing liquid phase. Introduction of Al from Mg Alloy may further delay the formation of Mg_xZn_y phases.

Absence of a number of Mg_xZn_y phases was also noted while further heating the Mg(Pure and Alloy)/Sn-9Zn couple to 450°C. Only $MgZn_2$ (i.e. Laves C14) remained. No expected initial melting was observed at ~340°C. However both, the DSC cooling traces and the microstructure of post 450°C heated samples showed the solidification of a liquid phase according to the Mg-Zn eutectic reaction. Evolution of Mg/Sn-9Zn complex diffusion couple between 350°C and 450°C was investigated at 375°C, 400°C and 425°C. Evidence of a Mg-Zn eutectic reaction was absent during heating, while during cooling, all samples (except the Mg Alloy couple cooled from 350°C) exhibit a small exothermic solidification peak at ~330°C (undercooled Mg-Zn

eutectic) whose magnitude increases with an increase in maximum heating temperature.

From the experimental observations using Sn-9Zn filler metal, it is clear that a Mg-Zn rich eutectic liquid formation around 342°C first requires the presence of the solid Mg_7Zn_3 intermetallic phase, which itself forms through the solid-state eutectoid reaction ($MgZn + (Mg) \leftrightarrow Mg_7Zn_3$) at lower temperatures (≈ 321°C). A metastable interface between the (Mg) and Mg_2Sn must exist which prevents the eutectoid reaction and the formation of Mg_7Zn_3 during heating. The solidification event must be according to the peritectic reaction ($Mg_7Zn_3 \leftrightarrow (Mg) + L$) (or its ternary form ($Mg_7Zn_3 + Mg_2Sn \leftrightarrow MgZn + L$)). Heating above 375°C, develops a liquid phase that, upon cooling, solidifies through the eutectic reaction ($Mg_7Zn_3 + MgZn \leftrightarrow L$) (or its ternary form ($MgZn + Mg_2Sn \leftrightarrow Mg_2Zn_3 + L$)). Pure Mg and Mg Alloy systems were observed to behave in a similar fashion with the primary difference in Mg Alloy system being the delay in the formation of Mg_7Zn_3 and the associated liquid phase formation until temperatures are as high as 400°C. This is likely due to the added presence of Al in the system which alters the complex phase equilibria necessary for the microstructural changes needed for liquid formation.

A wide gap TLPB was carried out by adding increments of 10wt% Mg to Sn-9Zn filler metal. The liquid volume fraction on solidification was observed to decrease with increase in Magnesium additions as well as an increase in heating temperatures. At 30wt% Mg and 450°C, a melting peak was noted however no significant solidification peak was observed indicating complete consumption of the filler metal. Microstructural events were noted to be similar to Sn-9Zn filler metal.

Lastly, in order to evaluate the effect of not having Sn in the system to produce Mg_2Sn, a 50:50 wt% Mg-Zn powder mixture was used as a filler metal. Melting upon initial heating supports binary system's liquid phase formation at

342°C. Mg-Zn solid solution zones, unreacted Mg particles and the presence of solid Mg_7Zn_3 were evident in the microstructure of samples heated to 350°C. Limited melting and alloying between Zn and Mg powders was found, likely due to the large Mg particle sizes used, slowing the dissolution of Mg particles into a Zn rich liquid, thus shifting the bulk composition of the filler metal to a Mg rich hypoeutectic value, preventing full liquid filler metal layer. Heating to higher temperatures produced more diffusional solidification as Zn diffuses further into the unreacted Mg powder and the Mg base metal.

Sn-9Zn eutectic powder added to the Mg-Zn filler metal mixture had a pronounced influence over the diffusion couple microstructural development. It accelerated the alloying and dissolution of the Pure Mg particles in the filler metal. No melting of Sn-9Zn was observed during initial heating indicating that all of the Sn-9Zn was consumed in solid state. However, further heating to ~350°C results in liquid formation similar to that seen in the Mg/Mg-Zn couple. The cooling traces for the Mg/Mg-Zn couple with and without Sn-9Zn exhibit a noticeable solidification peak. Diffusional solidification is evident from the fact that the area under the DSC trace for 450°C has a smaller area than at 350°C. In the case of the filler containing 10% Sn-9Zn, no Mg powder remained in the complex solidified microstructure indicative of a large volume fraction of liquid present at 450°C. The primary cellular grains of (Mg) grow from the Mg base metal substrate and Mg_7Zn_3 solidifies in the intercellular region. This solidification mode eventually develops into a well developed eutectic solidification microstructure. In the original filler metal portion of the diffusion couple, a similar mixture of (Mg), Mg_7Zn_3 and eutectic appears but with a more dispersed character indicative of an equiaxed growth process. Further work is required to investigate the filler metal composition of 45Mg:45Zn:10(Sn-9Zn) wt% and peak heating temperature of 450°C which shows promising results which can eventually be developed into a commercial application.

References

[1] S. Davis, S. Diegel and R. Boundy, Transportation Energy Data Book Ed. 29, Oak Ridge, TN: U.S.Department of Energy, 2010.

[2] A. Boby et al., "Developments in Magnesium Alloys for Transport Applications–An Overview," *Indian Foundary Journal*, vol. 57, no. 1, pp. 29-37, 2011.

[3] S. Gautam, "What Factors Affect Average Fuel Economy of US Passenger Vehicles?," 2010. [Online]. Available: http://digitalcommons.iwu.edu/econ_honproj/104.

[4] G. Cole and A. Sherman, "Lightweight Materials for Automotive Applications," *Materials Characterization*, Vols. 35, No. 1, pp. 3-9, 1995.

[5] E. Aghion and B. Bronfin, "Magnesium Alloys Development towards the 21st Century," *Materials Science Forum*, Vols. 350-351, pp. 19-30, 2000.

[6] X. Cao et al., "A review of Laser Welding Techniques for Magnesium Alloys," *Journal of Materials Processing Technology*, vol. 171, pp. 188 - 204, 2006.

[7] B. Mordike and T. Ebert, "Magnesium: Propeties - Applicaitons - Potential," *Materials Science and Engineering: A*, vol. 302, no. 1, pp. 37-45, 2001.

[8] E. Hombergsmeir, "AEROMAG-Aeronautic Application of Wrought Magnesium," in *Magnesium: 8th International conference on Magnesium Alloys and their Applications*, Wiley-VCH (Edited: K.Kainer), 2010, pp. 1383-1391.

[9] H. Furuya et al., "Applications of Magnesium Alloys for Aerospace Structural systems," *Materials Science Forum*, Vols. 350-351, pp. 341-348, 2000.

[10] B.-A. Behrens and J. Knigge, "EU Project Magforming: Development of a Magnesium Forging process for Aeronautical Applications," in *Magnesium: 8th International Conference on Magnesium Alloys and their Applications*, Wiley-VCH (Edited: K.Kainer), 2010, pp. 633-638.

[11] A. Guillan et al., "Mechanical properties of Advanced Magnesium Alloys for Application on Airbus Aircrafts," in *Magnesium: 8th International Conference on Magnesium Alloys and their Applications*, Wiley-VCH (Edited: K.Kainer), 2010, pp. 719-730.

[12] K. Kainer, Magnesium: 8th International Conference on Magnesium Alloys and their Applicaitons, Wiley-VCH (Edited: K.Kainer), 2010.

[13] C. Schille et al., "Corrosion of Experimental Magnesium Alloys for use as a Possible Bone Replacement Material," in *Magnesim: 8th International Conference on Magnesium Alloys and their Applications*, Wiley-VCH (Edited: K.Kainer), 2010, pp. 1195 - 1200.

[14] D. Vojtech, "Applications of Magnesium Alloys for Hydrogen Storage," in *Magnesim: 8th International Conference on Magnesium Alloys and their Applications*, Wiley-VCH (Edited: K.Kainer), 2010, pp. 1066-1072.

[15] R. E. Sanders, "Lightweight Armor Plate and Method". United States of America Patent 4,626,294, 2 Dec 1986.

[16] T. Jones, R. DeLorme and M. Burkins, "Ballistic Evaluation of Commercially Rolled AZ31B-H24 Magnesium Alloy Plate," in *Magnesium: 8th International Conference on Magnesium Alloys and their Applications*, Wiley-VCH (Edited: K.Kainer), 2010, pp. 1049-1058.

[17] I. McNeil, An Encylopedia of the History of Technology, NY: Routledge, 1990.

[18] D. Turriff, S. Corbin and M. Kozdras, "Diffusional Solidificaiton Phenomena in Clad Aluminum Automotive Braze Sheet," *Acta Materialia,* vol. 58, pp. 1332-1341, 2010.

[19] Burke et al., "Transient Liquid Phase Bonding Repair for Advanced Turbine Blades and vanes". USA Patent US 6,508,000 B2, 21 January 2003.

[20] ASM International, ASM Handbook, Vol. 7, Liquid Phase Sintering, ASM International, 1998.

[21] M. Kuntz, Y. Zhou and S. Corbin, "A Study of Transient Liquid Phase Bonding of Ag-Cu Using Differential Scanning Calorimetry," *Metallurgical and Materials Transactions A,* vol. 37A, pp. 2493 - 2504, 2006.

[22] R. M. German, Sintering Theory and Practice, NY: Wiley-Interscience, 1996.

[23] R. M. German, Liquid Phase Sintering, NewYork: Springer, 1985.

[24] Y. Zhou, "Analytical Modeling of Isothermal Solidification during transient liquid phase (TLP) bonding," *Journal of Materials Science Letters,* vol. 20, pp. 841 - 844, 2001.

[25] S. Corbin and D. Cluff, "Determining the rate of (B-Ti) decay and its influence on the sintering behavior of NiTi," *Journal of Alloys and Compounds,* vol. 487, no. 1-2, pp. 179-186, 2009.

[26] W. MacDonald and T. Eagar, "Isothermal Solidification Kinetics of Diffusion Brazing," *Metallurgical and Materials Transactions A,* vol. 29, no. 1, pp. 315-325, 1998.

[27] D. Turriff and S. Corbin, "Quantitative Thermal Analysis of Transient Liquid Phase Sintered Cu-Ni Powders," *Metallurgical and Materials Transactions A,* vol. 39, no. 1, pp. 28-38, 2008.

[28] B. Wielage, S. Muecklich and T. Grund, "Corrosion behaviour of soldered joints of magnesium alloys and dissimilar materials," *Microchimica Acta,* vol. 156, no. 1-2, pp. 151-157, 2007.

[29] B. Wielage and S. Muecklich, "Improving the Soldering of magnesium alloys," *Welding Journal - Brazing and Soldering Today,* vol. 85, no. 9, pp. 48-51, 2006.

[30] L. Liu et al., "The relationship between microstructure and properties of Mg/Al brazed joints using Zn filler metal," *Materials Characterization,* vol. 59, no. 4, pp. 479-483, 2008.

[31] K. Bobzin et al., "A look at the development of Magnesium-Based Filler Metals," *Welding Journal - Brazing and Soldering Today,* vol. 87, no. 3, pp. 38-40, 2008.

[32] D. Sun, X. Gu and W. Liu, "Transient liquid phase bonding of magnesium alloy (Mg-3Al-1Zn) using aluminium interlayer," *Materials Science and Engineering: A,* vol. 391, no. 1-2, pp. 29 - 33, 2005.

[33] ASM International, ASM Handbook, Vol. 3, Alloy Phase Diagram, ASM Handbook International, 1992.

[34] L. Rokhlin, "Magnesium-Tin-Zinc," *SpringerMaterials - The Landolt Bornstein Database*, vol. 11A4 Light Metal Systems Part 4.

[35] G. Hoehne, W. Hemminger and H.-J. Flammersheim, Differential Scanning Calorimetry 2nd Ed., Heidelberg: Springer-Verlag, 2003.

[36] G. Svehla, Comprehensive Analytical Chemistry: Thermal Analysis Part B, NewYork: Elsevier Scientific Publishing Company, 1982.

[37] Y. Cengel, Heat Transfer: A practical approach, NewYork: McGraw-Hill Companies, 2002.

[38] M. Brown, Introduction to Thermal Analysis, NewYork: Chapman and Hall, 1988.

[39] Netzsch Group, Instrument Manual for Netzsch Thermal Analysis Software, Germany: Netzch.

[40] M. Kuntz, Quantifying Isothermal Solidification Kinetics during Transient Liquid Phase Bonding using Differential Scanning Calorimetry, PhD Thesis, Waterloo: Mechanical Engineering, University of Waterloo, 2006.

[41] S. Corbin, "High-Temperature Variable Melting Point Sn-Sb Lead-Free Solder Pastes Using Transient Liquid Phase Powder Processing," *Journal of Electronic Materials*, vol. 34, no. 7, pp. 1016-1025, 2005.

[42] M. Kuntz, S. Corbin and Y. Zhou, "Quantifying Metallurgical Interactions in solid/liquid diffusion couples using differential scanning calorimetry," *Acta Materialia*, vol. 53, pp. 3071 - 3082, 2005.

[43] T. D'Hondt and S. Corbin, "Thermal Analysis of the compositional shift in a transient liquid phase during sintering of a ternary Cu-Sn-Bi Powder Mixture," *Metallurgical and Materials Transactions A*, vol. 37, no. 1, pp. 217 - 224, 2006.

[44] W. Yu-Feng, D. Wen-bo and Z. Tie-yong, "Synthesis kinetics of Mg2Sn in Mg-Sn powder mixture using non-isothermal differential scanning calorimetry," *Trans. Nonferrous Met Soc. China*, vol. 19, pp. 1196 - 1200, 2009.

[45] S. Corbin and P. Lucier, "Thermal Analysis of Isothermal Solidification Kinetics during Transient Liquid Phase Sintering," *Metallurgical and Materials Transactions A*, vol. 32, no. 4, pp. 971 - 978, 2001.

[46] F. Czerwinski, "Factors affecting the oxidation nature of Magnesium alloys," *JOM Journal of the Minerals, Metals and Materials Society*, vol. 56, no. 5, pp. 29 - 31, 2004.

[47] F. Altmayer, "Plating Magnesium," *Advice and Council - Plating and Surface Finishing*, Feb, 2005.

[48] L. Zhu, W. Li and D. Shan, "Effects of low temperature thermal treatment on zinc and/or tin plated coatings of AZ91D magnesium alloy," *Surface & Coatings Technology*, vol. 201, pp. 2768 - 2275, 2006.

[49] J. Chen et al., "A zinc transition layer in electroless nickel plating," *Surface & Coatings Technology*, vol. 201, pp. 686 - 690, 2006.

[50] ASM International, ASM Handbook, Vol. 5, Surface Engineering, ASM Handbook International, 1994.

[51] H. Zhao, Z. Huang and J. Cui, "Electroless plating of copper on AZ31 magnesium alloy substrates," *Microelectronic Engineering*, vol. 85, pp. 253 - 258, 2008.

[52] Y. Song, D. Shan and E. Han, "Initial deposition mechanism of electroless nickel plating on AZ91D Magnesium alloys," *Canadian Metallurgical Quarterly*, vol. 45, no. 2, pp. 215 - 222, 2006.

[53] X. Wang et al., "One-step pickling-activation before magnesium alloy plating," *Transactions of Nonferrous Metals Society of China*, vol. 19, no. 2, pp. 504 - 510, 2009.

[54] S.Rohrbacher, *Millennium Plating Company Inc.*, Lowell, MA.

[55] AM&M, *Advanced Machine and Materials Inc.*, Kanata, Ontario.

[56] Alfa Aesar, *Research Chemicals and Materials Company*, MA, USA.

[57] Netzch, *Analysing and Testing Business Unit*, Selb, Germany.

[58] F. Meng et al., "Thermodynamic modelling of the Mg-Sn-Zn ternary system," *Journal of Alloys and Compounds,* vol. 508, no. 2, pp. 570 - 581, 2010.

[59] C. Bale, P. Chartrand, S. Degterov, R. Mahfoud, J. Melacon, A. Pelton, G. Eriksson, K. Hack and S. Petersen, "FactSage Thermochemical Software and Databases", Calphad, vol. 26, no. 2, pp. 189-228, 2002.

[60] P. Ghosh, M. Mezbahul-Islam and M. Medraj, "Critical Assessment and thermodynamic modeling of Mg-Zn, Mg-Sn, Sn-Zn and Mg-Sn-Zn systems," *Calphad: Computer Coupling of Phase Diagrams and Thermochemistry,* vol. 36, pp. 28 - 43, 2012.

[61] M. Bamberger, "Phase formation in Mg-Sn-Zn alloys - thermodynamic calculations vs experimental verification," *Journal of Materials Science,* vol. 41, no. 10, pp. 2821-2829, 2006.

APPENDIX I

SEM Micrographs

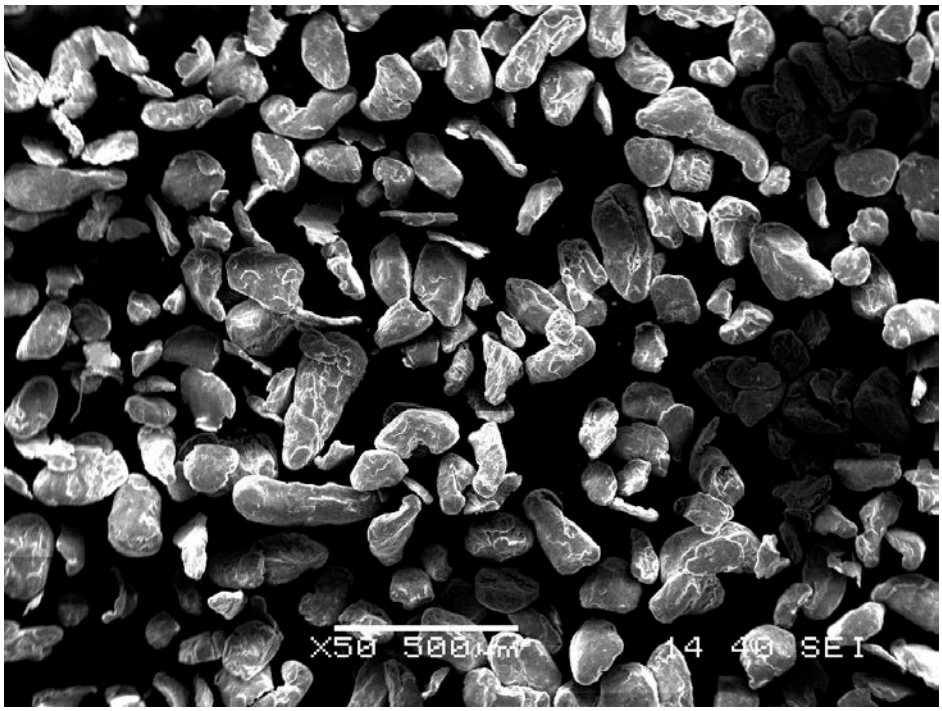

Figure I.1: SEM of Mg Powder

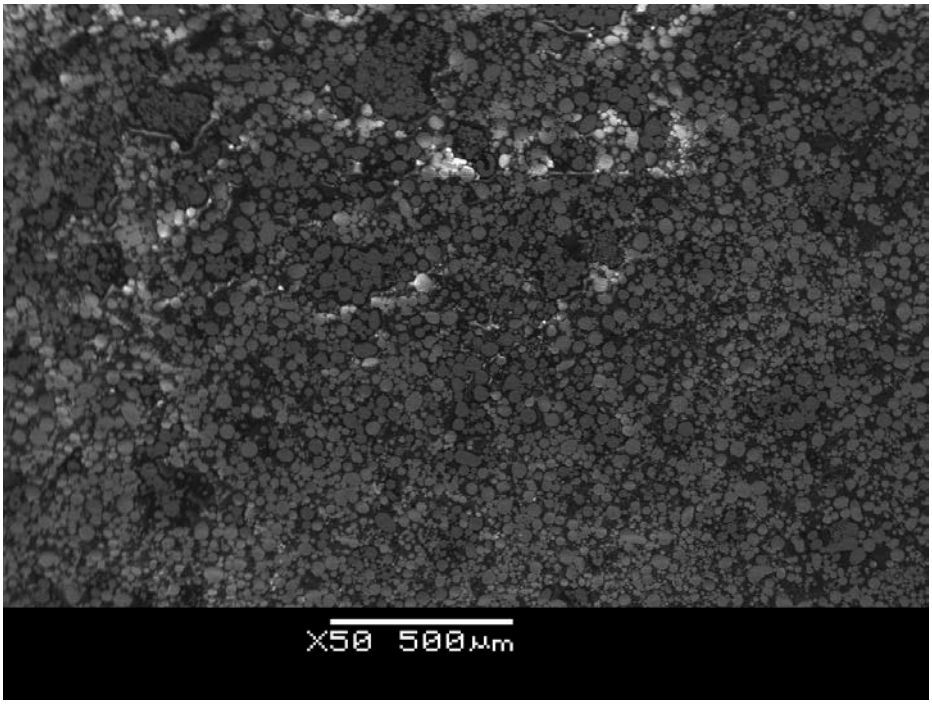

Figure I.2: SEM of Sn9Zn Powder

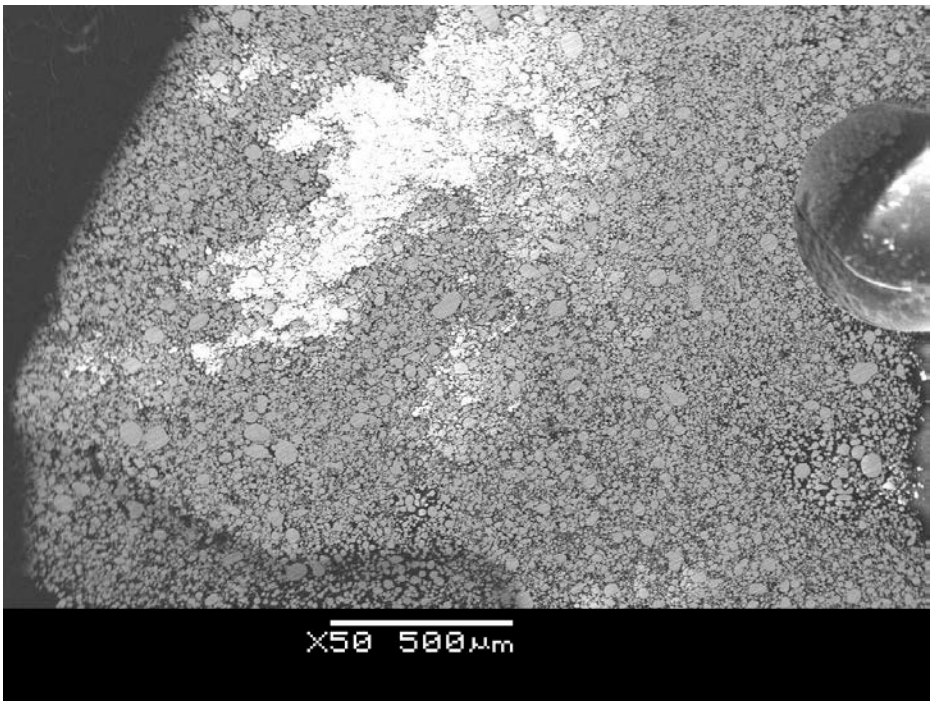

Figure I.3: SEM of Sn Powder

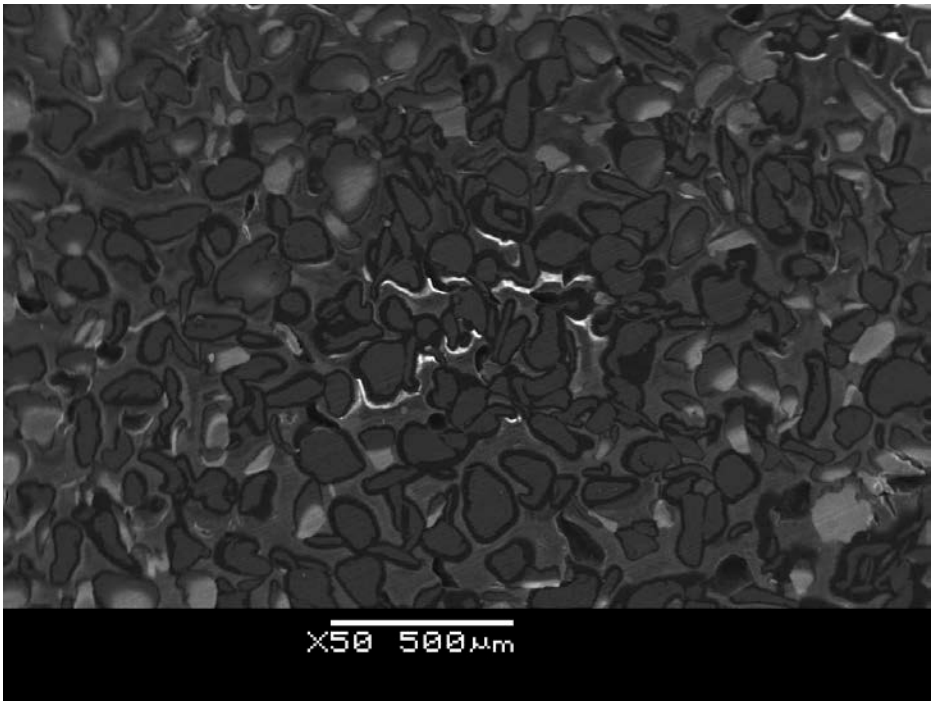

Figure I.4: SEM of Zn Powder

APPENDIX II

ISOTHERMS

Computed from FactSage Software

(C. Bale, P. Chartrand, S. Degterov, R. Mahfoud, J. Melacon, A. Pelton,
G. Eriksson, K. Hack and S. Petersen, "FactSage Thermochemical Software and Databases")

Mg - Sn - Zn

250°C

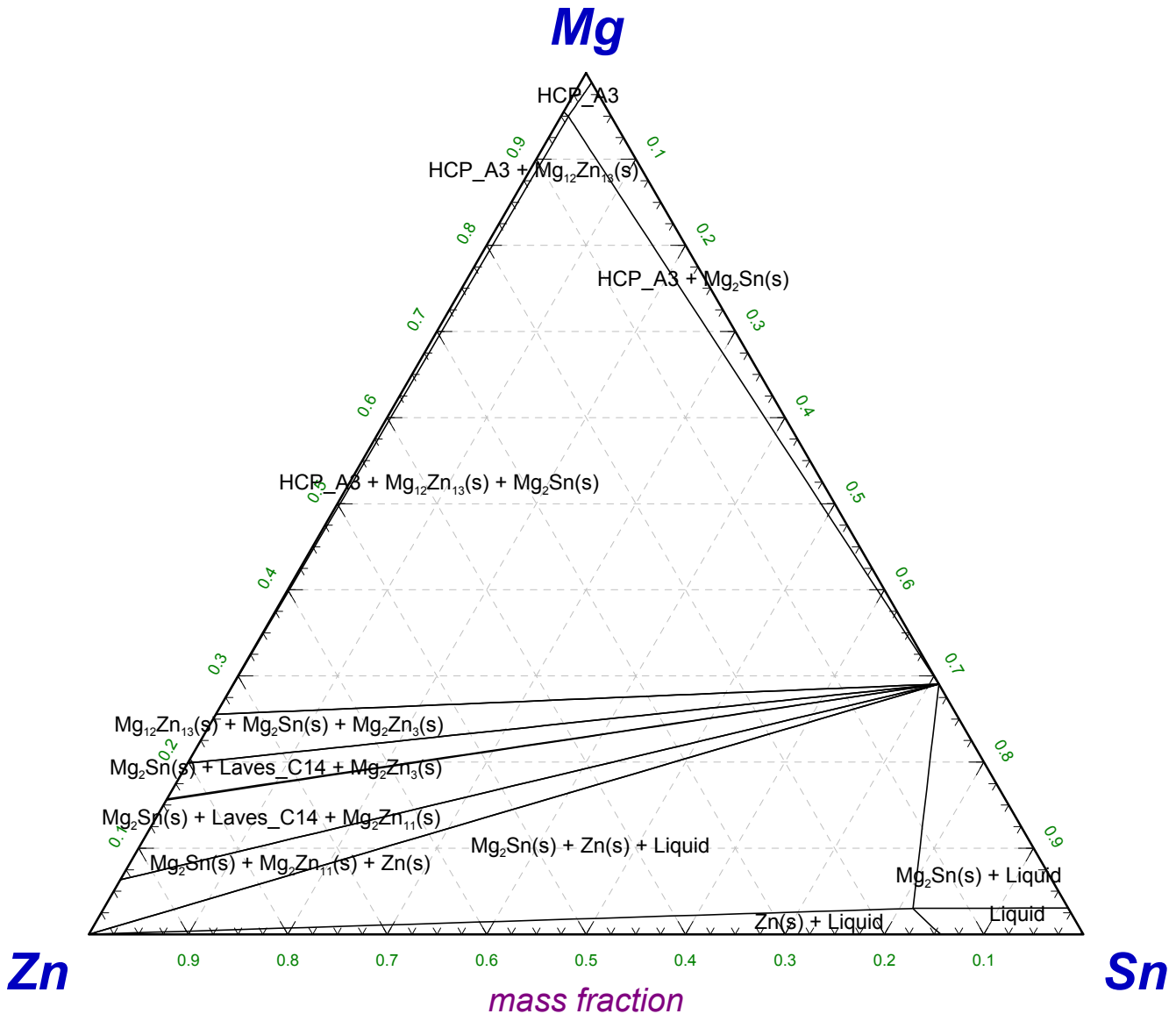
Mg
HCP_A3
HCP_A3 + Mg12Zn13(s)
HCP_A3 + Mg2Sn(s)
HCP_A3 + Mg12Zn13(s) + Mg2Sn(s)
Mg12Zn13(s) + Mg2Sn(s) + Mg2Zn3(s)
Mg2Sn(s) + Laves_C14 + Mg2Zn3(s)
Mg2Sn(s) + Laves_C14 + Mg2Zn11(s)
Mg2Sn(s) + Mg2Zn11(s) + Zn(s)
Mg2Sn(s) + Zn(s) + Liquid
Mg2Sn(s) + Liquid
Zn(s) + Liquid
Liquid
0.9
0.8
0.7
0.6
0.5
0.4
0.3
0.2
0.1
Zn
Sn
mass fraction

Mg - Sn - Zn

350°C

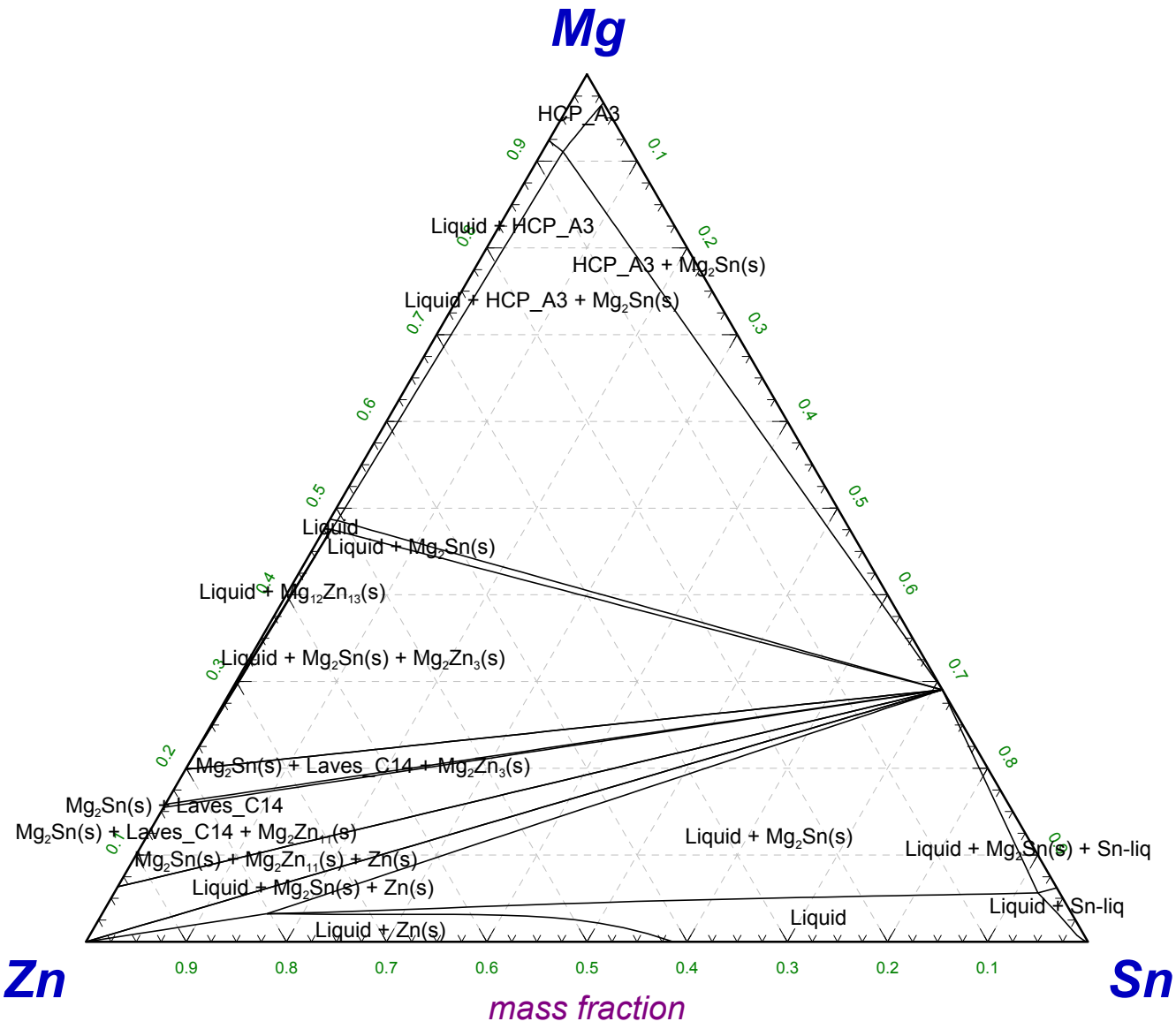
Mg
HCP_A3
Liquid + HCP_A3
HCP_A3 + Mg2Sn(s)
Liquid + HCP_A3 + Mg2Sn(s)
Liquid
Liquid + Mg2Sn(s)
Liquid + Mg12Zn13(s)
Liquid + Mg2Sn(s) + Mg2Zn3(s)
Mg2Sn(s) + Laves_C14 + Mg2Zn3(s)
Mg2Sn(s) + Laves_C14
Mg2Sn(s) + Laves_C14 + Mg2Zn11(s)
Mg2Sn(s) + Mg2Zn11(s) + Zn(s)
Liquid + Mg2Sn(s) + Zn(s)
Liquid + Zn(s)
Liquid + Mg2Sn(s)
Liquid + Mg2Sn(s) + Sn-liq
Liquid
Liquid + Sn-liq
0.9
0.8
0.7
0.6
0.5
0.4
0.3
0.2
0.1
Zn
Sn
mass fraction

Mg - Sn - Zn

375°C

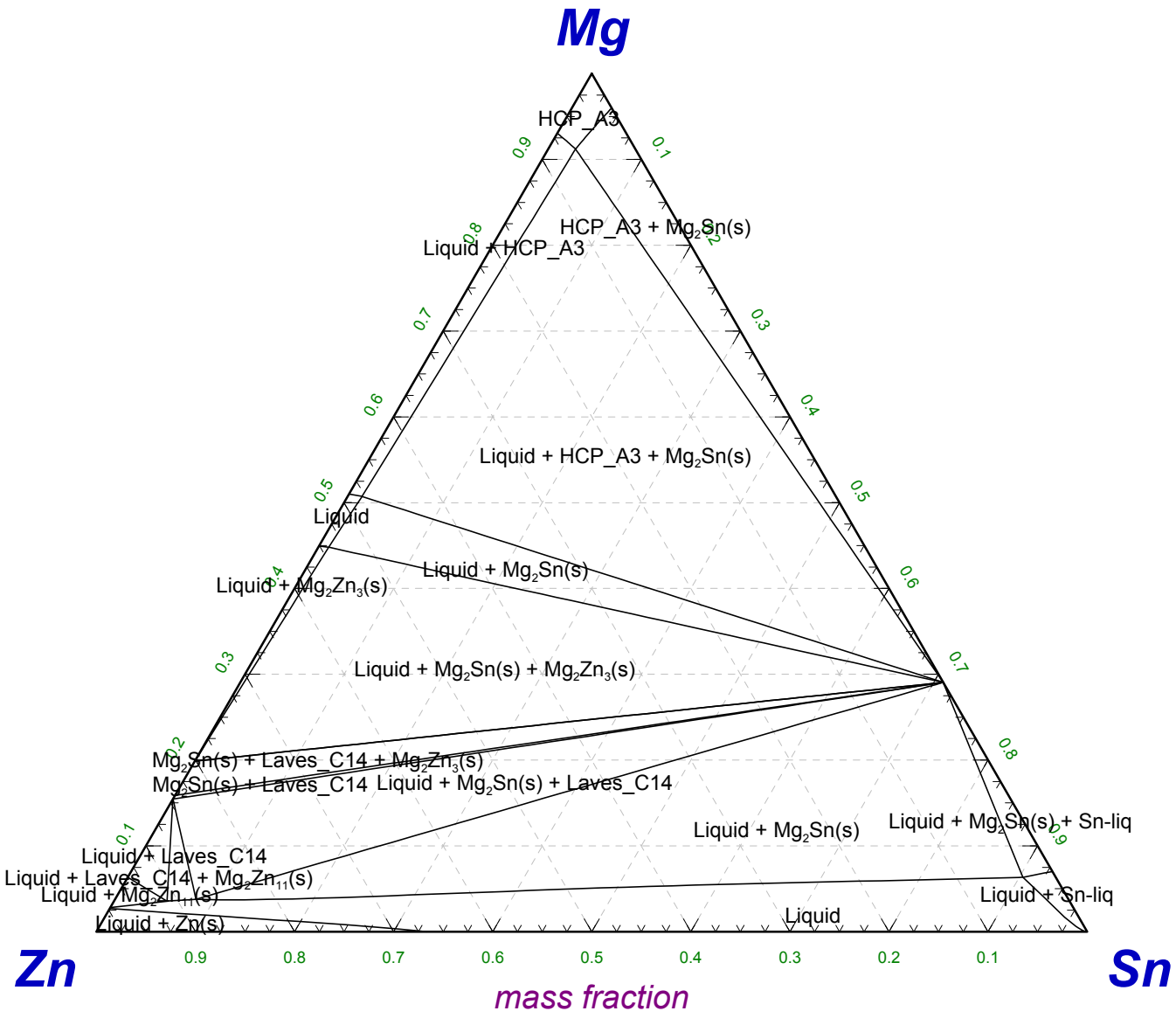
Mg
HCP_A3
HCP_A3 + Mg2Sn(s)
Liquid + HCP_A3
Liquid + HCP_A3 + Mg2Sn(s)
Liquid
Liquid + Mg2Sn(s)
Liquid + Mg2Zn3(s)
Liquid + Mg2Sn(s) + Mg2Zn3(s)
Mg2Sn(s) + Laves_C14 + Mg2Zn3(s)
Mg2Sn(s) + Laves_C14
Liquid + Mg2Sn(s) + Laves_C14
Liquid + Mg2Sn(s)
Liquid + Mg2Sn(s) + Sn-liq
Liquid + Laves_C14
Liquid + Laves_C14 + Mg2Zn11(s)
Liquid + Mg2Zn11(s)
Liquid + Sn-liq
Liquid + Zn(s)
Liquid
0.9
0.8
0.7
0.6
0.5
0.4
0.3
0.2
0.1
Zn
Sn
mass fraction

Mg - Sn - Zn

400°C

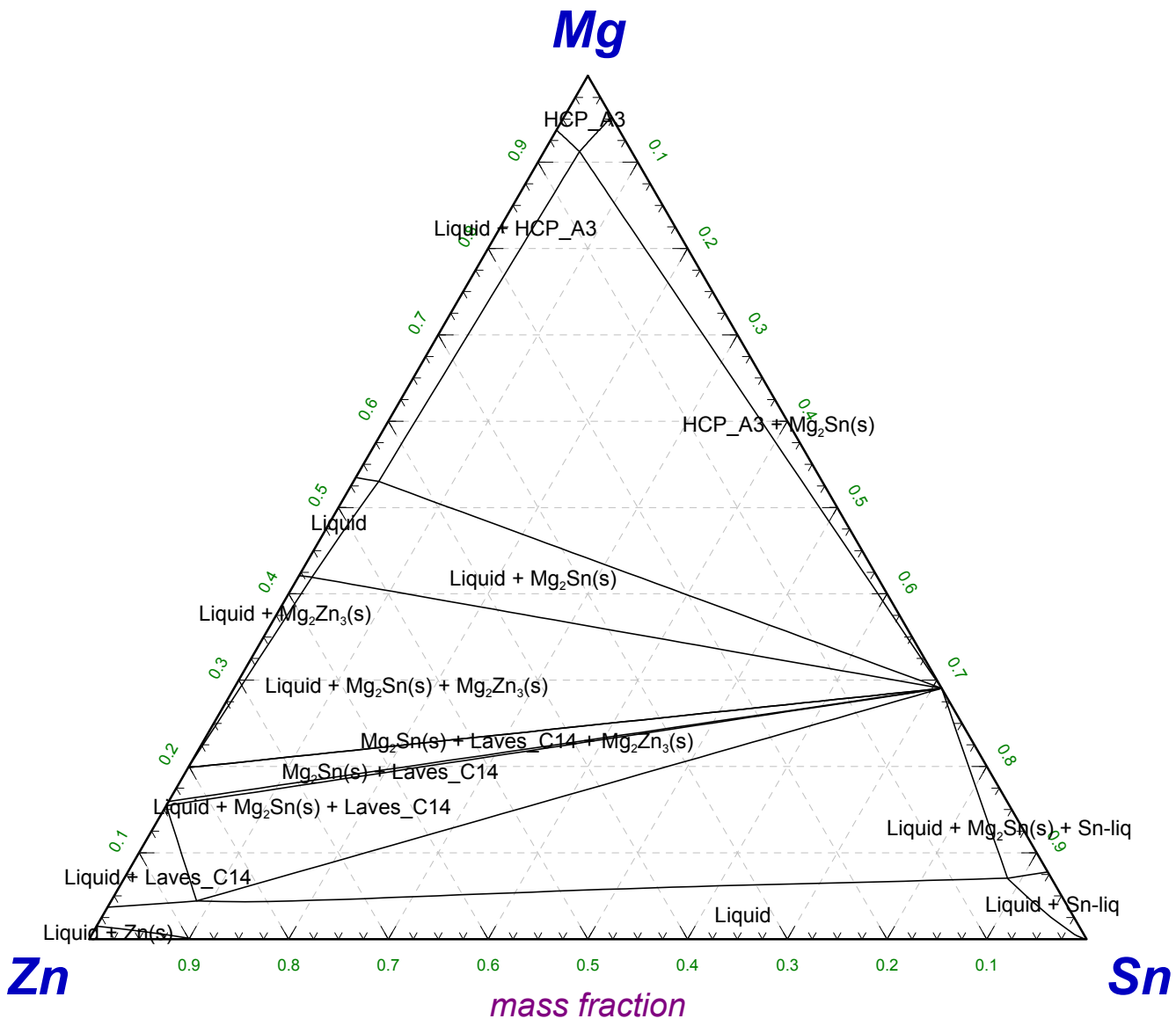
Mg
HCP_A3
Liquid + HCP_A3
HCP_A3 + Mg2Sn(s)
Liquid
Liquid + Mg2Sn(s)
Liquid + Mg2Zn3(s)
Liquid + Mg2Sn(s) + Mg2Zn3(s)
Mg2Sn(s) + Laves_C14 + Mg2Zn3(s)
Mg2Sn(s) + Laves_C14
Liquid + Mg2Sn(s) + Laves_C14
Liquid + Mg2Sn(s) + Sn-liq
Liquid + Laves_C14
Liquid + Sn-liq
Liquid
Liquid + Zn(s)
Zn
Sn
mass fraction

Mg - Sn - Zn

425°C

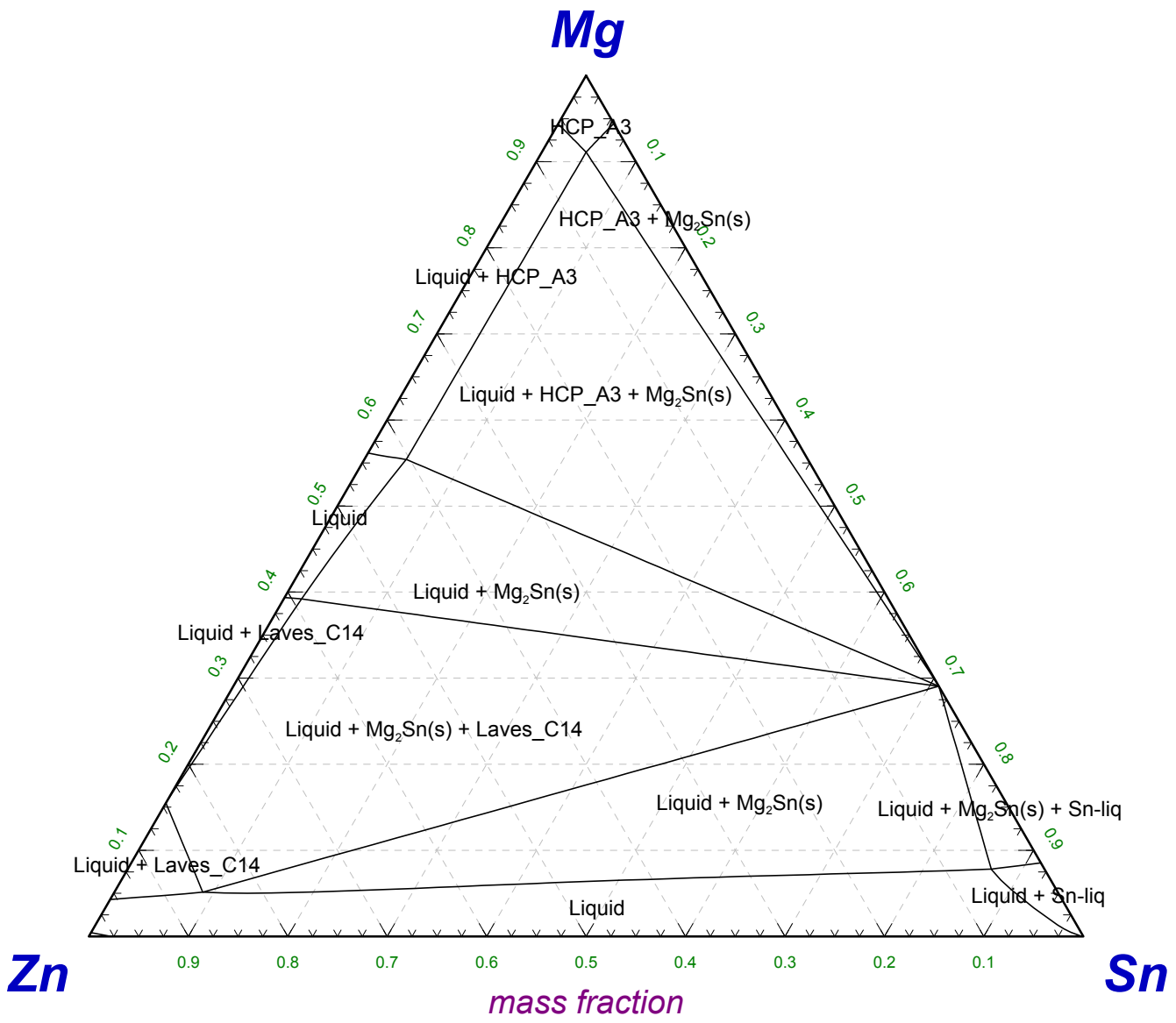
Mg
HCP_A3
HCP_A3 + Mg2Sn(s)
Liquid + HCP_A3
Liquid + HCP_A3 + Mg2Sn(s)
Liquid
Liquid + Mg2Sn(s)
Liquid + Laves_C14
Liquid + Mg2Sn(s) + Laves_C14
Liquid + Mg2Sn(s)
Liquid + Mg2Sn(s) + Sn-liq
Liquid + Laves_C14
Liquid
Liquid + Sn-liq
0.9
0.8
0.7
0.6
0.5
0.4
0.3
0.2
0.1
Zn
Sn
mass fraction

Mg - Sn - Zn

450°C

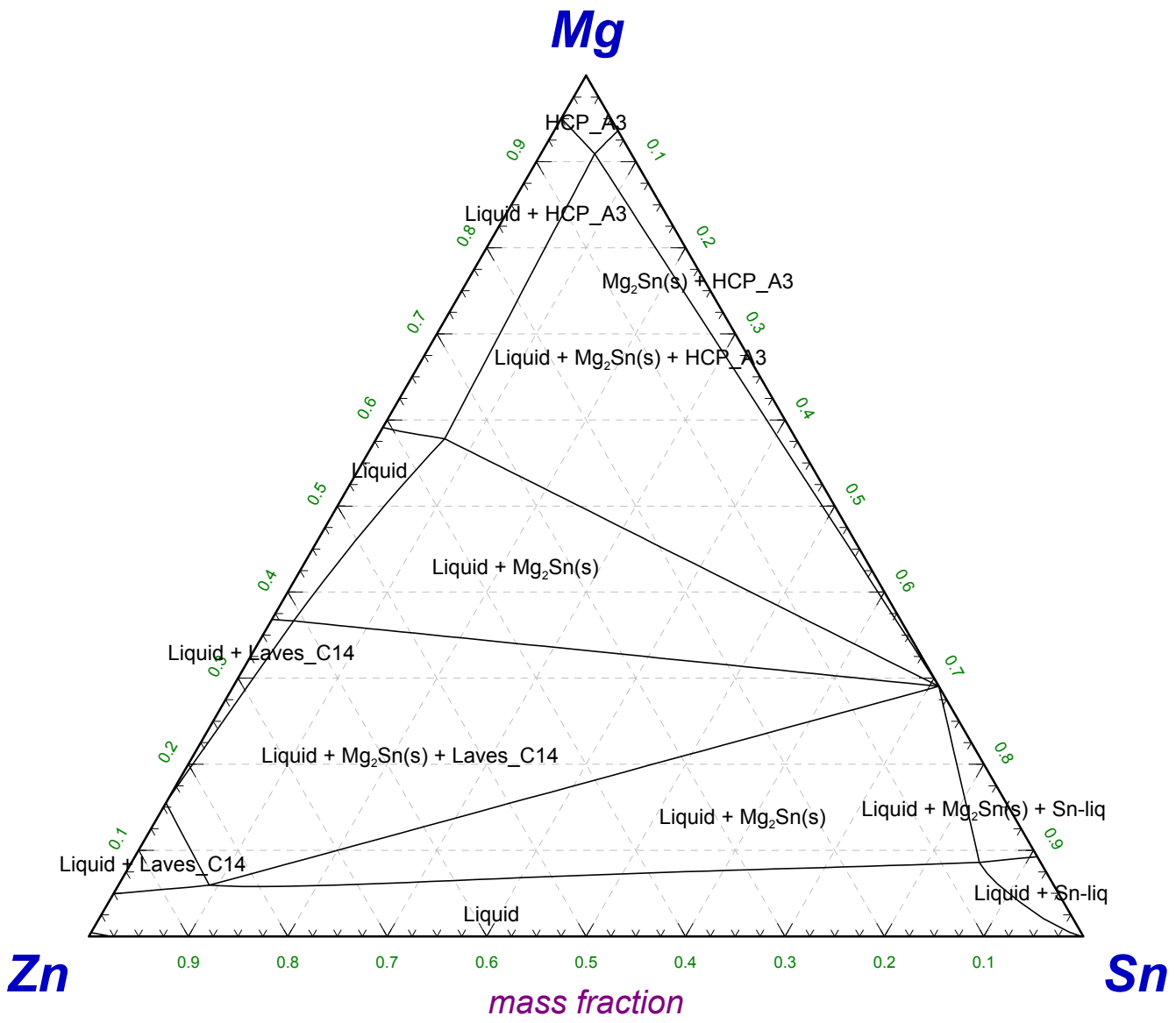
Mg
HCP_A3
Liquid + HCP_A3
Mg2Sn(s) + HCP_A3
Liquid + Mg2Sn(s) + HCP_A3
Liquid
Liquid + Mg2Sn(s)
Liquid + Laves_C14
Liquid + Mg2Sn(s) + Laves_C14
Liquid + Mg2Sn(s)
Liquid + Mg2Sn(s) + Sn-liq
Liquid + Laves_C14
Liquid + Sn-liq
Liquid
0.9
0.8
0.7
0.6
0.5
0.4
0.3
0.2
0.1
Zn
Sn
mass fraction